Title
Further Development of the Tail-Equivalent Linearization Method for Nonlinear Stochastic Dynamics

Author
Broccardo, Marco

Publication Date
2014

Peer reviewed|Thesis/dissertation

Further Development of the Tail-Equivalent Linearization Method for Nonlinear Stochastic Dynamics

by

Marco Broccardo

A dissertation submitted in partial satisfaction of the

requirements for the degree of

Doctor of Philosophy

in

Engineering – Civil and Environmental Engineering

and the Designated Emphasis

in

Computational Science and Engineering

in the

Graduate Division

of the

University of California, Berkeley

Committee in charge:

Professor Armen Der Kiureghian, Chair
Professor Sanjay Govindjee
Professor David Ross Brillinger

Fall 2014

Further Development of the Tail-Equivalent Linearization Method for Nonlinear Stochastic Dynamics

Abstract

Further Development of the Tail-Equivalent Linearization Method for Nonlinear Stochastic Dynamics

by

Marco Broccardo

Doctor of Philosophy in Engineering – Civil and Environmental Engineering

and the Designated Emphasis in

Computational Science and Engineering

University of California, Berkeley

Professor Armen Der Kiureghian, Chair

This dissertation provides the foundation for an in-depth understanding and significant development of the tail-equivalent linearization method (TELM) to solve different classes of nonlinear random vibration problems. The TELM is a linearization method that uses the first-order reliability method (FORM) to define a tail-equivalent linear system (TELS) and to estimate the tail of the response distribution for nonlinear systems under stochastic inputs. The method was originally developed in the time domain for inelastic systems. It was later extended in the frequency domain for a specific class of nonlinear excitations, while the frequency domain version for inelastic systems is covered in the present work.

This dissertation mathematically formalizes and extends TELM analysis with different types of discretization of the input process. A general formulation for discrete representation of a Gaussian band-limited, white-noise process is introduced, which employs the sum of deterministic and orthogonal basis functions weighted by random coefficients. The selection of the basis functions completely defines the two types of discretizations used in the earlier works. Specifically, a train of equally spaced time delta-Dirac functions leads to the current time-domain discretization, while harmonic functions with equally spaced frequencies lead to the current frequency-domain discretization. We show that other types of orthogonal basis functions can be used with advantage to represent a Gaussian band-limited white noise and in particular we employ sinc basis functions, which are at the base of the Whittaker-Shannon interpolation formula. We demonstrate that this representation is suitable for reducing the total number of random variables that are necessary to describe the process, since it decouples the computational-time discretization from the band-limit of the process.

Next, the dissertation tackles the problem of a nonlinear system subjected to multi-component excitations by defining an augmented standard normal space composed of all the

random variables that define the multiple components of the excitation. The tail-equivalent linearization and definition of the TELS is taken in this new space. Once the augmented TELS is defined, response statistics of interest are determined by linear random vibration analysis by superposition of responses due to each component of the excitation. The method is numerically examined for an asymmetric structure with varying eccentricity and subjected to two statistically independent components of excitation.

Several practical problems require analysis for non-stationary excitations. For this important class of problems the original TELM requires linearization for a series of points in time to study the evolution of response statistics. This procedure turns out to be computationally onerous. As an approximate alternative, we propose the evolutionary TELM, ETELM. In particular, we adopt the concepts of the evolutionary process theory, to define an evolutionary TELS, ETELS. The ETELS approximately estimates the continuous time evolution of the design point by only one TELM analysis. This is the essence of its efficiency compared to the standard TELM analysis. Among response statistics of interest, the first-passage probability represents the most important one for this class of problems. This statistic is efficiently computed by using the Au-Beck important sampling algorithm, which requires knowledge of the evolving design points, in conjunction with the ETELS. The method is successfully tested for five types of excitation: (I) uniformly modulated white noise, (II) uniformly modulated broad-band excitation, (III) uniformly modulated narrow-band excitation, (IV) time- and frequency-modulated broad-band excitation, and (V) time- and frequency-modulated narrow-band excitation.

to Gemma Carron, Giovanni and Leone Broccardo.

Contents

Contents **ii**

List of Figures **iv**

List of Tables **vii**

1 Introduction **1**
1.1 Nonlinear random vibration in the scientific literature 3
1.2 Objective 6
1.3 Organization of the dissertation 7

2 The state of art of TELM **9**
2.1 Introduction: TELM at a glance 9
2.2 TELM in the time domain 10
2.3 TELM in frequency domain 14
2.4 Numerical example 16
2.5 Conclusion 25

3 Sampling and Interpolation **27**
3.1 Introduction: Sampling and Interpolation at a glance 27
3.2 The Shah Distribution 27
3.3 Interpolation Problem 32
3.4 Functional spaces interpretation 33
3.5 Conclusion 36

4 Band-limited stochastic processes **37**
4.1 Introduction: Band-limited stochastic processes at a glance 37
4.2 General representation of stochastic processes 37
4.3 Vectorial Representation of stochastic processes 39
4.4 Band-limit white noise by Whittaker-Shannon expansion 40
4.5 TELM analysis 44
4.6 Conclusion 46

5 Multi-component TELM analysis **49**
5.1 Introduction multi-component TELM at a glance 49
5.2 Stochastic representation of input excitations 49
5.3 Multi-component TELM analysis 51
5.4 DDM in multi-component TELM analysis 54
5.5 Random vibration analysis 60
5.6 Multi-component TELM analysis, summary 60
5.7 Numerical example 61
5.8 Conclusion 65

6 Non-stationary TELM analysis **78**
6.1 Introduction non-stationary TELM at a glance 78
6.2 Evolutionary TELM 79
6.3 The Au-Beck algorithm in the ETELM context 85
6.4 Example I, separable modulating function 88
6.5 Example II, non-separable modulating function 92
6.6 Conclusion 94

7 Conclusion **106**
7.1 Introduction 106
7.2 State of art of TELM 106
7.3 Limitations and shortcomings of TELM 109
7.4 Further studies 113

Bibliography **115**

Index **123**

List of Figures

1.1 Flow chart of PBEE 2

2.1 TELS of the non linear response for a given threshold x and point in time t_x . . 13
2.2 a) Design point excitation, b) Design point response for $x = 3\bar{\sigma}$ and $t_x = 15$[s] . 18
2.3 Hysteresis loop for design point excitation-response pair 19
2.4 a) IRF, b) FRF for $x = 3\bar{\sigma}$ and $t_x = 15$[s] 19
2.5 IRFs, FRFs of the TELS for 3 different thresholds: $x = 0.5\bar{\sigma}$, $x = 1.5\bar{\sigma}$, $x = 5\bar{\sigma}$. 20
2.6 Sequence of Reliability index 21
2.7 a) Complemetary CDF and b) PDF of the response 21
2.8 Mean up-crossing rate of the nonlinear response. 22
2.9 First passage probability of the nonlinear response for a time interval of 10[s] . . 23
2.10 Tail Probability of the nonlinear response at threshold $x = 3\bar{\sigma}$ and scaled white-noise input 25
2.11 Tail Probability of the maximum response at threshold $x = 3\bar{\sigma}$ and scaled white-noise input 26

4.1 a) Design point excitation, b) Design point response for $x = 3\sigma_0$ 47
4.2 IRF and FRF of the nonlinear system for $x = 3\sigma_0$ 48

5.1 Structural archetype 66
5.2 Hysteretic behavior of the frames 67
5.3 Power spectral densities: a) band-limit white noise, b) Kanai-Tajimi 67
5.4 Design-point input, white noise input 68
5.5 Design-point input, Kanai-Tajimi inputs 68
5.6 Global response to white noise design-point input and design-point response . . 69
5.7 Global response to Kanai Tajimi design-point input and design-point response . 70
5.8 Impulse-response functions, white noise inputs 70
5.9 Frequency-response functions modulus and phase, white noise inputs 71
5.10 Frequency-response functions real and imaginary part, white noise inputs 72
5.11 Impulse-response functions, Kanai-Tajimi inputs 72
5.12 Frequency-response functions modulus and phase, Kanai-Tajimi inputs 73
5.13 Frequency-response functions, real and imaginary part, Kanai-Tajimi inputs . . 74

5.14 Reliability index and point in time probability, white noise inputs 74
5.15 Reliability index and point in time probability, Kanai-Tajimi inputs 75
5.16 Mean up-crossing and Probability of maximum response, white noise inputs . . 75
5.17 Mean up-crossing and probability of maximum response, Kanai-Tajimi inputs . 76
5.18 Tail-fragility curve of maximum response, white noise inputs 76
5.19 Tail-fragility curve of maximum response, Kanai-Tajimi inputs 77
5.20 a) Reliability index b) Probability of failure for different eccentricities 77

6.1 Time modulating function $q(t)$ 94
6.2 EPSD of modulated white noise excitation (excitation I) 95
6.3 EPSD modulated broad-band excitation (excitation II) 95
6.4 EPSD modulated narrow-band excitation (excitation III) 96
6.5 Hysteresis loop, for modulated broad-a) and narrow-b) band excitation 96
6.6 Reliability index for response to modulated white-noise (excitation I) 97
6.7 Reliability index for response to modulated broad-band excitation (excitation II) 97
6.8 Reliability index for response to modulated narrow-band excitation (excitation III) 98
6.9 EFRF for response to modulated white-noise (excitation I), the grey line corresponds to the linear case 98
6.10 EFRF modulated broad-band excitation (excitation II), the grey line correspond to the linear case 99
6.11 EFRF modulated narrow-band excitation (excitation II), the grey line correspond to the linear case 99
6.12 Convergence of $\hat{P}(F)$ for the case with modulated white-noise excitation (excitation I) 100
6.13 Convergence of $\hat{P}(F)$ for the case with modulated broad-band excitation (excitation II) 100
6.14 Convergence of $\hat{P}(F)$ for the case with modulated narrow-band excitation (excitation III) 101
6.15 EPSD fully non stationary broad-band excitation (excitation IV) 102
6.16 EPSD fully non stationary narrow-band excitation (excitation V) 102
6.17 Reliability index for response to fully non-stationary broad-band excitation (excitation IV) 103
6.18 Reliability index for response to fully non-stationary narrow-band excitation (excitation V) 103
6.19 EFRF fully non-stationary broad-band excitation (excitation IV), the grey line correspond to the linear case 104
6.20 EFRF fully non-stationary narrow-band excitation (excitation V), the grey line correspond to the linear case 104
6.21 Convergence of $\hat{P}(F)$ for the case with fully non-stationary broad-band excitation (excitation IV) 105
6.22 Convergence of $\hat{P}(F)$ for the case with fully non-stationary narrow-band excitation (excitation V) 105

7.1 χ convergence for $N \to \infty$ 110
7.2 Volume error concept 111
7.3 Limit state functions for different physical systems. a) FORM correct solution, b) FORM not applicable, c) FORM accurate solution 112
7.4 Limit state functions shapes a) FORM overestimates the response, b) FORM underestimates the response, c) FORM, the overestimation and underestimation error compensate 113

List of Tables

2.1 Structural and Excitation Properties 18

4.1 Structural and Excitation Properties 47
4.2 Efficiency of the TELM based on sinc basis functions 47

5.1 Structural and Excitation Properties 66

6.1 Excitation Properties 89
6.2 System Properties 90
6.3 ETELM output 91
6.4 Estimates of first-passage probability by ETELM and MCS 92
6.5 Excitation Properties fully non-stationary excitation 93
6.6 ETELM output fully non-stationary excitation 93
6.7 Estimates of first-passage probability by ETELM and MCS fully non-stationary excitation 94

Acknowledgments

My deepest and sincerest gratitude is to my advisor Professor Armen Der Kiureghian. He is not only an advisor and a professor, but during these years he has also been a guide, a friend, and a true academic father. He is an example of how a professor and researcher should be: wise, patient, organized, and always available. His style and integrity will always motivate me in my career.

I am also deeply in debt to all UC Berkeley community; the 5 years spent in this beautiful place have shaped my personality and have given me the opportunity of looking backward and being happy with my life path. In particular, I would like to thank to the International House and all the friends that I met there (mentioning them would be too long). I lived there for almost a year and it was absolutely one of the highest pinnacles of my experience at Berkeley.

Next I want to give my gratitude to my sweet Mina for supporting me, and to my fellow colleagues who became lifetime friends, I shared with them the good and the bad of what a Ph.D. program has to offer. Our joys, our tears, and our discussions are all stories that contributed to shape what the most beautiful thing a human being has: his memories. Thank you (in alphabetical order) to Ahmet, Bin Bin, Gerd, James, Juan, Mayssa, Micheal, Mohamed, Panos, Simon, Sunny, Tea, and Yuan.

In ultima istanza vorrei usare la mia lingua madre per ringraziare mia madre, Gemma e mio padre Giovanni. Miei cari genitori a voi devo tutto e nessuna parola o frase può comunicare la mia gratitudine, ma un particolare sopra ogni altro mi fa piacere menzionare. Nel contemporaneo mondo occidentale vi ringrazio per essere ciò che di più complesso c'è, due persone semplici.

Notation

set of natural numbers	$\mathbb{N}$	0 1 2...
set of integer numbers	$\mathbb{Z}$	$... -2, -1, 0, 1, 2, ...$
set of real numbers	$\mathbb{R}$	$(-\infty, \infty)$
set of complex numbers	$\mathbb{C}$	$a + ib;\ a, b \in \mathbb{R}$
vector space	$\mathbb{V}$	
Hilbert space	$\mathbb{H}$	
complex number	z	$a + ib; z \in \mathbb{C}$
Hermitian conjugate	z^{H}	$a - ib;\ z^{\mathrm{H}} \in \mathbb{C}$
derivative-integral operator	$u_{,x^n}$	$\frac{\partial^n u}{\partial x^n};\ n > 0$
		$\int^{(n)} u; n < 0$
standard inner product on $\mathbb{C}^N$	$\langle \boldsymbol{u}, \boldsymbol{v} \rangle$	$\sum_n u_n v_n^{\mathrm{H}}$
standard inner product on $\mathbb{C}^{\mathbb{R}}$	$\langle x(t), y(t) \rangle$	$\int_{-\infty}^{\infty} x(t) y(t)^{\mathrm{H}} dx$
standard inner product on $\mathbb{C}^{[a,b]}$	$\langle x(t), y(t) \rangle$	$\int_a^b x(t) y(t)^{\mathrm{H}} dx$
time sampling interval	Δt	$\Delta t \in \mathbb{R}^+$
period of a periodic time function	T	$T \in \mathbb{R}^+$

functions in the time domain	$f; g$	$f(t); g(t) \in \mathbb{R}$
frequency sampling interval	$\Delta\omega$	$\Delta\omega \in \mathbb{R}^+$
band limit of band limited function	$\frac{\Omega}{2}$	$\Omega \in \mathbb{R}^+$
functions in the frequency domain	$F; G$	$F(\omega); G(\omega) \in \mathbb{C}$
convolution	$f * g$	$\int_{-\infty}^{\infty} f(t-x)g(x)dx$
	$F * G$	$\int_{-\infty}^{\infty} F(\omega-x)G(x)dx$
general temporal stochastic process	$\mathrm{F}(t)$	
white noise	$W(t)$	
Fourier Transform	$\mathscr{F}[f](\omega)$	$\langle f(t), e^{i\omega t}\rangle$
Inverse Fourier Transform	$\mathscr{F}^{-1}[F](t)$	$\frac{1}{2\pi}\langle F(\omega), e^{-i\omega t}\rangle$
Dirac distribution	$\delta(t-a)$	$\langle f(t), \delta(t-a)\rangle \triangleq f(a)$
Sampling Shah distribution, time domain	$\mathrm{Ш}_{\Delta t}$	$\sum_{n=-\infty}^{\infty} \delta(t-n\Delta t)$
Periodizing Shah distribution, time domain	$\mathrm{Ш}_{T}$	$\sum_{n=-\infty}^{\infty} \delta(t-nT)$
Sampling Shah distribution, frequency domain	$\mathrm{Ш}_{\Delta\omega}$	$\Delta\omega \sum_{k=-\infty}^{\infty} \delta(\omega-\Delta\omega k)$
Periodizing Shah distribution, frequency domain	$\mathrm{Ш}_{\Omega}$	$\Omega \sum_{k=-\infty}^{\infty} \delta(\omega-\Omega k)$
rectangular function	$\Pi_a(t)$	$1, \lvert t\rvert < a; 0, \lvert t\rvert \geq a$
sinc function	$\mathrm{sinc}_T(t)$	$\frac{\sin(\pi t/T)}{\pi t/T}$
Kronecker delta (signal processing)	$\delta[n]$	$1,\ n = 0;$
		$0,\ n \neq 0$

Quick Reference

Proprieties Fourier Transform

Linearity	$\mathscr{F}[\alpha f(t) + \beta g(t)](\omega) = \alpha\mathscr{F}[f](\omega) + \beta\mathscr{F}[g](\omega)$ $\alpha, \beta \in \mathbb{C}$
Symmetry	$\mathscr{F}[f](-\omega) = 2\pi\mathscr{F}^{-1}[f](\omega)$ $2\pi\mathscr{F}^{-1}[F](-t) = \mathscr{F}[F](t)$ $\mathscr{F}[F(t)](\omega) = 2\pi f(-\omega)$
Shifting	$\mathscr{F}[f(t+a)](\omega) = e^{i\omega a}\mathscr{F}[f](\omega) = e^{i\omega a}F$ $\mathscr{F}^{-1}[F(\omega+a)](t) = e^{-i\omega a}\mathscr{F}^{-1}[F](t) = e^{-i\omega a}f$
Scaling	$\mathscr{F}[f(at)](\omega) = \frac{1}{\lvert a\rvert}\mathscr{F}[f]\left(\frac{\omega}{a}\right) = \frac{1}{\lvert a\rvert}F\left(\frac{\omega}{a}\right)$
Differentiation, Integration	$\mathscr{F}[f_{,t^n}] = (i\omega)^n\mathscr{F}[f](\omega) = (i\omega)^n F$ $\mathscr{F}^{-1}[F_{,\omega^k}] = (-it)^k\mathscr{F}^{-1}[F](t) = (-it)^k f$
Convolution	$\mathscr{F}[f * g](\omega) = \mathscr{F}[f](\omega)\mathscr{F}[g](\omega) = FG$ $\mathscr{F}^{-1}[F * G](t) = 2\pi\mathscr{F}^{-1}[F](t)\mathscr{F}^{-1}[G](t) = 2\pi fg$
Parseval's identity	$\langle f, g\rangle = \frac{1}{2\pi}\langle F, G\rangle$
Poisson summation formula	$\sum_{n=-\infty}^{\infty} f(nT) = \sum_{k=-\infty}^{\infty} F\left(\frac{2\pi k}{T}\right)$

Proprieties Dirac distribution

sampling	$u(x)\delta(x-x_0) = u(x_0)\delta(x-x_0)$
shifting	$u(x) * \delta(x-x_0) = u(x-x_0)$
summation	$\delta(x-x_0) * \delta(x-x_1) = \delta\left(x-(x_0+x_1)\right)$
scaling	$\delta(xa) = \frac{1}{\lvert a\rvert}\delta(x)$ for a given constant a

Proprieties Shah distribution

sampling in the time domain	$f\text{Ш}_{\Delta t} = f(\Delta t n)\sum_n \delta(t-n\Delta t)$
periodising in the time domain	$(f * \text{Ш}_T) = \sum_n f(t-nT)$
sampling in the frequency domain	$F(\omega)\text{Ш}_{\Delta\omega} = \Delta\omega\sum_k F(\Delta\omega k)\delta(t-k\Delta\omega)$
periodizing in the frequency domain	$(F * \text{Ш}_\Omega) = \Omega\sum_k F(\omega-k\Omega)$

Quick Fourier Transform

Dirac distribution	$\mathscr{F}[\delta(t-a)](\omega) = e^{-i\omega a}$ $\mathscr{F}^{-1}[\delta(\omega-a)](t) = \frac{1}{2\pi}e^{i\omega a}$
Rectangular function	$\mathscr{F}^{-1}[T\Pi_{\pi/T}](t) = \text{sinc}_T$
Shah function	$\mathscr{F}[\text{Ш}_a](\omega) = \frac{2\pi}{a}\text{Ш}_{\frac{2\pi}{a}}$
Shah function time domain	$\mathscr{F}[\text{Ш}_{\Delta t}](\omega) = \text{Ш}_\Omega,\ \Omega = \frac{2\pi}{\Delta t}$ $\mathscr{F}[\text{Ш}_T](\omega) = \text{Ш}_{\Delta\omega},\ \Delta\omega = \frac{2\pi}{T}$

ABBREVIATIONS

CDF	Cumulative Distribution Function
DFT	Discrete Fourier Transform
ELM	Equivalent Linearization methods
FFT	Fast Fourier Transform
EPSD	Evolutionary Power Spectral Density
ETELM	Evolutionary Tail-Equivalent Linearization Method
ETELS	Evolutionary Tail-Equivalent Linear System
FD	Frequency Domain
FORM	First-Order Reliability Method
FP	Fokker-Planck equation
FRF	Frequency-Response Function
IRF	Impulse-Response Function
IS	Important Sampling
ISD	Important Sampling Density
MCS	Monte Carlo Simulation
MDOF	Multy Degree Of Freedom
MSE	Mean Square Error
PDF	Probability Density Function
PSD	Power Spectral Density
SDOF	Single Degree Of Freedom
TD	Time Domain
TELM	Tail-Equivalent Linearization Method
TELS	Tail-Equivalent Linear System

Chapter 1

Introduction

Safety analysis of structures subjected to stochastic excitations, such as earthquake, wind or wave loading, is a primary goal of structural engineering. In the last few decades, considerable amount of progress has been made in developing mathematical models and computational methods that are able to predict the response of deterministic complex and nonlinear structures under deterministic excitations. In the real world, however, uncertainties in the geometry, material and excitations of structures are present, and they play a key role in determining the accuracy in predicting responses of interest. While in engineering practices that involve control, manufacturing and industrial production uncertainties can be controlled and reduced to a sufficient degree, in most civil facilities this is generally not possible. Therefore, prediction of the structural response under uncertain conditions, either in the structural characteristics or in the input excitations, is a more realistic approach for the civil engineering field. There is, therefore, a need to improve the design flow and to adopt a probabilistic approach that includes the definition of the so-called probabilistic structural analysis (PSA), which defines modes of structural failure and determines their likelihoods.

In recent years, the Pacific Earthquake Engineering Research Center (PEER) has invested a major effort in establishing and adopting the PSA as a vital element of structural analysis and design. The outcome of these efforts is the so called Performance Based Earthquake Engineering (PBEE) . The PBEE is divided into four major tasks: hazard analysis, structural analysis, damage analysis, and decision making. Figure 1.1 shows a flow chart of the PBEE. The first three tasks serve the purpose to create a probabilistic framework as a foundation for risk-based decision making. One approach to solve this part of PBEE is presented in this dissertation. The goal is to obtain the probability distribution of the response of interest. These include the first-passage probability for a selected response, or the conditional probability with respect to a given measure of intensity of the excitation, commonly known as fragility curve.

An important aspect of evaluating the failure probability and fragility curves is to correctly estimate the tail of the distributions, since that is where failure events for highly reliable systems are located. Moreover, failure events inevitably involve nonlinear response.

Therefore, there are two overriding elements in the PSA for PBEE:

- Accurate modeling of the **nonlinear response** of structures.
- Accurate estimation of the **tail distribution** of the nonlinear response.

The failure probability of large linear and nonlinear structures is usually evaluated by methods of structural reliability for static and pseudo-dynamic loads [30], and by linear and nonlinear random vibration analysis for dynamic problems with stochastic inputs [68, 77, 78]. Our work falls in the second category and is driven by the aforementioned two overriding elements.

Current methods available for nonlinear random vibration analysis can be divided into three classifications:

- **Classical methods**: Perturbation methods, Fokker-Plank equation, stochastic averaging, moment closure, etc.
- **Simulation methods**: Monte Carlo Simulation (MCS), Importance Sampling (IS), Markov Chain Monte Carlo (MCMC), Latin Hypercube Sampling (LHS), Orthogonal plane sampling, etc.
- **Linearization methods:** Classical Equivalent Linearization Method (ELM), Tail-Equivalent Linearization Method (TELM).

The classical methods are important and elegant approaches, but are limited to specialized systems or excitations. The broad family of simulation methods has no theoretical limits;

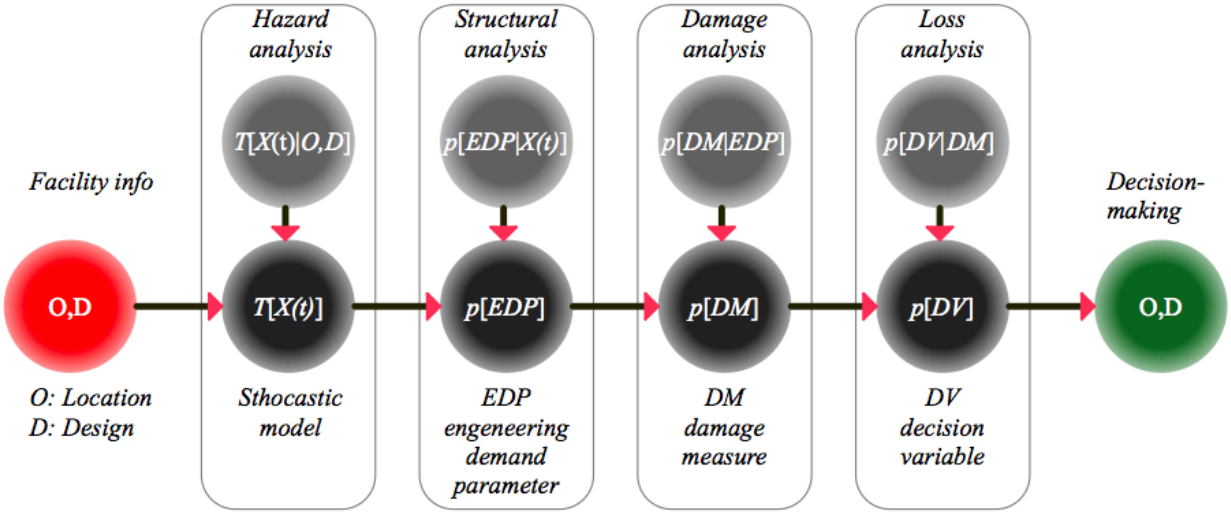

Figure 1.1: Flow chart of PBEE

however, some of these methods are computationally inefficient for high reliability problems (such as most civil structures). The final class of methods offers an efficient and fairly accurate estimation of the response distribution for many structural problems. However, the standard ELM, which is a parametric method, is designed to accurately estimate the first- and the second-moments of the response distribution. Since the method is not meant for estimating the tail of the distribution, it is not accurate for computing the probability of failure for highly reliable systems. The TELM is a recent linearization method based on the first-order reliability method (FORM) developed by Fujimura and Der Kiureghian [37, 38, 55]. It aims at providing a good estimation of the tail probability of the nonlinear response for this class of problems. Taking the pioneering work of Fujimura and Der Kiureghian as a starting point, this dissertation aims at formalizing and generalizing the TELM as a robust mathematical approach to estimate the tail probability of the response of general nonlinear systems subjected to stochastic excitations.

1.1 Nonlinear random vibration in the scientific literature

Classical methods

Among the classical methods, *perturbation methods* are probably the first ones to be used in nonlinear random vibration. First introduced in this field by Crandall [27], these are fairly general methods to solve deterministic and/or stochastic nonlinear mechanics problems. Perturbation methods are based on power series expansion of the solution, where only "significant" terms are retained. The differential equations are formulated for each term of the expansion. The procedure is rather straightforward. However, due to the nature of the formulation, the expansion terms rapidly increase in complexity when high-order terms are considered. In addition, these methods are usually limited to lightly nonlinear systems. A comprehensive overview of the topic can be found in [76].

The *Fokker-Planck equation* was derived in the context of statistical mechanics [12, 13]; it is a partial differential equation that describes the evolution in time of the probability density function of a non-stationary process. Several texts on stochastic processes describe solutions of the FP equations; noteworthy are [39, 66, 68, 78, 87, 101]. The solution of this equation provides the exact probabilistic structure of the response at all times. However, solutions for nonlinear problems are scarce and typically are limited to situations where the response process is Markovian. Moreover, the required computational effort rapidly increases with the number of degrees of freedom of the structure.

Moment of closure is an approximate method for estimating the statistical moments of a stochastic process [25, 26, 49, 52, 61, 64]. The method is based on the derivation of the equations for statistical moment of the response from the FP equation. In general, the statistical moments are governed by an infinite number of coupled equations; a closure

technique is used to obtain an approximate solution in terms of a finite set of moments. The accuracy of the solution depends on the order of closure. However, this comes at a price because the method turns out to be impractical for high orders, which are needed for highly nonlinear systems.

The *stochastic averaging* method was first introduced by Stratonovich in solving nonlinear oscillations of electrical systems under noisy excitations, while a robust mathematical foundation has been established in [54, 79, 80]. In the field of stochastic dynamics most of the works on this topic has been done by Roberts, Spanos and Zhu [89, 113, 114]. Essentially, the method approximates the response vector with a diffusive Markov vector with the probability density function governed by the FP equation. The method is designed to calculate the coefficient function in the FP equation by eliminating the effect of periodic terms by stochastic averaging. The method is applicable to a wide variety of single degree of freedom systems, but it finds its limitation when applied to multi-degree-of-freedom (MDOF) systems.

Simulations methods

Due to its simplicity, *Monte Carlo Simulations* is the most frequently applied method to solve random vibration problems [96, 98]. There are no theoretical limitations owing to the nature of the approach; however, for the crude version of MCS, there are computational limitations when the tail of the response distribution is of interest. For highly reliable systems, where the interest is in the far tail of the distribution, many alternative simulation methods have been developed in the recent years. The two principal categories are the IS and MCMC methods.

The *importance sampling* is a rather straightforward method. The inefficiency of the crude MCS for low probability events lies in the fact that only few samples fall in the failure domain. To avoid this problem, an importance sampling distribution is used in order to generate more samples in the failure domain, making the method more efficient [11, 31, 33, 48, 71, 72, 73, 83]. However, particular care must be taken in using this method in high dimensions [5, 53, 59, 58, 59, 93], such as in conjunction with discretized stochastic processes. For Gaussian processes in high dimensional spaces, a suitable importance sampling distribution is formulated by Au and Beck [4]. This method is adapted in this dissertation to estimate the first-passage probability of the equivalent linear system obtained by the TELM.

The *Markov Chain Monte Carlo* methods are a collection of schemes for sampling from complex probability densities by constructing a Markov chain that has the desired distribution in its equilibrium state [43, 107]. There are different algorithms in this class. The most widely used ones, which can be considered as the parents of all other schemes, are the Metropolis-Hasting algorithm [74, 75] and the Gibbs sampling algorithm [42]. Initially developed outside the field of statistics, these methods greatly impacted statistical analysis in the early 90's [41], especially in Bayesian computational statistics. In particular, the Metropolis-Hasting algorithm was developed in physics in an attempt to calculate complex integrals as

the expected value of random variables by sampling from their distributions. Gibbs sampling found its roots in image processing. Good references for MCMC methods [90, 102]. MCMC methods are suitable for high-dimensional problems and can be efficiently used to sample in rare failure domains. For this class of problems, the subset simulation method proposed by Au and Beck [3, 6, 7] represents one the most popular simulation method to solve high reliability problems under stochastic excitations.

Linearization methods

The *equivalent linearization method* is the most popular method used in nonlinear stochastic dynamics. Its popularity is based on its simplicity and its wide range of applicability. In particular, its complexity does not increase for MDOF systems and thus it is suitable for civil structures. The general idea behind the method is to replace the nonlinear system by a parameterized equivalent linear system. The method possibly finds its roots in the deterministic linearization method introduced in mechanics by Krylov and Bogolubov [63]. The most appealing feature of every linearization method is that, once the linear system is obtained, all the linear theory can be effortlessly applied. In the original versions of the ELM [2, 8, 23, 50, 51, 60, 88, 108], the linear system is identified by minimizing the mean-square error of the response of interest between the linear and the nonlinear systems, thereby determining the linear system parameters. An alternative version, based on energy minimization, is given in [32]. In recent years, the method has been used in conjunction with the Karhune-Loeve expansion to solve nonlinear stochastic dynamic problems for significantly large finite element models [81, 91]. Usually, the response is assumed to be Gaussian and, due to the nature of the minimization, the method provides a rather good estimate of the variance of the nonlinear response. The major drawback of the ELM is its lack of accuracy in estimating the tail of the distribution, particularly when the system experiences strongly nonlinear behavior. The major reason underlying this problem is the Gaussian assumption adopted by the method. While this assumption is doing a fair job in estimating the variance, it completely loses its validity for tail probabilities. To overcome this issue, Casciati *et al.* [22] introduced an alternative linearization based on the mean level-crossing rate. The linear system is identified by equating the mean level-crossing rates of the equivalent linear system and the nonlinear system. While this approach can be accurate in estimating the tail distribution, it becomes significantly complex for MDOF systems and for certain nonlinear systems. This is due to the fact that the approach requires knowledge of the joint probability distribution of the response and its derivative, which in most nonlinear systems is difficult to obtain.

The *tail-equivalent linearization method* is a recent method that aims at providing an adequate estimation of the tail distribution of the response of a nonlinear system under stochastic input. The method was introduced by Fujimura and Der Kiureghian [37, 38, 55]. The work found its genesis in the earlier works of Li and Der Kiureghian [65], Franchin [36] and Koo *et al.* in applying the FORM to solve nonlinear random vibration problems. The

solution by this time-invariant structural reliability method requires discretization of the input in terms of a finite set of random variables, and the definition of the failure event as a limit-state function. The limit-state function is defined by the difference between the critical response threshold level and the nonlinear system response, which is an implicit function of the random variables defining the discretized input excitation. Negative values of the limit-state function identify the failure domain and zero values define the frontier of the failure domain, the limit-state surface. The limit-state surface is generally nonlinear for nonlinear systems; the tail probability is then obtained by FORM approximation. In this method, the limit state-surface is approximated by an hyperplane tangent to the point belonging to the limit-state surface and having the highest probability density value. This point, known as the "design point" in structural reliability theory, contains important physical information regarding the behavior of the nonlinear system. Departing from these early works, Fujimura and Der Kiureghian developed the TELM and formalized the concept of the tail-equivalent linear System (TELS). Briefly stated, the TELS is defined by the hyperplane introduced by the linearization at the design point and is identified numerically in terms of its Impulse-Response Function (IRF) or Frequency-Response Function (FRF). The main objective of the method is to estimate the statistics of responses of interest for highly reliable nonlinear structural system in the context of PBEE. The original method was developed in the time domain for inelastic systems and, in 2008, was extended in frequency domain by Garrè and Der Kiureghian in the context of marine structures for a nonlinear type of loading [40]. Chapter 2 of this work is dedicated to a review of the method both in the original time domain and in the frequency domain; for the latter approach, a generalization for inelastic system is presented.

1.2 Objective

The goal of this dissertation is to extend the original work of Fujimura and Der Kiureghian to solve different problems, such as nonlinear systems subjected multi-component excitations and non-stationary excitations. The second major objective is to provide a deeper mathematical foundation that leads to an improvement in the efficiency of the method. The latter goal is achieved by using a general representation of a Gaussian process as a weighted random sum of basis functions. The basis functions are time dependent, and the coefficients are Gaussian random variables. The split between the time-dependence carried by the basis function and the randomness carried by the coefficient of the series is a requirement in order to apply time-invariant reliability methods. It turns out that the choice of the basis functions determines the nature of the discretization. In particular, if the time-domain basis function are chosen to be equally spaced delta-Dirac functions, the obtained discretization is in the time domain. If harmonic functions, i.e. sine and cosine, are chosen as the basis functions, the discretization is in the frequency domain. In this dissertation, we show that other basis functions can be used to represent Gaussian inputs and, notably, we explore the convenience of using the sinc functions. It is found that the discretization is especially useful

in solving nonlinear softening systems, since it provides a remarkable reduction in the number of random variables needed to represent the input excitation. The analysis also indicates that the efficiency of TELM depends on the total number of random variables used, and, consequently, the use of sinc basis functions becomes highly effective for softening systems.

After introducing the general representation of the Gaussian stochastic input, we analyze the case of a nonlinear system under multi-component stochastic excitations. It turns out that the extension of TELM can be achieved quite straightforwardly by introducing an augmented standard normal space and by solving the TELM analysis in this new space.

We finally tackle the challenging task of solving the nonlinear system under non-stationary excitation. We make use of concepts from evolutionary theory proposed by Priestley [82] to introduce an evolutionary tail-equivalent System (ETELM). Once the ETELM is identified, we use the Au-Beck importance sampling method [4] to estimate the first-passage probability of the nonlinear system under non-stationary input. The method proves to be fairly accurate and its power lies in its computational efficiency. This last application is best applicable in the context of PBEE.

1.3 Organization of the dissertation

The goal of this work is to provide the foundation for an in-depth understanding and further development of the tail-linearization method to solve nonlinear random vibration problems. A modern and deep understanding of the subject requires some advanced mathematical formality, as presented in Chapters 3 and Chapter 4. This is not done to make the underlying concepts more difficult to understand or more esoteric, but because once the basic mathematical formality is absorbed, the understanding of the subject becomes deeper and more concise and neat. For those who love mathematics and want much more than that presented here, we give references and hope to share their passion to further improve and develop this subject. Keeping in mind that this work lies on a bridge between the two communities of engineers and mathematicians, we start our journey with a review of the basics of TELM analysis, then go into more mathematical treatments in the following chapter, which serves as a basis in defining the general representation of Gaussian processes. We finally dedicate the last two chapters to the extension of TELM to multi-component analysis and to non-stationary excitations, respectively. Specifically, after this introductory chapter, the contents of the dissertation are as follows:

Chapter 2 reviews the current state-of-the-art of TELM analysis. The first section describes the original work of K. Fujimura and A. Der Kiureghian in the time domain [37, 38], while the second section describes the extension of TELM in the frequency domain by L. Garrè and A. Der Kiureghian [40]. The last section compares results obtained by the two methods for an example hysteretic oscillator.

Chapter 3 introduces the concept of a band-limited function, which is the building block for defining stationary band-limited stochastic processes. We explore how we can represent a band-limited function as a weighted series of orthogonal basis functions through the

Whittaker-Shannon interpolation formula [70]. We assume that the reader is not familiar with these concepts so all necessary proofs are presented.

Chapter 4 considers a band-limited function as a realization of an underling stochastic process; we explore the benefit of TELM analysis with such a representation. Issues such as approximation errors and convergence are explored in detail. Part of this work has been published in [17].

Chapter 5 extends the TELM analysis for multi-component excitations. The solution is obtained by introducing an augmented standard normal space. The method is illustrated by investigating the response of an inelastic eccentric structure subjected to bi-directional seismic input. Part of this work has been published in [18].

Chapter 6 is dedicated to non-stationary stochastic processes, in particular to the broad family of modulated stochastic processes. We introduce concepts such as temporal and spectral non-stationarity, modulating function and evolutionary power spectral density. We then introduce the concept of the ETELS and apply the Au-Beck algorithm to approximately solve the first-passage probability of the response of the nonlinear system. Example applications showing the evolutionary behavior of a nonlinear system demonstrate the methodology. Part of this work has been published in [19].

Chapter 7 provides a summary of the dissertation and the major findings of the study. It also discusses the limitations and drawbacks of TELM, of which the user must be aware of when applying this linearization method.

Chapter 2

The state of art of TELM

2.1 Introduction: TELM at a glance

This chapter reviews and revisits the current state-of-the-art of the tail-equivalent linearization method, TELM. TELM is a new linearization method for nonlinear stochastic dynamic analysis introduced by Fujimura and Der Kiureghian [37, 38, 55]. It makes use of the time-invariant first-order reliability method (FORM) to accurately estimate the tail of the distribution of the response of a nonlinear system that is subjected to a stochastic input.

Briefly stated, in TELM the input process is discretized and represented by a set of standard normal random variables. Each response threshold defines a limit state surface in the space of these variables with the "design point" being the point on the surface that is nearest to the origin. Linearization of the limit-state surface at this point uniquely and non-parametrically defines a linear system, denoted as the tail-equivalent linear system, TELS. The tail probability of the response of the TELS for the specified threshold is equal to the first-order approximation of the tail probability of the nonlinear system response for the same threshold.

Once the TELS is defined for a specific response threshold of the nonlinear system, methods of linear random vibration analysis are used to compute various response statistics of interest, such as the mean crossing rate and the tail probabilities of local and extreme peaks. The method has been developed for application in both time, [37, 38, 55], and frequency domains, [40], and it has been applied for inelastic structures as well as structures experiencing geometric nonlinearities. The first section in this chapter reviews the time-domain formulation, the second section reviews the frequency-domain formulation, and the third section shows a numerical example, where results from the two formulations are compared with each other and with results obtained from Monte Carlo Simulation (MCS) analysis.

2.2 TELM in the time domain

Discrete representation of the stochastic excitation

The stochastic excitation in TELM analysis is represented by a linear combination of basis functions, $\boldsymbol{s}(t)$, with standard normal independent random coefficients, $\boldsymbol{u}$:

$$F(t) = \boldsymbol{s}(t)\boldsymbol{u}, \tag{2.1}$$

where

$$\boldsymbol{s}(t) = [s_1(t), \ldots, s_N(t)], \tag{2.2}$$

and

$$\boldsymbol{u} = [u_1, \ldots, u_N]^\intercal. \tag{2.3}$$

The vector $\boldsymbol{s}(t)$ is deterministic and depends on the covariance structure of the excitation process. Time-domain TELM uses a filtered white-noise representation of the input excitation [29]. Following this formulation, the excitation is defined as

$$F(t) = [\eta(t) * W(t)]U(t) = \int_0^t \eta(t-\tau)W(t)d\tau, \tag{2.4}$$

where $*$ denotes convolution, $U(t)$ is the unit step function, $W(t)$ is a white-noise process and $\eta(t)$ is the impulse-response function, IRF, of a stable linear filter. Implementation of (2.4) in TELM requires discretization of the time axis. For a selected time step Δt and initial time $t_0 = 0$, we approximate the white noise $W(t)$ with the rectangular wave process

$$\hat{W}(t) = \frac{1}{\Delta t}\int_{t_{n-1}}^{t_n} W(\tau)d\tau, \quad t_{n-1} < t \leq t_n \;\; n \in [1, \ldots, N]. \tag{2.5}$$

This define a square-wave process, where the wave amplitudes $\hat{w}_n = \hat{W}(t),\ t_{n-1} < t \leq t_n,\ n \in [1, \ldots, N]$, are statistically independent normal random variables with zero means and variance dictated by the band limit $\bar{\omega} = \pi/\Delta t$ [rad/s] of the discretized process, i.e. $\sigma^2 = 2\pi S_0/\Delta t$, where S_0 denotes the spectral density of the white noise. In the original formulation of TELM [37, 38], the discretization time step is dictated by the integration step of the numerical scheme adopted to solve the differential equation governing the nonlinear system response. When dealing with highly nonlinear problems, the integration time step must be taken sufficiently small to guarantee convergence. It follows that in the original TELM we do not have control over the band limit of the process, which is controlled by the integration step required by the numerical solver scheme.

Defining the standard normal random variables $u_n = \hat{w}_n/\sigma$, (2.5) can be written in the form

$$\hat{W}(t) = \boldsymbol{s}(t)\boldsymbol{u} \tag{2.6}$$

$$s_n(t) = \sigma, \quad t_{n-1} < t < t_n$$
$$= 0 \;\text{ otherwise.} \tag{2.7}$$

The discrete version of (2.4), $\hat{F}(t)$, is obtained by replacing $W(t)$ with $\hat{W}(t)$

$$\begin{aligned} \hat{F}(t) &= [\eta(t) * \hat{W}(t)]U(t) = \boldsymbol{s}(t)\boldsymbol{u} && (2.8) \\ s_n(t) &= \sigma \int_{t_{n-1}}^{t_n} \eta(t-\tau)d\tau \quad t_{n-1} < t \leq t_n,\ n \in [1,\ldots,N] && (2.9) \\ &= 0 \quad t \leq t_{n-1}. \end{aligned}$$

The above formulation represents a Gaussian process with zero mean and variance function $\sigma^2(t) = |\boldsymbol{s}(t)|^2$. This discrete representation of a Gaussian process is not the only one available in literature, but it is the one that is employed in TELM because it has the advantage of splitting the time dependence of the process, carried by the set of basis functions $\boldsymbol{s}(t)$, and the randomness of process carried by the set of random variables $\boldsymbol{u}$. In Chapters 3 and 4, we formalize and extend this representation with the aim of making it more efficient for TELM analysis.

Definition of TELS and application of TELM

The governing equation of a stable system subject to stochastic input can be written as

$$L[X(t)] = F(t), \tag{2.10}$$

where $L[\cdot]$ is a differential operator. If the system is linear, the response can be obtained by convolving its IRF, $h(t)$, with the input excitation:

$$X(t) = [h(t) * F(t)]U(t). \tag{2.11}$$

If the input is discretized according to (2.8) we can write:

$$\begin{aligned} X(t) &= [h(t) * \hat{F}(t)]U(t), && (2.12) \\ &= \sum_{n=1}^{N} \int_0^t h(t-\tau)s_n(\tau)d\tau u_n = \boldsymbol{a}(t)\boldsymbol{u}, && (2.13) \end{aligned}$$

with

$$a_n(t) = \int_0^t h(t-\tau)s_n(\tau)d\tau. \tag{2.14}$$

If the system is nonlinear, a numerical solution can be used to compute the response $X(t)$. Thus, given the representation of the input excitation in (2.1), the response $X(t)$ is either an implicit or an explicit function of the standard normal variables $\boldsymbol{u}$, i.e., $X(t) = X(t, \boldsymbol{u})$.

Given a response threshold of interest x, at a specific time $t_x = t_N$, the tail probability is defined as $Pr[x \leq X(t_x, \boldsymbol{u})]$. Reliability theory is used to compute this probability by defining a limit-state surface $g(x, t_x, \boldsymbol{u}) = x - X(t_x, \boldsymbol{u})$ and rewriting the probability statement as

$Pr[x \leq X(t_x, \boldsymbol{u})]$=$Pr[g(x, t_x, \boldsymbol{u}) \leq 0]$. In particular, TELM employs the first-order reliability method, FORM, in which a first-order approximation of the probability is computed by defining, in the standard normal space, the so-called design point $\boldsymbol{u}^*$, which belongs to the limit state surface $g(x, t_x, \boldsymbol{u}) = 0$ and has minimum distance from the origin. This distance is known as the reliability index. The significance of this point is described in [57]. If the system is linear, the limit state surface is an hyperplane with gradient $\boldsymbol{a}(t)$ and the design point and the reliability index are given in closed form as

$$\boldsymbol{u}^*(x, t_x) = \frac{x}{||\boldsymbol{a}(t_x)||} \frac{\boldsymbol{a}(t_x)^\intercal}{||\boldsymbol{a}(t_x)||}, \tag{2.15}$$

$$\beta(x, t_x) = \frac{x}{||\boldsymbol{a}(t_x)||}. \tag{2.16}$$

Moreover the gradient $\boldsymbol{a}(t_x)$ can be written explicitly in terms of the given design point [38],

$$\boldsymbol{a}(t_x) = \frac{x}{||\boldsymbol{u}^*(x, t_x)||} \frac{\boldsymbol{u}^*(x, t_x)^\intercal}{||\boldsymbol{u}^*(x, t_x)||}. \tag{2.17}$$

In this case, the tail probability has the simple solution

$$Pr[g(x, t_x, \boldsymbol{u}) < 0] = \Phi[-\beta(x, t_x)], \tag{2.18}$$

where $\Phi[\cdot]$ is the standard normal cumulative probability function.

In the more general nonlinear case, first the design point $\boldsymbol{u}^*$ is computed by solving the constrained optimization problem

$$\boldsymbol{u}^* = \text{argmin}\{||\boldsymbol{u}|| \ | g(x, t_x, \boldsymbol{u}) = 0\}. \tag{2.19}$$

Then, the nonlinear limit-state function is expanded in Taylor series at the design point:

$$g(x, t_x, \boldsymbol{u}) = x - [X(t_x, \boldsymbol{u}^*) + \nabla_{\boldsymbol{u}} X(t_x, \boldsymbol{u}^*) \cdot (\boldsymbol{u} - \boldsymbol{u}^*) + \text{h.o.t.}], \tag{2.20}$$

$$= -\nabla_{\boldsymbol{u}} X(t_x, \boldsymbol{u}^*) \cdot (\boldsymbol{u} - \boldsymbol{u}^*) + \text{h.o.t.} \tag{2.21}$$

The first-order approximation of $P[g(x, t_x, \boldsymbol{u}) < 0]$ is obtained by keeping the linear terms in (2.21) resulting in

$$P[g(x, t_x, \boldsymbol{u}) \leq 0] \simeq \Phi[-\beta(x, t_x)], \tag{2.22}$$

where the reliability index of the linearized system is given by

$$\beta(x, t_x) = ||\boldsymbol{u}^*(x, t_x)|| = \boldsymbol{\alpha}(x, t_x)\boldsymbol{u}^*(x, t_x), \tag{2.23}$$

with α being the negative normalized gradient vector of the limit-state function

$$\boldsymbol{\alpha}(x, t_x) = -\frac{\nabla_{\boldsymbol{u}} g(x, t_X, \boldsymbol{u}^*)}{||\nabla_{\boldsymbol{u}} g(x, t_X, \boldsymbol{u}^*)||} = \frac{\nabla_{\boldsymbol{u}} X(t_X, \boldsymbol{u}^*)}{||\nabla_{\boldsymbol{u}} X(t_X, \boldsymbol{u}^*)||}, \tag{2.24}$$

which is identical to the normalized gradient vector of the nonlinear response. This corresponds to approximating the limit-state surface by its tangent hyperplane at the design point. This hyperplane, which is described by $\beta(x,t_x) - \boldsymbol{\alpha}(x,t_x)\boldsymbol{u} = 0$ or equivalently $x - \nabla_{\boldsymbol{u}} X(t_X, \boldsymbol{u}^*)\boldsymbol{u} = 0$, defines a linear system, which has the same tail probability as the first-order approximation of the tail probability of the nonlinear system.

At this point we have all the elements to give a formal definition of the TELS.

Definition 1. *Given the response of a nonlinear system, X(t), under the stochastic input excitation, F(t), and given a threshold x and a fixed time point t_x the **TELS** is the linear system that has the same tail probability as the first-order approximation of the tail probability of the nonlinear system.*

Figure 2.1 illustrates the geometric concept underlying the definition of the TELS.

The above definition is general, but in this context we have to specify that it is restricted for inputs represented by (2.1) and thus the TELS is defined in the standard normal space. Therefore, the FORM approximation of the tail probability of the non-linear system response coincides with the tail probability of the response of the TELS.

For a given pair of input and output processes, a linear system is characterized by its IRF. In TELM analysis this linear system is nonparametric. A nonparametric model is the opposite of what one might suppose from its name: not a model without parameters, but a model that cannot be parameterized by a finite dimensional parameter space. Videlicet, we may consider a nonparametric model as one having an infinite number of parameters [92]. Given the discrete excitation $\hat{F}(t)$ and the gradient vector $\boldsymbol{a}(t_x)$, the design point $\boldsymbol{u}^*(x,t_n)$ uniquely defines the IRF independently of the scaling of the excitation. This statement is

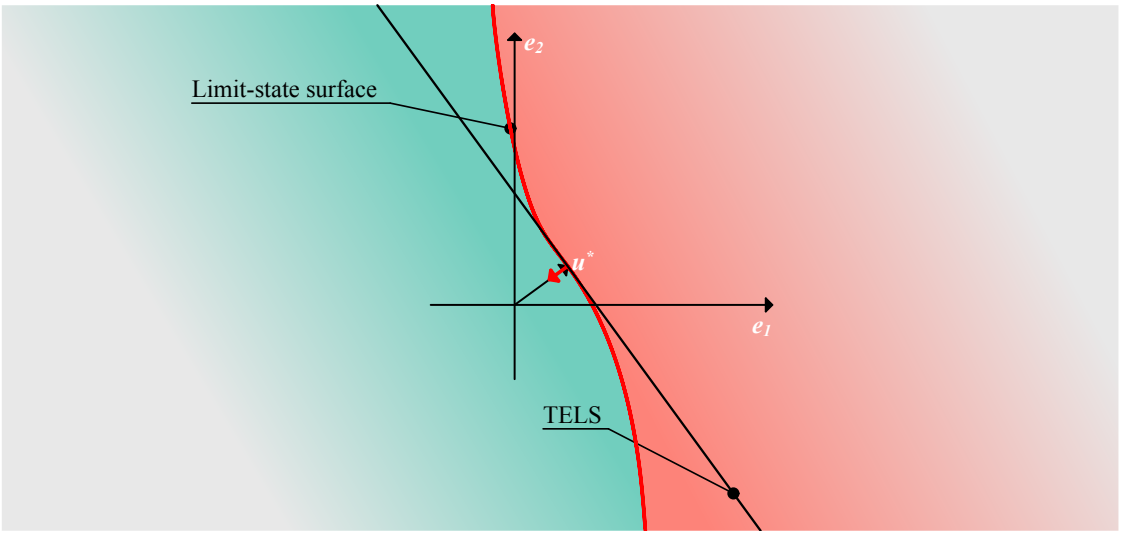

Figure 2.1: TELS of the non linear response for a given threshold x and point in time t_x

verified by considering the discrete version of the basic convolution formula (2.14):

$$\sum_{m=1}^{M} h(t_x - t_m) s_n(t_m) \Delta t = a_n(t_x),\ n \in [1, \ldots, N], \tag{2.25}$$

which in matrix form can be written as

$$\boldsymbol{S}\boldsymbol{h} = \boldsymbol{a}, \tag{2.26}$$

with

$$\boldsymbol{S} = \Delta t \begin{bmatrix} s_1(t_1) & \ldots & s_1(t_M) \\ \vdots & s_n(t_m) & \vdots \\ 0 & \ldots & s_N(t_M) \end{bmatrix},\ \boldsymbol{h} = \begin{bmatrix} h(t_M - t_1) \\ \vdots \\ h(t_M - t_M) \end{bmatrix},\ \boldsymbol{a} = \begin{bmatrix} a_1(t_N) \\ \vdots \\ a_N(t_N) \end{bmatrix}, \tag{2.27}$$

with $t_M \equiv t_x$ and $M \equiv N$. The IRF is determined in a discrete form by solving for $\boldsymbol{h}$ in (2.25). The matrix $\boldsymbol{S}$ in general is triangular because of the form of (2.9), and in the special case of a white-noise excitation it is diagonal. In this version of TELM, the resolution of the IRF is determined by the time interval Δt used in the discretization of the input excitation and numerical integration of the response. Once the IRF is determined, the frequency-response function, FRF, of the TELS is computed as the discrete Fourier transform of the IRF.

2.3 TELM in frequency domain

Discrete representation of the stochastic excitation

An alternative to the above formulation is to perform the discretization in the frequency domain. This formulation is particularly useful when the input and output processes are both stationary. Following the original work of Rice [86] and later extensions by Shinozuka [95], [97] and Deodatis [97], the basis functions $\boldsymbol{s}(t)$ in (2.1) are selected as the sine and cosine functions. The representation is the canonical Fourier series with random coefficients. For a selected frequency discretization step $\Delta\omega$, and given $[\omega_1, ..., \omega_K]$ with $\omega_k = \omega_{k-1} + \Delta\omega$, $k \in [1, \ldots, K]$, (2.8) is written as:

$$\hat{F}(t) = \sum_{k=1}^{K} \sigma_k [u_k \sin(\omega_k t) + u_{K+k} \cos(\omega_k t)] = \boldsymbol{s}(t)\boldsymbol{u}, \tag{2.28}$$

$$\boldsymbol{s}(t) = [s_1(t), ..., s_{2K}(t)], \tag{2.29}$$

$$\boldsymbol{u}(t) = [u_1, ..., u_{2K}]^{\intercal}, \tag{2.30}$$

$$s_k(t) = \sigma_k \sin(\omega_k t),\ k \in [1 \ldots K], \tag{2.31}$$

$$s_k(t) = \sigma_k \cos(\omega_k t),\ k \in [K+1 \ldots 2K]. \tag{2.32}$$

The discretization is located in the frequency domain because the spectrum of the Fourier series is a weighted train of equally spaced pulses along the frequency axis. We must select the frequency

sampling rate $\Delta\omega$ and the band limit $K\Delta\omega$. However, one has to be careful about the periodicity arising by the use of the Fourier series. In this case the period of the process is given by $T = 2\pi/\Delta\omega$. This period should be shorter than the duration of the excitation that is considered in the TELM analysis. The above discretization was first employed in TELM analysis by [40] for a marine application involving nonlinear loading and elastic material. In this study we use this formulation while considering inelasticity in the material behavior.

Determination of the TELS

The governing equation of a stable linear system in frequency domain can be written as

$$\begin{aligned} \mathscr{F}\{L[X(t)]\}(\omega) &= \mathscr{F}\{F(t)\}(\omega) && (2.33)\\ \mathscr{L}[\bar{X}(\omega)] &= \bar{F}(\omega), && (2.34) \end{aligned}$$

where $\bar{X}(\omega)$ and $\bar{F}(\omega)$ are the Fourier transforms of the response and the input excitation respectively. The steady-state response is obtained as:

$$\begin{aligned} \bar{X}(\omega) &= \mathscr{F}\{[h(t)F(t)]\}(\omega) && (2.35)\\ &= H(\omega)\bar{F}(\omega), && (2.36) \end{aligned}$$

where $H(\omega) = \mathscr{F}\{h(t)\}(\omega)$ is the FRF of the system. Given the stochastic representation in (2.28), using (2.36), the steady-state response of the linear system is obtained in the time domain as

$$\begin{aligned} X(t,\boldsymbol{u}) &= \mathscr{F}^{-1}\{\bar{X}(\omega)\}(t) && (2.37)\\ &= \sum_{k=0}^{K} \sigma_k |H(\omega_k)| [u_k \sin(\omega_k t - \varphi_k) + u_{K+k}\cos(\omega_k t - \varphi_k)] && (2.38)\\ &= \boldsymbol{a}(t)\boldsymbol{u}, && (2.39) \end{aligned}$$

where $\boldsymbol{a}(t)$ for a specific time t_x is written as

$$\begin{aligned} \boldsymbol{a}(t_x) &= [a_1(t_x), ..., a_K(t_x); a_{K+1}(t_x), ..., a_{2K}(t_x)], && (2.40)\\ a_k(t_x) &= |H(\omega_k)| \sin(\omega_k t_x - \varphi_k),\ k \in [1 \dots K], && (2.41)\\ a_K(t_x) &= |H(\omega_k)| \cos(\omega_k t_x - \varphi_k),\ k \in [K+1 \dots 2K], && (2.42) \end{aligned}$$

in which $|H(\omega_k)|$ and φ_k respectively represent the modulus and the phase of the FRF of the linear system. [40] have shown that the following relationships between the elements of the gradient vector $\boldsymbol{a}(t_x)$ and the FRF hold:

$$\begin{aligned} |H(\omega_k)| &= \frac{\sqrt{a_k^2 + a_{K+k}^2}}{\sigma_k},\ k \in [1, \dots, K], && (2.43)\\ \varphi_k &= \omega_k t_x - \tan^{-1}\left[\frac{a_k}{a_{K+k}}\right],\ k \in [1, \dots, K]. && (2.44) \end{aligned}$$

Given a general nonlinear system and a stationary stochastic input described by (2.28), the design point $\boldsymbol{u}^*$ for threshold x at time t_x is first determined and the gradient vector of the tangent plane, $\boldsymbol{a}(t_x)$, is computed from (2.17). The latter in conjunction with (2.43) and (2.44) uniquely defines the FRF of the TELS. Once the FRF is determined, methods of linear random vibration are used to compute the statistics of interest for the nonlinear response for the specified threshold x. In analogy with the time-domain formulation where the FRF of the system is determined as the DFT of the IRF, in the frequency-domain formulation the IRF is determined as the inverse DFT of the FRF.

In the next section we explore a numerical example where both formulations are used and their results compared.

2.4 Numerical example

In this section the properties of TELM are numerically investigated by considering a single-degree-of-freedom (SDOF) oscillator with inelastic material behavior. The problem is solved both in frequency and time domains. We use a symmetric Bouc-Wen material model [8, 14, 109] to describe the force-displacement relationship. Other inelastic material models can be used in the formulation. However, there is a fundamental condition for application of TELM: the limit-state function and, therefore, the response of the system must be differentiable with respect to the random variables $\boldsymbol{u}$ at the design point. This guarantees that the limit-state surface has a tangent hyperplane at the design point. It has been proven in [47] that, for an inelastic material, a necessary condition for the differentiability of the response is a smooth transition between material states except for elastic unloading. This condition is satisfied for the Bouc-Wen material model, but in other cases the material model may have to be modified to have smooth transitions.

The equation of an inelastic SDOF oscillator can be written as

$$m\ddot{X}(t) + c\dot{X}(t) + P_{inn}[X(t), \dot{X}(t)] = F(t) \text{ or } -m\ddot{U}_g(t), \tag{2.45}$$

where $P_{inn}[\cdot]$ is the restoring force and the second option on the right-hand side applies when the excitation is specified in terms of base acceleration $\ddot{U}_g(t)$. In the particular case of the hysteretic Bouc-Wen model, (2.45) is written as (see [109])

$$m\ddot{X}(t) + c\dot{X}(t) + k[\alpha X(t) + (1-\alpha)Z(t)] = F(t) \text{ or } -m\ddot{U}_g(t), \tag{2.46}$$

where α is a nonlinearity parameter with $\alpha = 1$ denoting a linear system, and $Z(t)$ follows the hystereris law

$$\dot{Z}(t) = -\gamma|\dot{X}(t)||Z(T)|^{\hat{n}-1}Z(t) - \eta|Z(t)|^{\hat{n}}\dot{X}(t) + A\dot{X}(t), \tag{2.47}$$

in which γ, η, A and $\hat{n}$ are model parameters. The first and computationally most expensive operation in TELM is numerical solution of the design point $\boldsymbol{u}^*$ according to (2.19). Different algorithms are available in the literature and a general review can be found in [67]. Here, we employ the improved HLRF (iHLRF) algorithm, which is a gradient-based method proposed in [112]. The cost of the algorithm is related to the computation of the gradient of the nonlinear limit-state function $g(t_x, x, \boldsymbol{u})$ with respect to $\boldsymbol{u}$, which in the present case is tantamount to computing the

gradient of the nonlinear system response. It follows that the cost of this computation is directly related to the size of vector $\boldsymbol{u}$ or, equivalently, the number of random variables used to describe the input excitation.

For a given threshold x and specified time t_x, the design point is the point with highest probability density among all realizations giving rise to the event $\{x < X(t, \boldsymbol{u})\}$. Thus, $f^*(t) = \boldsymbol{s}(t)\boldsymbol{u}^*$ (or in this example $\ddot{u}_g = \boldsymbol{s}(t)\boldsymbol{u}^*$) is the most likely realization among all realizations of the excitation process that lead to that event. Likewise, the response of the nonlinear system (2.45), $x^*(t) = X(t, \boldsymbol{u}^*)$, under the excitation $f^*(t)$, is the response with the highest likelihood among all possible responses leading to the event of interest. We can consequently give two formal definitions:

Definition 2. *Given a threshold x and a fixed point in time t_x,* ***the design-point excitation****, $f^*(t)$, is the realization with the highest likelihood among all realizations of the excitation process that give rise to the event $\{x < X(t_x, \boldsymbol{u})\}$.*

Definition 3. *Given a threshold x and a fixed point in time t_x,* ***the design-point response****, $x^*(t)$, is the realization of the response with the highest likelihood that leads to the event $\{x < X(t_x, \boldsymbol{u})\}$.*

Figure 2.2 shows the design-point excitation and the design-point response for the system described by (2.46)-(2.47) and the properties listed in Table 2.1. The excitation is white-noise base acceleration with spectral density amplitude $S = 1[\mathrm{m}^2/\mathrm{s}^3]$. The threshold $x = 3\bar{\sigma}$ and time $t_x = 15[\mathrm{s}]$ are considered, where $\bar{\sigma}^2 = \pi S_0 m^2/(ck)$ is the root-mean-square of the linear ($\alpha = 1$) system. The hysteretic relationship between the internal force P^*_{inn} and response $x^*(t)$ at the design points is shown in Figure 2.3. The analysis is carried out using both the time- (TD) and frequency-domain (FD) formulations and the results indicate close agreement of the two. The time/frequency increments used are $\Delta t = 0.01[\mathrm{s}]$ and $\Delta\omega/2\pi = 0.05[\mathrm{Hz}]$, respectively, and the number of random variables used to describe the input excitation are $N = 1500$ and $K = 400$, respectively. The frequency-domain formulation is a lot more efficient since it uses far fewer random variables. Of course this is achieved by using a much smaller cut-off frequency at 10[Hz], versus the cut-off frequency of 50[Hz] in the time-domain approach. The latter is dictated by the small time increment that is necessary for the numerical integration scheme used for computing the nonlinear response.

The core of TELM is in the definition of the TELS, which is completely characterized by its IRF or FRF. The two functions are Fourier transform pairs. In the time-domain approach, the IRF is directly determined by solving the linear system (2.25) and the FRF is computed as the DFT or FFT of the IRF. In the frequency-domain approach, the FRF is determined by solving (2.43) and (2.44) and the IRF is determined as the inverse DFT or the inverse FFT of the FRF. Figure 2.4 shows the IRFs and FRFs computed from time- and frequency-domain approaches for the considered threshold x and time t_x.

The TELS strongly depends on the considered threshold x of the nonlinear response. For each threshold different IRF and FRF are obtained. Figure2.5 shows the IRFs and FRFs obtained for three distinct response thresholds for the example system. It is of interest to examine the behavior of the FRFs as the threshold increases. As expected, the frequency content of the TELS response is migrating from the natural frequency of the system for low-amplitude vibrations to a range of lower frequencies due to the softening of the system; however, there is always a local maximum at the original natural period. The dependence of the TELS on the threshold of interest is a cornerstone of

TELM analysis. It is through this dependence that TELM is able to account for the non-Gaussian distribution of the nonlinear system response.

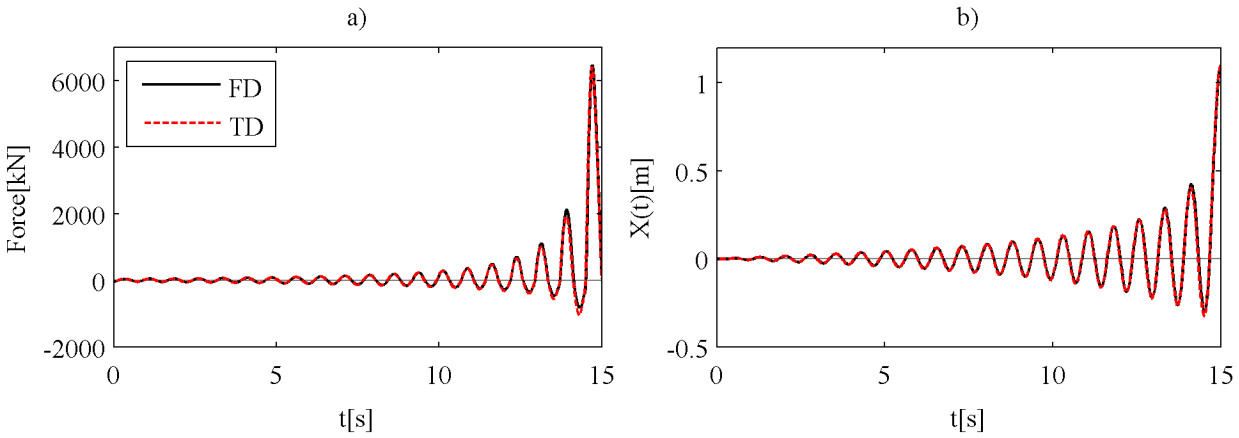

Figure 2.2: a) Design point excitation, b) Design point response for $x = 3\bar{\sigma}$ and $t_x = 15$[s]

Once the TELS is determined in terms of its IRF or FRF for a specified threshold, methods of linear random vibration theory can be used to compute various statistical quantities of interest for the nonlinear response. Below we describe four such quantities.

CDF and PDF of the point-in-time response distribution

The CDF is readily available from FORM analysis at each threshold of interest. With $\beta(x, t_x)$ as the reliability index at threshold x and time t_x, the first-order approximation of the CDF is given by

$$F_{X(t_x)}(x, t_x) \simeq 1 - \Phi[-\beta(x, t_x)]. \tag{2.48}$$

Table 2.1: Structural and Excitation Properties

Bouc-Wen	α	m[kg]	$c\left[\frac{\text{kNs}}{\text{m}}\right]$	k[kN]	$\gamma\left[\frac{1}{\text{m}^{\hat{n}}}\right]$	$\eta\left[\frac{1}{\text{m}^{\hat{n}}}\right]$	$\hat{n}$	A
	0.1	3.00E5	1.00E2	2.10E4	$1/2\bar{\sigma}^{\hat{n}}$	$1/2\bar{\sigma}^{\hat{n}}$	3	1
Excitation		$S_0[\frac{\text{m}^2}{\text{s}^3}]$	t_x[s]	Δt[s]	$\frac{\Delta\omega}{2\pi}$[Hz]	$\frac{\bar{\omega}}{2\pi}$[Hz]	N, K	
time domain		1	15	0.01		50	1500	
frequency domain		1	15		0.05	10	400	

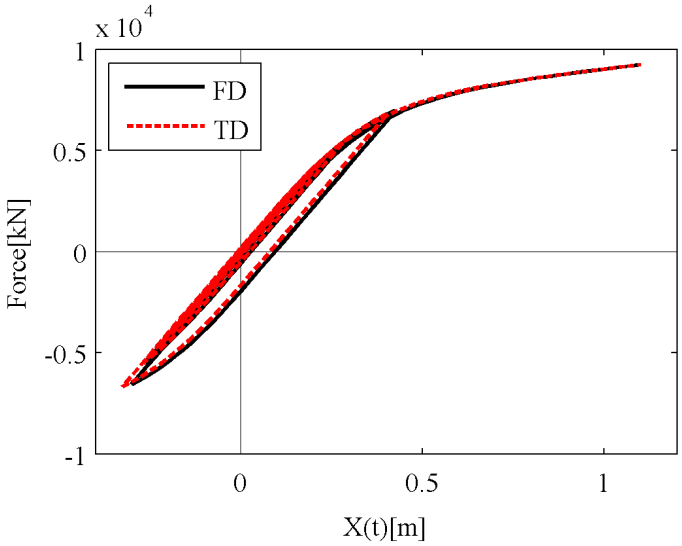

Figure 2.3: Hysteresis loop for design point excitation-response pair

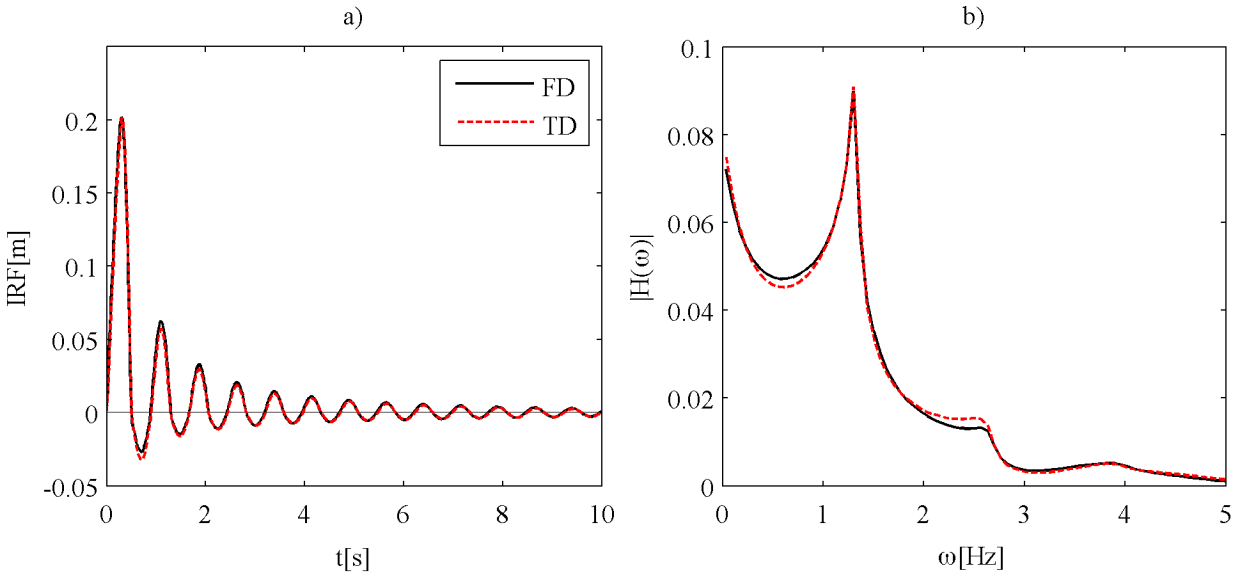

Figure 2.4: a) IRF, b) FRF for $x = 3\bar{\sigma}$ and $t_x = 15$[s]

The PDF is derived by differentiation of (2.48)

$$f_{X(t_x)}(x,t_x) = \phi[-\beta(x,t_x)]\frac{\partial\beta(x,t_x)}{\partial x} = \phi[-\beta(x,t_x)]\frac{1}{||\boldsymbol{a}(t_x)||}, \tag{2.49}$$

which leads to

$$f_{X(t_x)}(x,t_x) \simeq \frac{1}{||\boldsymbol{a}(t_x)||}\phi[-\beta(x,t_x)] = \frac{\beta(x,t_x)}{x}\phi[-\beta(x,t_x)]. \tag{2.50}$$

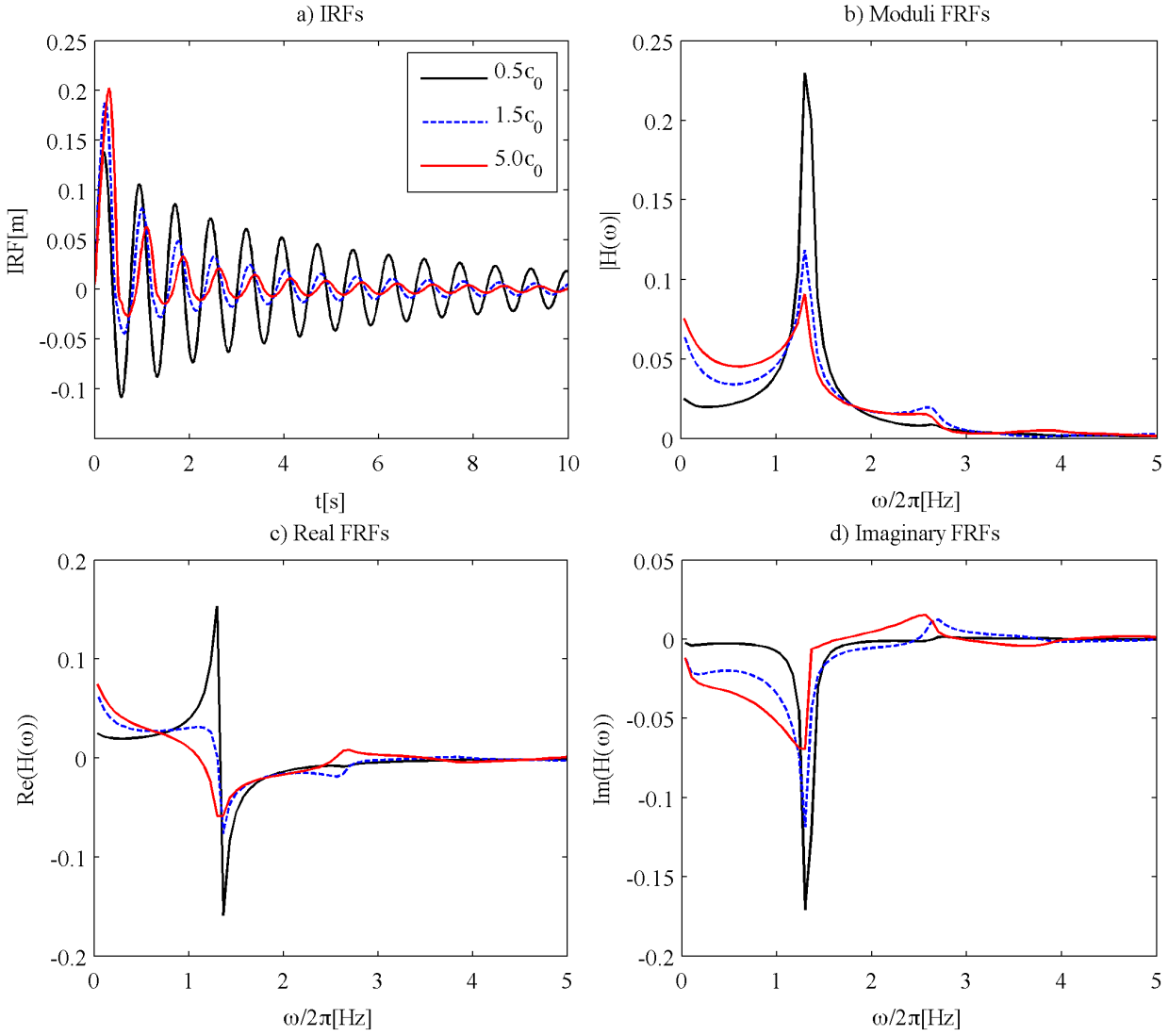

Figure 2.5: IRFs, FRFs of the TELS for 3 different thresholds: $x = 0.5\bar{\sigma}$, $x = 1.5\bar{\sigma}$, $x = 5\bar{\sigma}$

where $\phi[\cdot]$ denotes the standard normal PDF. Figure 2.6 shows the reliability index as a function of the normalized threshold, $x/\bar{\sigma}$, for the example system. The dashed line is for the linear ($\alpha = 1$) case, which has unitary slope because the threshold is normalized. Once the PDF is determined for all the thresholds, the moments of the distribution can be computed by numerical integration. Figure 2.7 comperes the TELM results with a crude MCS with different sample sizes ranging from 1,000 up to 1,000,000 simulations. The I-bars indicate one standard deviation bounds. The figure clearly indicates the non-Gaussian nature of the distribution of the nonlinear response.

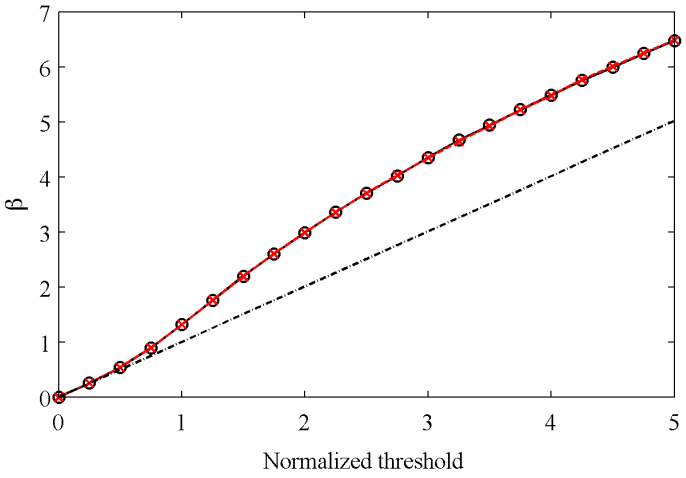

Figure 2.6: Sequence of Reliability index

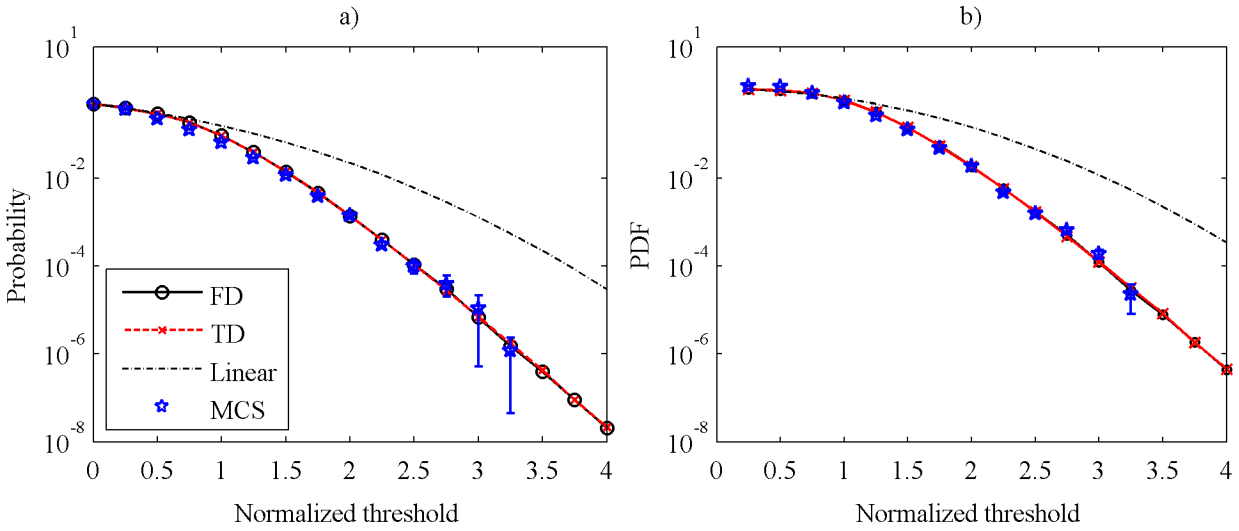

Figure 2.7: a) Complemetary CDF and b) PDF of the response

Mean up-crossing rate

Let $\nu^+(x, t_x)$ denote the mean rate of up-crossing the threshold x at a time t_x. There are different approaches available for computing $\nu^+(x, t_x)$. In this dissertation, we use the linear random vibration theory applied to the TELS. In the present case since t_x is sufficiently large so that the response of the system has reached stationary state, we use the well-known formula for a stationary Gaussian process derived by Rice [86],

$$\nu^+(x) = \frac{1}{2\pi}\sqrt{\frac{\lambda_2(x)}{\lambda_0(x)}}\exp\left(-\frac{1}{2}\frac{x^2}{\lambda_0(x)}\right), \tag{2.51}$$

where λ_m is the m-th spectral moment defined by

$$\lambda_m(x) = 2\int_0^\infty \omega^m |H(\omega, x)|^2 S_{FF}(\omega) d\omega. \tag{2.52}$$

Remark: The reader may be confused from the fact that the formula used is for a Gaussian process, while we know that the nonlinear response is not Gaussian. However, one should note that the non-Gaussianity is with respect of the threshold x. For a given threshold, once linearization is applied and the TELS is determined, the input-output relation is linear. The reader should also note that the spectral moments are functions of the threshold x. This is due to the non-Gaussian nature of the response process.

Figure 2.8 shows $\nu^+(x)$ computed with TELM analysis in the frequency domain compared with the results of a crude MCS analysis.

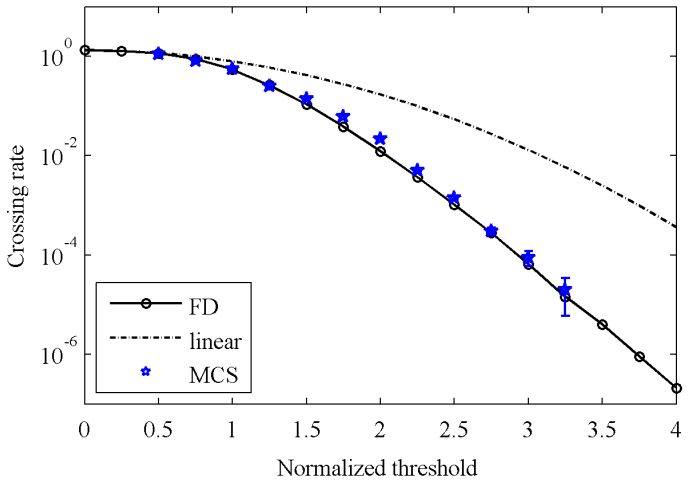

Figure 2.8: Mean up-crossing rate of the nonlinear response.

First-passage probability

In this section the analysis of the first-passage probability, i.e., the probability distribution of the maximum response over an interval of time is presented. Specifically, we are interested in the complementary CDF of the maximum absolute response over a defined interval $(0, T]$, i.e. $P[x < \max_{0<t\leq T} |X(t)|]$. Again, we make use of existing formulas for stationary Gaussian processes. According to the approximate solution proposed by Vanmarcke [105],

$$P\left[x \leq \max_{0<t\leq T} |X(t)|\right] \simeq 1 - \left[1 - \exp\left(-\frac{x^2}{2\lambda_0(x)}\right)\right] \exp[-\eta(x)T], \tag{2.53}$$

where $\eta(x)$ is defined by:

$$\eta(x) = \nu^+(x)\frac{\left[1 - \frac{x}{\lambda_0(x)}\exp\left(-\sqrt{2\pi\left(1 - \frac{\lambda_1^2(x)}{\lambda_2(x)\lambda_0(x)}\right)^{1.2}}\right)\right]}{\left[1 - \exp\left(-\frac{x^2}{2\lambda_0(x)}\right)\right]}. \tag{2.54}$$

Figure 2.9 shows the first-passage probability computed with TELM analysis in the frequency domain using Vanmarcke's formula in comparison with results obtained by crude MCS analysis.

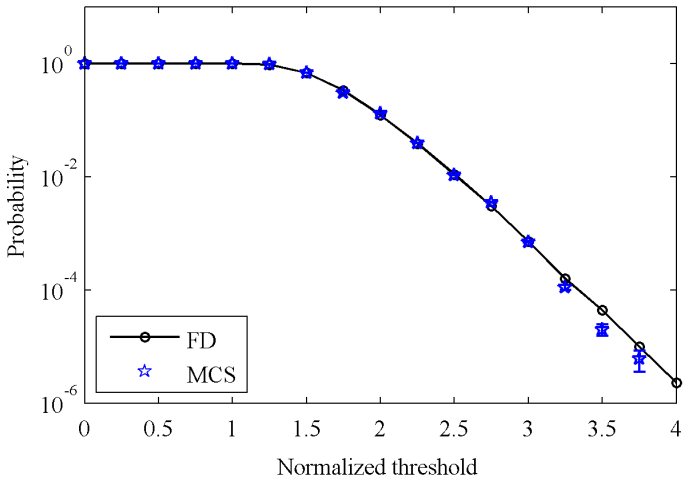

Figure 2.9: First passage probability of the nonlinear response for a time interval of 10[s] .

Fragility curve analysis

Given a failure threshold, the fragility curve is the conditional probability of failure plotted as a function of a given measure of the intensity of the excitation. The fragility curve plays an important role in performance-based earthquake engineering, where methods based on the so-called incremental dynamic analysis [104] have been developed to compute it through repeated time-history dynamic analysis using scaled ground motions. It turns out that TELM is particularly convenient for fragility analysis when the ground motion is specified as a stochastic process.

A remarkable result in TELM is that the TELS is independent of any scaling of the excitation. That is, given a scaled excitation $cF(t)$, the IRF and FRF of the TELS for a specific threshold x are independent of the scale factor c.

The proof is as follows: Let $cF(t) = \tilde{F}(t) = c\boldsymbol{s}(t)\tilde{\boldsymbol{u}} = \boldsymbol{s}(t)\boldsymbol{c}$ with $\boldsymbol{c} = c\tilde{\boldsymbol{u}}$, where $\tilde{\boldsymbol{u}}$ is the set of standard normal random variables of the scaled excitation and $\boldsymbol{c}$ is a vector of normal random variables of zero mean and standard deviation c. The design point for this problem, denoted $\tilde{\boldsymbol{u}}^*$, is the solution to (2.19) with $\boldsymbol{u}$ replaced by $\tilde{\boldsymbol{u}}$ and the limit-state function replaced by $g(x, t_x, \boldsymbol{c})$.

Multiplying the two sides of that equation by c, we obtain

$$\boldsymbol{c}^* = \text{argmin}\{||\boldsymbol{c}|| \ |g(x, t_x, \boldsymbol{c}) = 0\}, \tag{2.55}$$

This equation is identical in form to the equation for the unscaled problem; only the $\boldsymbol{u}$ has been replaced by $\boldsymbol{c}$. It follows that $\boldsymbol{c}^* = \boldsymbol{u}^*$ and thus

$$\boldsymbol{c}^* = \boldsymbol{u}^* = c\tilde{\boldsymbol{u}}^* \Rightarrow \tilde{\boldsymbol{u}}^* = \boldsymbol{u}^*/c. \tag{2.56}$$

Remark The probability space of $\boldsymbol{c}$ is of course different from the standard normal space; however, an isotropic scaling does not affect the axial symmetry of the Gaussian space. Indeed, the problem is still a norm minimization. Once established that the norm is the minimization criterion, the problem is completely deterministic and equivalent to (2.19).

The design point excitation is then written

$$\tilde{f}^*(t) = c\boldsymbol{s}(t)\tilde{\boldsymbol{u}}^* = \boldsymbol{s}(t)\boldsymbol{u}^* = f^*(t) \tag{2.57}$$

and

$$\tilde{f}^*(t) = f^*(t) \Rightarrow \tilde{x}^*(t) = x^*(t). \tag{2.58}$$

Thus for any scale factor c, the design-point excitation and the design-point response are unique for a given threshold x and point in time t_x. Because for a linear system the IRF or the FRF are completely characterized by the input-output pair, (2.58) implies that $h(t) = \tilde{h}(t)$ and $H(\omega) = \tilde{H}(\omega)$.

For a given threshold of interest, we define $L_{\text{TELS}}[\cdot]$ and $h_{\text{TELS}}(t)$ respectively as the linear operator and the IRF of the TELS. We can than write

$$L_{\text{TELS}}[X(t)] = cF(t) \tag{2.59}$$

$$X(t) = c[h_{\text{TELS}}(t) * \boldsymbol{s}(t)\tilde{\boldsymbol{u}}]U(t). \tag{2.60}$$

Remark The invariance of the design-point excitation and response relative to the scaling factor does not mean that the response is invariant to the scaling factor, as is clearly evident in (2.60).

Given (2.56), the first-order approximation of the CDF of the nonlinear response with respect to a scaled excitation is simply given by $\Phi[\beta(x, t_x)/c]$, where $\beta(x, t_x)$ denotes the reliability index for the unscaled problem. Thus, no extra computations are required for the scaled excitations. This is in contrast to the incremental dynamic analysis method [104], where repeated nonlinear dynamic analysis must be performed for each scaled time history. Figure 2.10 shows the complementary CDF of the response of the example system for a specified threshold as a function of the scale of the white-noise excitation. Only the frequency-domain results are compared with the results of a crude MCS analysis, since we have already established that the time- and frequency-domain analyses produce virtually identical results. The result in Figure 2.10 can be considered as the fragility curve for the selected threshold for the point-in-time failure event. The fragility curve due to the failure event

during an interval of time is computed by selecting the TELS corresponding to a specific threshold x and modifying (2.53)-(2.54) as

$$P\left[x \leq \max_{0<t\leq T} |X(t)| \Big| C = c\right] \simeq 1 - \left[1 - \exp\left(-\frac{x^2}{c2\lambda_0(x)}\right)\right] \exp[-\eta(x,c)T], \tag{2.61}$$

$$\eta(x,c) = \nu^+(x) \frac{\left[1 - \frac{x}{c\lambda_0(x)} \exp\left(-\sqrt{2\pi\left(1 - \frac{\lambda_1^2(x)}{\lambda_2(x)\lambda_0(x)}\right)^{1.2}}\right)\right]}{\left[1 - \exp\left(-\frac{x^2}{c2\lambda_0(x)}\right)\right]}. \tag{2.62}$$

Figure 2.11 shows the tail probability of the hysteretic oscillator maximum response at threshold $3\bar{\sigma}$ and a time interval of 10[s].

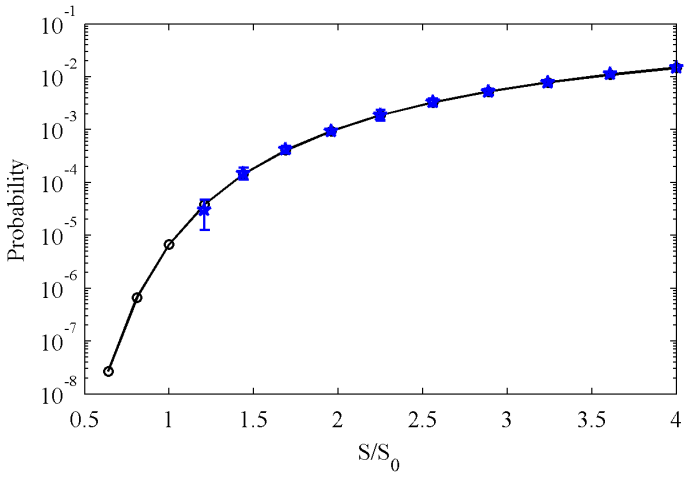

Figure 2.10: Tail Probability of the nonlinear response at threshold $x = 3\bar{\sigma}$ and scaled white-noise input

2.5 Conclusion

This chapter reviews the main aspects of the tail-equivalent linearization. The method is designed for Gaussian excitations and it employs two type of discretizations, one in the time domain and one in the frequency domain. The linearization is based on classical FORM analysis and, in particular, the equivalent linear system, named TELS, is defined by matching its design point with the one of the nonlinear system. Consequently the tail probability of the TELS coincides with first-order approximation of the tail probability of the nonlinear system. We have seen that the TELS has a nonparametric form and is strongly influenced by the response threshold of interest. As a consequence of these properties, TELM predicts the non-Gaussian distribution of the nonlinear response.

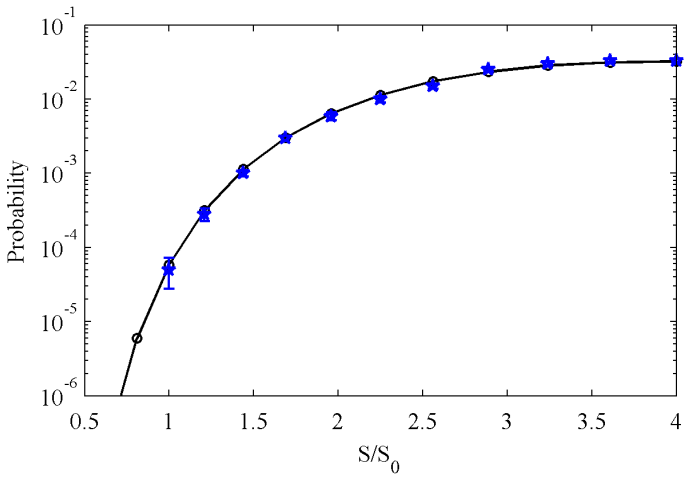

Figure 2.11: Tail Probability of the maximum response at threshold $x = 3\bar{\sigma}$ and scaled white-noise input

Another cornerstone of TELM analysis is its independence from the TELS to a scaling of the excitation, a characteristic that is particular appealing for incremental dynamic analysis. In the next chapter we explore the evolution of TELM for different types of input dicretizations.

Chapter 3

Sampling and Interpolation

3.1 Introduction: Sampling and Interpolation at a glance

This chapter first introduces the concept of sampling from a continuous function; this boils down to recording sample values of the original signal at selected discrete points. Next, we turn to the interpolation operation, which amounts to reconstructing the original function from its sampled values. Different interpolation schemes can be found in the literature. In this chapter, we focus on the well-known sinc interpolation formula, which is also known as the Whittaker-Shannon interpolation formula [44, 94, 110]. This is a remarkable rule, since it allows us to fully reconstruct a continuous-time, band-limited signal from a set of equally spaced samples. Here by following [16], we provide a modern description of the original problem, so that readers unfamiliar with the topic can have a gentle introduction. For this purpose, we recall some definitions and proofs from the theory of signal processing. These will be useful for the next chapter, where we will introduce discrete representation of band-limited stochastic processes.

3.2 The Shah Distribution

In electrical engineering literature a train of equally spaced pulses is known as the "Shah distribution".[1] The Shah distribution is defined as

$$\text{Ш}_a \triangleq \sum_{n=-\infty}^{\infty} \delta(t - na);\ a \in \mathbb{R}^+. \tag{3.1}$$

where $\delta(\cdot)$ denotes the Dirac delta function. The distribution function is widely used in signal processing due to its three fundamental properties: the sampling property, the periodizing property, and the Fourier Transform property. Here, we will make use of the original definition to describe

[1] This name was first introduced by Bracewell [15]in order to underline the similarity between the shape of the cyrillic letter Ш (Sha) and the graphic representation of a train of pulses.

four Shah distributions: two in the time domain and two in the frequency domain. These four distributions are not independent; in fact, they are Fourier transform pairs.

Sampling Shah distribution in the time domain

The sampling Shah distribution in the time domain is defined as

$$\text{Ш}_{\Delta t} = \sum_{n=-\infty}^{\infty} \delta(t - n\Delta t), \tag{3.2}$$

where Δt is the sampling rate. The choice of Δt is only related to the bandwidth of the signal and it can be selected differently from the time step of the structural dynamic analysis. This concept is elaborated upon later in this chapter

Periodizing Shah distribution in the time domain

The periodizing Shah distribution in the time domain is defined as

$$\text{Ш}_{T} = \sum_{n=-\infty}^{\infty} \delta(t - nT), \tag{3.3}$$

where T is the period. The choice of T is related to the total duration of the signal and should be selected with care to avoid aliasing. This is elaborated upon later in the chapter.

Sampling Shah distribution in the frequency domain

The sampling Shah distribution in the frequency domain is defined as:

$$\text{Ш}_{\Delta\omega} = \Delta\omega \sum_{k=-\infty}^{\infty} \delta\left(\omega - k\Delta\omega\right), \tag{3.4}$$

where $\Delta\omega$ is the sampling rate. The reader should note that the sampling rate also appears as a scaling factor of the entire summation. At the end of this section, we will see that this is a direct consequence of the Fourier transform propriety of the Dirac delta distribution.

Periodizing Shah distribution in the frequency domain

The periodizing Shah distribution in the frequency domain is defined as

$$\text{Ш}_{\Omega} = \Omega \sum_{k=-\infty}^{\infty} \delta\left(\omega - k\Omega\right), \tag{3.5}$$

where Ω is related to the bandwidth of the signal, which should be selected with care to avoid spectrum aliasing.

Sampling property

Given a function f in time domain, we can sample the function at equally spaced intervals by multiplying the function f with the Shah distribution $\text{Ш}_{\Delta t}$

$$f_{\Delta t}(t) = f\text{Ш}_{\Delta t} = \sum_{n=-\infty}^{\infty} f(n\Delta t)\delta(t - n\Delta t), \tag{3.6}$$

where the last equality is based on the sampling property of the delta Dirac distribution.

Given a spectrum F in the frequency domain, we can sample the spectrum at equally spaced intervals by multiplying it with the Shah distribution $\text{Ш}_{\Delta\omega}$

$$F_{\Delta\omega}(\omega) = F\text{Ш}_{\Delta\omega} = \Delta\omega \sum_{k=-\infty}^{\infty} F\left(k\Delta\omega\right)\delta\left(\omega - k\Delta\omega\right). \tag{3.7}$$

When sampling in time domain, we introduce a band-limited spectrum because we do not capture the fluctuations between two consecutive sampling points. Given a sampling rate Δt, the band limit is $\bar{\Omega}/2 = \pi/\Delta t$; consequently, if we have a signal band-limited to Ω, Δt should be selected satisfying the condition $\Delta t \leq \pi/\Omega$ so that $\bar{\Omega} \geq \Omega$. This condition is the well-known Nyquist rate.

Example Given a 25[Hz] band-limited signal we must select the sampling rate $\Delta t \leq \frac{1}{50}[s]$.

If, instead, we choose a spectral sampling method, we express the original function in terms of a Fourier Series. However, we should be aware of the fact that when we use the Fourier series, we periodize the original function f by a period T. In terms of the sampling rate $\Delta\omega$, the period is $T = 2\pi/\Delta\omega$. Thus, given a function f defined in the interval $[0, T]$, we must select $\Delta\omega \leq 2\pi/T$. Note that while the time is a continuous function defined on the interval $[0, T]$, the spectrum is a discrete and unbounded function.

Example Given a function f defined on the time interval [0,30][s], the correct sampling rate is $\Delta\omega \leq \frac{2\pi}{30}$[rad].

Periodizing property

A non-periodic function f in the time domain can be periodized by convolving it with the Shah distribution in the time domain, i.e.,

$$f_T(t) = f * \text{Ш}_T = \sum_{n=-\infty}^{\infty} f(t - nT), \tag{3.8}$$

where the last equality is based on the shifting property of the Dirac delta distribution. In (3.8), T is the periodization period. However, the period should be carefully selected. Suppose we have a signal over an interval $[0, \bar{T}]$ with $\bar{T} \in \mathbb{R}^+$. If we want to periodize the signal over $\mathbb{R}$ without

altering the original shape over the interval $[0, \bar{T}]$, we must select $T \geq \bar{T}$. Inappropriate selection of the period leads to aliasing of the signal in time domain.

Alternatively, a spectrum F in the frequency domain can be periodized (without scaling) by convolving it with a scaled Shah distribution in the frequency domain, i.e.,

$$F_\Omega(\omega) = F * \frac{1}{\Omega}\text{Ш}_\Omega = \sum_{k=-\infty}^{\infty} F(\omega - k\Omega), \tag{3.9}$$

where Ω is the periodization frequency. However, as in the time domain case, Ω should be taken with caution. Suppose we have a band-limited signal over an interval $[0, \bar{\Omega}]$ with $\bar{\Omega} \in \mathbb{R}^+$. If we wish to periodize the modulus of the spectrum without altering the original shape over the interval $[0, \bar{\Omega}]$, we must select $\Omega \geq \bar{\Omega}$. Often, inappropriate selection of Ω leads to spectrum aliasing.

Fourier transform

Until now we have used two versions of the Shah distribution: the time domain version and the frequency domain version. But what is the link between the two? In this subsection we will prove that the two definitions are Fourier transform pairs. We start by taking the Fourier transform of Ш_T:

$$\mathscr{F}[\text{Ш}_T](\omega) = \sum_{k=-\infty}^{\infty} \mathscr{F}[\delta(t - kT)](\omega) = \sum_{k=-\infty}^{\infty} e^{-i\omega kT}. \tag{3.10}$$

This is an infinite series of harmonic functions with constant coefficients equal to 1. On the other hand, Ш_T is a periodic function of period T. Hence, it can be expressed in terms of Fourier series as

$$\text{Ш}_T = \sum_{k=-\infty}^{\infty} c_k e^{ik\frac{2\pi}{T}t}, \tag{3.11}$$

where the Fourier coefficients c_k can be determined over any interval T. In particular,

$$\begin{aligned}
c_k &= \frac{1}{T}\int_{-T/2}^{T/2} \text{Ш}_T e^{-ik\frac{2\pi}{T}t} dt && (3.12)\\
&= \frac{1}{T}\int_{-T/2}^{T/2} \delta(t) e^{-ik\frac{2\pi}{T}t} dt && (3.13)\\
&= \frac{1}{T}\left\langle \delta(t), e^{ik\frac{2\pi}{T}t} \right\rangle && (3.14)\\
&= \frac{1}{T} e^{-ik\frac{2\pi}{T}0} && (3.15)\\
&= \frac{1}{T}, && (3.16)
\end{aligned}$$

which leads to

$$\text{Ш}_T = \frac{1}{T}\sum_{k=-\infty}^{\infty} e^{ik\frac{2\pi}{T}t}. \tag{3.17}$$

Now, we take the Fourier transform of (3.17)

$$\mathscr{F}[\text{Ш}_T](\omega) = \frac{1}{T}\sum_{k=-\infty}^{\infty} \mathscr{F}[e^{ik\frac{2\pi}{T}t}](\omega), \tag{3.18}$$

and by using the symmetry property of the Fourier Transform $\mathscr{F}[F(-t)] = 2\pi f(\omega)$ and the Dirac distribution Fourier pairs $\mathscr{F}[\delta(t-a)](\omega) = e^{-i\omega a}$, we can write

$$\begin{aligned}
\mathscr{F}[\text{Ш}_T](\omega) &= \frac{1}{T}\sum_{k=-\infty}^{\infty} \mathscr{F}[e^{-ik\frac{2\pi}{T}(-t)}](\omega) && (3.19)\\
&= \frac{1}{T}\sum_{k=-\infty}^{\infty} \mathscr{F}[e^{-ia(-t)}](\omega) && (3.20)\\
&= \frac{2\pi}{T}\sum_{k=-\infty}^{\infty} \delta(\omega - a) && (3.21)\\
&= \frac{2\pi}{T}\sum_{k=-\infty}^{\infty} \delta\left(\omega - k\frac{2\pi}{T}\right). && (3.22)
\end{aligned}$$

This leads to the definition of the Shah distribution ($\text{Ш}_{\Delta\omega}$) in the frequency domain

$$\begin{aligned}
\text{Ш}_{2\pi/T} &= \frac{2\pi}{T}\sum_{-\infty}^{\infty}\delta\left(\omega - k\frac{2\pi}{T}\right), && (3.23)\\
\text{Ш}_{\Delta\omega} &\triangleq \Delta\omega\sum_{-\infty}^{\infty}\delta(\omega - k\Delta\omega), && (3.24)
\end{aligned}$$

with $\Delta\omega = 2\pi/T$.

We can see that the a periodic function of period T corresponds to a discrete spectrum. If we replace T with Δt, we obtain:

$$\begin{aligned}
\text{Ш}_{2\pi/\Delta t} &= \frac{2\pi}{\Delta t}\sum_{-\infty}^{\infty}\delta\left(\omega - k\frac{2\pi}{\Delta t}\right), && (3.25)\\
\text{Ш}_{\Omega} &\triangleq \Omega\sum_{-\infty}^{\infty}\delta(\omega - k\Omega), && (3.26)
\end{aligned}$$

with $\Omega = 2\pi/\Delta t$.

3.3 Interpolation Problem

The interpolation problem arises from the desire to reconstruct the exact original time-continuous, band-limited signal from a set of equally spaced values. A function f is band-limited if its Fourier transform $F = 0$ for $|\omega| \geq \bar{\Omega}$, where $\bar{\Omega}$ is the bandwidth. The claim is that if a function f is band-limited, the interpolation problem can be solved exactly. In other words, we provide a formula of f continuous on the variable t in terms of the sample values $f(nT)$. Before doing that, we need to review what the sinc function and its Fourier transform are.

The original sinc function is defined as

$$\text{sinc}(t) = \frac{\sin(\pi t)}{\pi t}. \tag{3.27}$$

In this dissertation we use a scaled version of the sic function defined as

$$\text{sinc}_{\Delta t}(t) = \frac{\sin\left(\dfrac{\pi t}{\Delta t}\right)}{\left(\dfrac{\pi t}{\Delta t}\right)}. \tag{3.28}$$

It is easy to prove that the Fourier transform of (3.28) is

$$\mathscr{F}[\text{sinc}_{\Delta t}(t)](\omega) = \Delta t \Pi_{\pi/\Delta t}, \tag{3.29}$$

where $\Pi_{\pi/\Delta t}$ is the rectangular function defined as $\Pi_{\pi/\Delta t} = 1$ for $|\omega\| < \pi/\Delta t$, and $\Pi_{\pi/\Delta t} = 0$ otherwise. Now we have all the elements to prove the previous statement.

For a given function f in time domain, band-limited at $\bar{\Omega}$, we select the sampling rate as $\Delta t = \pi/\bar{\Omega}$ and we use Ш_Ω to periodize the corresponding spectrum, F, as

$$F_p = \frac{1}{\Omega}\text{Ш}_\Omega * F = \frac{\Delta t}{2\pi}(\text{Ш}_\Omega * F), \tag{3.30}$$

with $\Omega = 2\bar{\Omega} = 2\pi/\Delta t$. Recall from the definition in (3.9) that the latter periodization does not scale the original spectrum. As suggested in [16], we can regain the original spectrum by multiplying the periodic spectrum with a rectangular low-pass filter

$$F = \frac{\Delta t}{2\pi}\Pi_{\Omega/2}(\text{Ш}_\Omega * F). \tag{3.31}$$

Finally, we apply the inverse Fourier transform to get back the original time-domain function

$$\begin{aligned} f &= \frac{1}{2\pi}\mathscr{F}^{-1}\left[\Delta t \Pi_{\Omega/2}(\text{Ш}_\Omega * F)\right](t) \\ &= \frac{1}{2\pi}\mathscr{F}^{-1}[(\Delta t \Pi_{\Omega/2})](t) * \mathscr{F}^{-1}[(\text{Ш}_\Omega * F)](t) \\ &= \mathscr{F}^{-1}[\Delta t \Pi_{\Omega/2}](t) * \frac{2\pi}{2\pi}\mathscr{F}^{-1}[F](t)\mathscr{F}^{-1}[\text{Ш}_\Omega](t) \\ &= \text{sinc}_{\Delta t}(t) * \sum_{n=-\infty}^{\infty} f(n\Delta t)\delta(t - n\Delta t) \\ &= \sum_{n=-\infty}^{\infty} f(n\Delta t)\text{sinc}_{\Delta t}(t) * \delta(t - n\Delta t) \\ &= \sum_{n=-\infty}^{\infty} f(n\Delta t)\text{sinc}_{\Delta t}(t - n\Delta t). \end{aligned} \tag{3.32}$$

We rewrite the final result in order to highlight its importance:

$$f = \sum_{n=-\infty}^{\infty} f(n\Delta t)\text{sinc}_{\Delta t}(t - n\Delta t). \tag{3.33}$$

In the signal processing field (3.33) is known as "Whittaker-Shannon interpolation formula" or "Whittaker-Shannon interpolation formula." It is a remarkable formula, because for a band-limited process it yields back the exact original function from its samples. Moreover, we will see in the next section that the $\text{sinc}_{\Delta t}$ functions can be interpreted as orthogonal bases for the original function f. Without much elaboration here, (3.33) (like the Fourier series) can be viewed as an infinite series, where the samples are the coefficients of the series and the $\text{sinc}_{\Delta t}$ functions are the orthogonal bases.

3.4 Functional spaces interpretation

We can review the problem described above also in the context of functional spaces. It is assumed that the reader is familiar with the concepts of vector space in $\mathbb{R}^N$, Euclidean norm, and orthogonality. A good reference for these topics is [62].

If the dimensionality of the vector space $\mathbb{R}^N$ is pushed to infinity, each vector can be thought of as an infinite number of components and, in the limit, as a function. We equip this new space with a norm which defines the length of our function. Because the dimensionality is not finite, we restrict the function to finite norm. The notion of inner product and orthogonality can be extended to this space by considering the usual limit of the Riemann sum pushed to an integral. With this in mind, the inner product of two vectors is viewed as the integration of the product of two functions with finite norm. The concept of orthogonality is thus easily extendable. Two functions are said to be orthogonal if their inner product is zero. The concept of inner product is more profound as it has to obey certain rules, which are discussed in details in [62]. A vector space equipped with an inner product is said to be an inner product space. Functions $(f_1, f_2 ... f_m ...)$ are said to be linearly

independent if $\sum_{m=1}^{\infty} a_m f_m = 0$ is true only if $a_m = 0$ for all m. The span of a set of functions is the subspace consisting of all linear combinations of the functions in the set. A subset of a functional space is called a basis when the functions in the subset are linearly independent and their span covers the entire space. A set of orthonormal functions is a set of functions which are orthogonal with unitary norm.

A complete inner product space is called a Hilbert space. The concept of completeness is rather detailed (it needs the concept of Cauchy sequences [62]), but here it is sufficient to say that the examples considered below can be cast in the Hilbert space framework. An example of a Hilbert space is the space of square-integrable functions over the interval $[-\pi, \pi]$, for which the set of sines and cosines are a complete set of basis and the Fourier series expansion is the synthesis formula.

It should be intuitive that any valid set of basis functions can be used to describe a particular class of functions. Thus, in general, we can write

$$f(t) = \sum_{m=-\infty}^{\infty} a_m \psi_m(t) \tag{3.34}$$

$$= \sum_{m=-\infty}^{\infty} \langle \psi_m(t), f \rangle \psi_m(t). \tag{3.35}$$

In the next subsection we prove that the sinc interpolation formula can be viewed as a particular case of (3.34), where $\psi_m(t)$ are selected to be the sinc functions.

Before moving to the next section, it is worth briefly describing why the expansion (3.34) and its functional space interpretation are so suitable to describe a general function. For example, in a practical application, the expansion (3.34) has to be truncated and the question that we may want to ask is: what is the error in doing that? A vector in a finite space or a function in the Hilbert space can be completely described if all the coordinates of the expansion (3.34) are provided. In practice, we truncate the infinite series up to a "sufficiently" large M. If we consider only a finite number of basis functions, we constrain our work into a subspace $\mathbb{V}$, which is the span of the finite set of these basis functions. The approximate realization is the orthogonal projection of the real realization into this subspace. This has an important consequence for it guarantees the best approximation of the real realization for the given basis. In other words, it consists of the least-square approximation of our original function for a given subspace. Moreover, as we will see in the next chapter, if we randomize the coefficients of the series, we obtain a random process in which the "randomness" is distinguished from its time or space dependence.

The sinc basis functions

In this subsection we show that sinc functions are a suitable orthogonal set of functions to describe band-limited signals. First, we check the orthogonality condition, and then we derive the coefficients a_m of expansion (3.34).

Orthogonality

To address this task we make use of the Parseval identity $\langle f^{\mathrm{H}}, g\rangle = \frac{1}{2\pi}\langle F^{\mathrm{H}}, G\rangle$ (where the superscript $\cdot^{\mathrm{H}}$ denotes the Hermitian conjugate) and the Fourier transform of the sinc function (3.29). Given two distinct sinc functions from expansion (3.34) we can write:

$$\begin{aligned}
\langle \mathrm{sinc}_{\Delta t}(t - n\Delta t), \mathrm{sinc}_{\Delta t}(t - m\Delta t)\rangle &= \langle \mathrm{sinc}_{\Delta t}(t) * \delta(t - n\Delta t), \mathrm{sinc}_{\Delta t}(t) * \delta(t - m\Delta t)\rangle \\
&= \frac{1}{2\pi}\left\langle \Delta t \mathbf{\Pi}_{\pi/\Delta t}(\omega) e^{in\omega}, \Delta t \mathbf{\Pi}_{\pi/\Delta t}(\omega) e^{-im\omega}\right\rangle \\
&= \frac{1}{2\pi}\left\langle \Delta t^2 \mathbf{\Pi}_{\pi/\Delta t}(\omega), e^{i(n-m)\Delta t\omega}\right\rangle \\
&= \frac{\Delta t}{2\pi}\left\langle \Delta t \mathbf{\Pi}_{\pi/\Delta t}(\omega), e^{i(n-m)\Delta t\omega}\right\rangle \\
&= \Delta t \mathrm{sinc}_{\Delta t}[(n-m)\Delta t] \\
&= \Delta t \mathrm{sinc}(n-m) = \Delta t \delta[n-m]. \qquad (3.36)
\end{aligned}$$

Indeed, the sinc functions are orthogonal but not orthonormal. We can easily make them orthonormal by scaling with $1/\sqrt{\Delta t}$. Thus, we define the orthonormal basis

$$\psi_m(t) = \frac{1}{\sqrt{\Delta t}}\mathrm{sinc}(t - \Delta t m). \qquad (3.37)$$

The coefficients of the series

In this subsection we compute the coefficients of the orthonormal series expansion, that is,

$$a_m = \langle \psi_m(t), f\rangle, \qquad (3.38)$$

where $\psi_m(t)$ is the scaled sinc function (3.37). Again, we make use of the Parseval identity and the Fourier transform of the sinc function:

$$\begin{aligned}
a_m &= \frac{1}{2\pi}\left\langle \sqrt{\Delta t}\Pi_{\pi/\Delta t} e^{-i\omega m\Delta t}, F\right\rangle \\
&= \frac{\sqrt{\Delta t}}{2\pi}\langle e^{i\omega m\Delta t}, F\rangle \\
&= \sqrt{\Delta t} f(m\Delta t), \qquad (3.39)
\end{aligned}$$

where the second equality is justified by the fact that F is band-limited to $\bar{\Omega}$, so that the rectangular function is not altering the spectrum. The last equality is a direct application of the definition of inverse Fourier transform. It is clear now that the scaled sinc functions are a suitable set of orthonormal basis functions.

3.5 Conclusion

This chapter serves as a foundation for the following Chapter 4. In particular, we have introduced the definition of the Shah distribution in time and frequency domains and its two fundamental properties, i.e., the sampling property and the periodizing property. Moreover, we have seen that Shah in the time domain is Fourier pair with the Shah in the frequency domain. We use these properties to review, in a modern perspective, the classical sinc interpolation formula, which is also known as the Whittaker-Shannon interpolation formula [44, 94, 110]. We finally studied the properties of this remarkable formula, which will be of fundamental importance in the next chapter, when we will deal with the general representation of a stochastic process based on white noise.

Chapter 4

Band-limited stochastic processes

4.1 Introduction: Band-limited stochastic processes at a glance

In the previous chapter we introduced the sinc interpolation formula to represent band-limited functions. We saw that this is a remarkable formula because the original continuous signal can be reconstructed from a suitable set of sample values. Roughly speaking, the set of samples is a "sufficient statistic" for the function f. In this chapter, we consider each individual band-limited function, f, as a realization of an underlying stochastic process. Starting from the general representation (3.34), we transform each coefficient a_m into a random variable. In particular, if we choose Gaussian random variables, the linear combination (3.34) leads to a Gaussian process. This representation is suitable for TELM analysis because it allows distinguishing the "randomness" of the process from its time evolution. Moreover, if we choose $\psi_m(t)$ as sine and cosine functions, we recover the classical random Fourier series proposed by Shinozuka [95, 97] Shinozuka and Deodatis and used in the frequency domain version of the TELM by Garrè and Der Kiureghian [40].

As mentioned above, in this chapter we select $\psi_m(t)$ to be the sinc functions. The resulting stochastic process is band-limited, but the advantage in this case is given by the full control of the band limit, which is uncoupled from the time integration step required by the numerical analysis. We finally apply this expansion to TELM analysis and examine the computational efficiency gained from that formulation.

Part of the material covered in this chapter has been published in [17].

4.2 General representation of stochastic processes

In the previous chapter, we described discrete representation of deterministic functions, but we are mainly interested in stochastic processes. It is convenient to approach the description of general stochastic processes using the general representation of deterministic functions. As we have already seen in (3.34), a general function can be represented as a linear combination of an infinite set of basis functions. We have already seen two example of this representation:

I The Fourier series expansion for periodic functions:

$$\begin{aligned} f &= \sum_{k=-\infty}^{\infty} c_k e^{ik\frac{2\pi}{T}t}, \\ m &= k \\ a_m &= c_k \\ \psi_m(t) &= e^{ik\frac{2\pi}{T}t}. \end{aligned} \tag{4.1}$$

II The Whittaker-Shannon expansion for band-limited functions:

$$\begin{aligned} f &= \sum_{n=-\infty}^{\infty} f(n\Delta t)\mathrm{sinc}_{\Delta t}(t - n\Delta t), \\ m &= n \\ a_m &= f(n\Delta t) \\ \psi_m(t) &= \mathrm{sinc}_{\Delta t}(t - n\Delta t). \end{aligned} \tag{4.2}$$

One way to obtain a stochastic process from these representations is to consider these single functions as particular realizations of a sample space. In this approach, we decide to treat the coefficients of the series as random variables. This, of course, is not the only available choice. We adopt this representation because we aim to decouple the "randomness" of the process from its time evolution, as required in TELM analysis. Indeed, a stochastic process can be represented as:

$$F(t) = \sum_{m=-\infty}^{\infty} A_m \psi_m(t), \tag{4.3}$$

where the deterministic coefficient a_m is replaced by the random variable coefficient A_m.

Example We construct a "Gaussian-noise" version of (4.3) as:

$$F(t) = \sum_{m=-\infty}^{\infty} A_m \psi_m(t), \tag{4.4}$$

$$A_m \sim a_m + N(0, \sigma), \tag{4.5}$$

$$\mu_F(t) = \mathrm{E}[F(t)] = \sum_{m=-\infty}^{\infty} \mathrm{E}[A_m]\psi_m(t) = \sum_{m=-\infty}^{\infty} a_m \psi_m(t), \tag{4.6}$$

$$\sigma^2_{F(t)}(t) = \mathrm{Var}[F(t)] = \sum_{m=-\infty}^{\infty} \mathrm{Var}[A_m]\psi_m^2(t) = \sigma^2 \sum_{m=-\infty}^{\infty} \psi_m^2(t), \tag{4.7}$$

with A_n and A_m being statistically independent for $m \neq n$.
Example A zero mean band-limited Gaussian noise can be represented as:

$$\begin{aligned} W(t) &= \sigma \sum_{m=-\infty}^{\infty} u_j \psi_m(t), && (4.8)\\ u_j &\sim \phi(u), && (4.9)\\ \mu_W(t) &= 0, && (4.10)\\ \sigma_W^2(t) &= \sigma^2 \sum_{m=-\infty}^{\infty} \psi_m^2(t). && (4.11) \end{aligned}$$

where $\phi(\cdot) = N(0,1)$ is the standard normal distribution.

In this study we use the zero-mean, band-limited Gaussian white noise as a building block for modeling stochastic processes. The rest of this chapter is focused on the simulation of the band-limited white-noise process and the implementation of the sinc expansion in TELM analysis.

4.3 Vectorial Representation of stochastic processes

As we have mentioned in the previous chapter, we cannot use infinite series in practice. When we introduce truncation, we can represent our approximate functions in a compact vectorial form. We restrict this section to zero-mean Gaussian processes, even though the same definitions can be extended to non-Gaussian processes. It is easy to see that the expansion (4.3) can be rewritten in the same format as used in Chapter 2, i.e.,

$$\begin{aligned} F(t) &= \boldsymbol{s}(t)\boldsymbol{u}, && (4.12)\\ \boldsymbol{s}(t) &= [s_1(t), \ldots, s_N(t)] = \sigma[\psi_1(t), \ldots, \psi_N(t)], && (4.13)\\ \boldsymbol{u} &= [u_1, \ldots, u_N]^\intercal, && (4.14) \end{aligned}$$

with u_i a set of statistically independent standard normal random variables and $s_i(t)$ a set of deterministic basis functions. It is appealing to examine this representation not only from the point of view of a functional space but also from the perspective of the time-invariant reliability formulation. We do this in the following section.

The Standard normal space

In reliability analysis, the above representation is viewed in the standard normal space, which is a $\mathbb{R}^N$ space spanned by a set of orthonormal vectors $\boldsymbol{e}_1, \boldsymbol{e}_2 ... \boldsymbol{e}_N$. In this space, $\boldsymbol{u}$ is a vector described by its coordinates $[u_1, \ldots, u_N]$, each $u_i \sim \phi(u)$, such that

$$\boldsymbol{u} = u_1\boldsymbol{e}_1 + u_2\boldsymbol{e}_2 + ...u_N\boldsymbol{e}_N. \quad (4.15)$$

A given vector $\bar{\boldsymbol{u}}$ in this space spans a line passing through the origin (which is a subspace of $\mathbb{R}^N$)

$$\mathcal{U} = \{\alpha\bar{\boldsymbol{u}}|\alpha \in \mathbb{R}\}. \tag{4.16}$$

Furthermore, for a fixed point in time t, the vector $\boldsymbol{s}(t)$ can be written as

$$\boldsymbol{s}(t) = s_1(t)\boldsymbol{e}_1 + s_2(t)\boldsymbol{e}_2 + ...s_N(t)\boldsymbol{e}_N. \tag{4.17}$$

As the time parameter t evolves, $\boldsymbol{s}(t)$ describes a parametric curve in space, which is a subset (though not generally a subspace) of $\mathbb{R}^N$. We can write this set as:

$$\mathcal{S} = \{\boldsymbol{s}(t)|t \in \mathbb{R}^+\}. \tag{4.18}$$

Thus, we can view the particular realization $f = \boldsymbol{s}(t)\bar{\boldsymbol{u}}$ as the orthogonal projection of the subset $\mathcal{S}$ onto the subspace $\mathcal{U}$. Each vector $\boldsymbol{u}$ of this space is equipped with a probability density defined by the standard multi-normal probability density function

$$\phi(\boldsymbol{u}) = \mathcal{N}(\boldsymbol{0}, \mathbb{I}^{(N)}). \tag{4.19}$$

where $\mathbb{I}^{(N)}$ is the N-dimension identity matrix. The following properties hold:

$$\sigma_F^2(t) = \mathrm{Var}[\boldsymbol{s}(t)\cdot\boldsymbol{u}] = ||\boldsymbol{s}(t)||^2, \tag{4.20}$$

$$K_{FF}(t,t') = \mathrm{E}[(\boldsymbol{s}(t)\cdot\boldsymbol{u})(\boldsymbol{s}(t')\cdot\boldsymbol{u})] = \boldsymbol{s}(t)\cdot\boldsymbol{s}(t'), \tag{4.21}$$

$$\rho_{FF}(t,t') = \frac{K_{FF}(t,t')}{\sigma_F(t)\sigma_F(t')} = \frac{\boldsymbol{s}(t)}{||s(t)||}\cdot\frac{\boldsymbol{s}(t')}{||s(t')||}. \tag{4.22}$$

Thus, the Euclidian norm of each vector in $\mathcal{S}$ is the variance of the process at a particular time. The auto-covariance (or auto-correlation) is the inner product of two elements of $\mathcal{S}$ defined by two distinct instants in time. The cosine of the angle between two elements of $\mathcal{S}$ is the correlation coefficient. The geometry of the set $\mathcal{S}$ underlies further interesting properties. For example, it is easy to show that a weakly Gaussian stationary process is in general described by segment of an hyper-sphere with radius equal to the standard deviation of the process. Readers interested in further geometric interpretations of random processes and random vibrations from the perspective of reliability analysis should consult [29].

4.4 Band-limit white noise by Whittaker-Shannon expansion

We saw in the preceding chapter that any band-limited function can be represented by the Whittaker-Shannon interpolation formula. Moreover, we proved that sinc functions are a valid set of orthogonal basis functions. In this section, we first examine if the sinc functions are a valid set of basis functions to represent the autocorrelation function of a stochastic process and, in particular, the autocorrelation function of a band-limited white noise. Next, we examine the convergence properties of the sinc expansion series. The first authors to explore the use of the Whittaker-Shannon interpolation formula to simulate Gaussian stationary processes are Grigoriu and Balopoulou [45].

The autocorrelation of the process

In this subsection we verify that the sinc expansion provides a valid autocorrelation function for a band-limited $[-\bar{\omega}, \bar{\omega}]$, zero mean, white-noise process. For such stationary process, we have a closed form solution for the autocorrelation function that is well-known to be again the sinc function:

$$R(\tau) = \text{sinc}_{\Delta t}(\tau), \tag{4.23}$$

with $\Delta t = \pi/\bar{\omega}$. Given (4.8), we can write:

$$W(t) = \sum_{n=-\infty}^{\infty} u_n \text{sinc}_{\Delta t}(t - n\Delta t). \tag{4.24}$$

The autocorrelation (or autocovariance) function can be written as:

$$\begin{aligned} K(t,\bar{t}) &= \text{E}[W(t)W(\bar{t})] && (4.25)\\ &= \sum_{m=-\infty}^{\infty}\sum_{n=-\infty}^{\infty} \text{E}[u_m u_n]\text{sinc}_{\Delta t}(\bar{t} - m\Delta t)\text{sinc}_{\Delta t}(t - n\Delta t) && (4.26)\\ &= \sum_{n=-\infty}^{\infty} \text{E}[u_n^2]\text{sinc}_{\Delta t}(\bar{t} - n\Delta t)\text{sinc}_{\Delta t}(t - n\Delta t) && (4.27)\\ &= \sum_{n=-\infty}^{\infty} \text{sinc}_{\Delta t}(\bar{t} - n\Delta t)\text{sinc}_{\Delta t}(t - n\Delta t). && (4.28) \end{aligned}$$

The question now is: Does the series (4.28) converge to the correct autocorrelation function in (1.23)? The answer is yes, and it requires a small trick to show it. Let us represent the function $\text{sinc}_{\Delta t}(t - \bar{t})$, for a fixed $\bar{t}$, through the sinc expansion, i.e.

$$\begin{aligned} \text{sinc}_{\Delta t}(t - \bar{t}) &= \sum_{n=-\infty}^{\infty} a_n \text{sinc}_{\Delta t}(t - n\Delta t) && (4.29)\\ &= \sum_{n=-\infty}^{\infty} \text{sinc}_{\Delta t}(n\Delta t - \bar{t})\text{sinc}_{\Delta t}(t - n\Delta t) && (4.30)\\ &= \sum_{n=-\infty}^{\infty} \text{sinc}_{\Delta t}(\bar{t} - n\Delta t)\text{sinc}_{\Delta t}(t - n\Delta t), && (4.31) \end{aligned}$$

where in the transition from (4.29) to (4.30) we have made use of the interpolation theorem for band-limited functions described in (3.33), and the transition from (4.30) to (4.31) is achieved by the symmetry of the sinc function. This result is identical to 4.28. Thus, for the autocorrelation function we can write:

$$\begin{aligned} K(t,\bar{t}) &= \text{sinc}_{\Delta t}(t - \bar{t})\\ &= \text{sinc}_{\Delta t}(\tau)\\ &= R(\tau). && (4.32) \end{aligned}$$

and the power spectral density (PSD):

$$\begin{aligned} S(\omega) &= \mathscr{F}[\mathrm{sinc}_{\Delta t}(\tau)], (\omega) && (4.33)\\ &= (2\pi\Delta t)\Pi_{\pi/\Delta t}. && (4.34)\end{aligned}$$

The area of the PSD integrates to one, which is the initially assumed variance.

The convergence of the process

We have seen in the previous section that the autocorrelation function of the band-limited white-noise process represented by (4.24) is the sinc function. As a consequence any band-limited stochastic process with the same or compatible bandwidth derived by filtering the previous band-limited white noise has an autocorrelation function that is correctly represented by the interpolation formula. By using this observation, we show-mean square convergence of a band-limited stochastic process (on the interval $[-\bar{\omega}, \bar{\omega}]$) represented by the interpolation formula and here denoted by $\hat{F}(t)$, to the original band-limited stochastic process, denoted by $F(t)$. We start by writing $\hat{F}(t)$ as

$$\hat{F}(t) = \sum_{n=-\infty}^{\infty} F(n\Delta t)\mathrm{sinc}_{\Delta t}(t - n\Delta t). \tag{4.35}$$

This implies $R_{\hat{F}}(\tau) = R_F(\tau)$, as previously demonstrated. Then we say that $\hat{F}$ converges in the mean-square sense if

$$E\left[(F(t) - \hat{F}(t))^2\right] = 0. \tag{4.36}$$

By writing $F \equiv F(t)$ and $\hat{F} \equiv \hat{F}(t)$ for convenience, we expand (4.36) as

$$\begin{aligned} E\left[(F - \hat{F})^2\right] &= E\left[F^2\right] + E\left[\hat{F}^2\right] - 2E\left[F\hat{F}\right] && (4.37)\\ &= E\left[F^2\right] \\ &\quad + \sum_{m=-\infty}^{\infty}\sum_{n=-\infty}^{\infty} E[F(n\Delta t)F(m\Delta t)]\mathrm{sinc}_{\Delta t}(t - n\Delta t)\mathrm{sinc}_{\Delta t}(t - m\Delta t) \\ &\quad -2\sum_{n=-\infty}^{\infty} E[FF(n\Delta t)]\mathrm{sinc}_{\Delta t}(t - n\Delta t), && (4.38)\\ &= E\left[F^2\right] \\ &\quad + \sum_{m=-\infty}^{\infty}\sum_{n=-\infty}^{\infty} R_F\left((n-m)\Delta t\right)\mathrm{sinc}_{\Delta t}(t - n\Delta t)\mathrm{sinc}_{\Delta t}(t - m\Delta t) \\ &\quad -2\sum_{n=-\infty}^{\infty} R_F(t - n\Delta t)\mathrm{sinc}_{\Delta t}(t - n\Delta t). && (4.39)\end{aligned}$$

The last term of (4.39) can be rewritten by considering the sinc expansion of the function $R_F(t-\bar{t})$,

$$R_F(t-\bar{t}) = \sum_{n=-\infty}^{\infty} R_F(n\Delta t - \bar{t})\mathrm{sinc}_{\Delta t}(t-n\Delta t). \tag{4.40}$$

By the symmetry property of the autocorrelation function

$$R_F(t-\bar{t}) = \sum_{n=-\infty}^{\infty} R_F(\bar{t} - n\Delta t)\mathrm{sinc}_{\Delta t}(t-n\Delta t), \tag{4.41}$$

and by imposing $t = \bar{t}$

$$R_F(0) = E[F^2] = \sum_{n=-\infty}^{\infty} R_F(t-n\Delta t)\mathrm{sinc}_{\Delta t}(t-n\Delta t), \tag{4.42}$$

which is identical to the last term in (4.39). The second term of the expansion (4.39) can be simplified by introducing the index $l = n - m$ as

$$\sum_{l=-\infty}^{\infty} R_F\left(l\Delta t\right) \sum_{n=-\infty}^{\infty} \mathrm{sinc}_{\Delta t}(t-(n-l)\Delta t)\mathrm{sinc}_{\Delta t}(t-n\Delta t). \tag{4.43}$$

Now we consider the sinc expansion of the sinc function

$$\mathrm{sinc}_{\Delta t}\left(t-\bar{t}\right) = \sum_{n=-\infty}^{\infty} \mathrm{sinc}_{\Delta t}\left(n\Delta t - \bar{t}\right)\mathrm{sinc}_{\Delta t}(t-n\Delta t). \tag{4.44}$$

letting $\bar{t} = t + l\Delta t$ and using the symmetry property of the sinc function, we obtain the equivalence

$$\begin{aligned} \mathrm{sinc}_{\Delta t}\left(t-\bar{t}\right) &= \mathrm{sinc}_{\Delta t}(l\Delta t), & (4.45)\\ &= \delta[l], & (4.46)\\ &= \sum_{n=-\infty}^{\infty} \mathrm{sinc}_{\Delta t}(t-(n-l)\Delta t)\mathrm{sinc}_{\Delta t}(t-n\Delta t), & (4.47) \end{aligned}$$

where $\delta[l] = 1$ for $l = 0$ and $\delta[l] = 0$ otherwise. We finally write (4.43) as

$$\sum_{l=-\infty}^{\infty} R_F\left(l\Delta t\right)\delta[l] = R_F(0) = E[F^2]. \tag{4.48}$$

We conclude the proof by combining the different terms composing (4.39) as

$$E\left[(F-\hat{F})^2\right] = E[F^2] + E[F^2] - 2E[F^2] = 0. \tag{4.49}$$

By introducing the truncation N on the infinity sum, we can write

$$\hat{F}_N = \sum_{n=-N}^{N} F(n\Delta t)\text{sinc}_{\Delta t}(t - n\Delta t), \tag{4.50}$$

and

$$\lim_{N\to\infty} E\left[(\hat{F}_N - F)^2\right] \to 0. \tag{4.51}$$

4.5 TELM analysis

The application in TELM analysis of the Whittaker-Shannon expansion is straightforward. The theory described in Chapter 2 is still valid because the input is defined with (4.12), (4.13) and (4.14). However, the choice of two time steps is a fundamental advantage in the new formulation. Let Δt_s denote the sampling rate for the sinc expansion formula (4.8). This time step is only related to the band limit of the input process. Provided Δt_s satisfies the condition $\Delta t_s \leq \pi/\bar{\Omega}$, where $\bar{\Omega}$ is the desired bandwidth, (4.8) gives a time-continuous representation of the process. We can select a different discretization time step, Δt_a, for numerical analysis. Δt_a should be sufficiently small to assure convergence in the nonlinear response analysis. In this formulation, the time step of the numerical analysis is completely decoupled from the band-limit of the input process.

Example We explore the difference in the total number of random variables between the existing representation method as described in Chapter 2 and the sinc expansion for simulation of a band-limited white-noise process defined on the time span [0,30][s]. Assume that the "physical" band-limit of interest is [0,10][Hz], i.e., frequencies above 10[Hz] are not significant for the response of the particular structure under consideration.

If we use the time-discretization method of the original TELM (2.9), the number of random variables is defined by the integration time step required in the numerical analysis. Recall that the minimization problem in (2.19) for finding the design point requires computation of the nonlinear response and its gradient by numerical analysis. A typical integration step is $\Delta t_a = 0.01$[s]. This leads to a band-limit of 50[Hz] and the total number of random variables is $30/0.01 = 3000$. Obviously, a large number of the random variables are used to represent frequencies in the range of [10-50][Hz], which are not physically significant for the structural response.

Let us reverse the problem: because our interest is up to 10[Hz], we define $\Delta t_s = 0.05$[s]. We then have $30/0.05 = 600$ random variables. At this point we can use (4.8) to reconstruct a continuous time approximation of the band-limited white noise. Sampling at a rate $\Delta t_a = 0.01$[s], we get back a suitable representation of the signal for the numerical analysis. Using this approach, the total number of random variable has been reduced by a factor 5.

Because the efficiency of TELM is related to the minimization problem (2.19), which depends on the the total number of random variables, the sinc expansion can represent an interesting alternative for using the "right" amount of random variables for a defined physical problem. The advantage compared to the frequency-domain version is that the spectrum is continuous, not discrete; furthermore, we do not have the problem of periodicity of the process.

The last issue to cover before providing a numerical example of TELM analysis is the computation of the IRF of the TELS in the sinc representation. In the original time-domain formulation, this IRF is computed by solving the linear system (2.25), the solution of which requires inversion of the matrix $\boldsymbol{S}$ in (2.27). The matrix is $N \times N$ because the number of random variables is the same as the number of time steps in the numerical integration. On the other hand, when the sinc expansion formulation is used, we have to solve the system of equations

$$\sum_{m=1}^{M} h(t_x - t_m) s_n(t_m) \Delta t = a_n(t_x), \tag{4.52}$$

which in matrix form is rewritten here for convenience

$$\boldsymbol{S}\boldsymbol{h} = \boldsymbol{a}(t_x), \tag{4.53}$$

with

$$\boldsymbol{S} = \Delta t \begin{bmatrix} s_1(t_1) & \dots & s_1(t_M) \\ \vdots & s_n(t_m) & \vdots \\ 0 & \dots & s_N(t_M) \end{bmatrix} \boldsymbol{h} = \begin{bmatrix} h(t_M - t_1) \\ \vdots \\ h(t_M - t_M) \end{bmatrix} \boldsymbol{a}(t_x) = \begin{bmatrix} a_n(t_M) \\ \vdots \\ a_N(t_M) \end{bmatrix}, \tag{4.54}$$

where M is the number of time steps in the numerical analysis, which is usually much greater than N, the number of random variables used in the sinc expansion formulation. Moreover, we have $t_M \equiv t_x$. As can be seen, the system of equations (4.53) is rectangular in form. The solution can be found as the min-norm solution of the system. However, there is an alternative and more elegant way to proceed. Consider the IRF as a band limited function that can be expressed in terms of the sinc expansion. Then, it is sufficient to compute the samples of the IRF and to reconstruct the continuous function by the sinc expansion. In other words, we enforce $M' \equiv N$, where M' is the minimum sufficient number of time points to describe the IRF with the sinc expansion. This leads to a system of N equations with N unknowns, which is solved by inversion as before. Note, however, that the size of this system is much smaller than in the original formulation. Once the N samples of the IRF are computed, the IRF is completely determined by the sinc expansion i.e.

$$h(t) \simeq \sum_{n=0}^{N} h(n\Delta t) \mathrm{sinc}_{\Delta t}(t - n\Delta t). \tag{4.55}$$

Numerical example

In this example, we analyze the computational efficiency gained by implementation of the sinc expansion. We analyze the SDOF Bouc-Wen hysteretic model [8, 14, 109] under white noise excitation modeled with the sinc expansion. The equations governing the dynamical system are (2.45), (2.46), and (2.47) and the structural properties are listed in Table 4.1. The time point is selected as $t_x = 10$[s], and the limit state function is defined by the threshold $x = 3\sigma_0$. Table 4.2 shows the results of TELM analysis for several selected band-limited white noise inputs. In all cases

$\Delta t_a = 0.01$ is used for numerical integration of the nonlinear response, while Δt_s is different for each analysis. Figure 4.1 shows the design point excitation and response and the IRF and FRF of the TELS for the two extreme cases in Table 4.2. Examining the FRF in Figure 4.2, we clearly see that frequencies above 2.5-4[Hz] are not playing a fundamental role; indeed, we can select a Δt_s according to this band-limit and use the "right" number of random variables. It is clear from the last two columns of Table 4.2, which list the reliability index and the CPU time, that this approach can lead to significant savings in computational time at practically no loss in accuracy.

However, this expansion should be used with caution. The analyst should have a "feel" for the physics underlying the problem. In the present example, we know that the system is softening when experiencing plasticity, so that the frequency content is migrating towards a lower values. Moreover, we know that in the linear elastic case the natural frequency is 1[Hz] and that the FRF has a decaying tail with a power of four. Based on this we can determine a "suitable" band-limit.

On the other hand, for stiffening systems, such as a Duffing oscillator [10], the frequency content in the response migrates towards higher values. In such cases, apriori selection of an upper bound frequency can be tricky. Therefore, for such systems, the upper band limit should be selected with extra caution.

4.6 Conclusion

In this chapter we investigate an alternative and broader method to represent stochastic processes in discrete form and its application on TELM analysis. We start from the concept of Hilbert space to represent general signals in series expansion of basis functions. From this representation we generate a stochastic process by randomizing the coefficients of the expansion. In particular we study the simulation of band-limited white noise, which is widely used in practice. If the random variables are selected to be Gaussian the process is Gaussian. At the current state we are using sinc functions as a set of orthonormal basis but in general any valid set of basis can be used to decompose signals and in general to describe stochastic processes. The author aims to investigate Lagrange polynomials expansion and more generally the use of wavelets based on the proposed decomposition. Finally we extend TELM analysis to the sinc representation. Compared to the original time-domain formulation, the advantage of TELM analysis with the proposed formulation lies in the complete separation and control of the band-limit of the process from the time integration step used in analysis. For problems in which the high frequency content is not important, the number of random variables used to describe the process can be significantly reduced. The advantage compared to the frequency-domain formulation is that there are no issues with periodicity and the spectrum is continuous. Furthermore, the formulation is simpler since it does not require splitting the basis functions into sine and cosine terms. The drawback of the sinc expansion is that the function does not die off, even for times distant from t_n, and this reduces its efficiency. This is the reason why the author is considering a low-order Lagrange polynomial expansion to further improve the efficiency.

Table 4.1: Structural and Excitation Properties

Bouc-Wen	α	m[kg]	$c\left[\frac{\text{Ns}}{\text{m}}\right]$	k[N]	$\gamma\left[\frac{1}{\text{m}^{\hat{n}}}\right]$	$\eta\left[\frac{1}{\text{m}^{\hat{n}}}\right]$	$\hat{n}$	A
	0.1	1.00E3	6.28E2	3.95E4	$1/2\bar{\sigma}^{\hat{n}}$	$1/2\bar{\sigma}^{\hat{n}}$	1	1
Excitation		$S_0[\frac{\text{m}^2}{\text{s}^3}]$	t_x[s]	Δt[s]	$\frac{\bar{\omega}}{2\pi}$[Hz]	N		
		1	10	var	10	var		

Table 4.2: Efficiency of the TELM based on sinc basis functions

Sampling rate[s]	Band limit[Hz]	N.Random Variables	Reliability index	Computational time[s]
0.01	50.0	1000	3.122	836
0.02	25.0	500	3.135	322
0.05	10.0	200	3.122	292
0.10	5.0	100	3.122	113
0.20	2.5	50	3.133	51

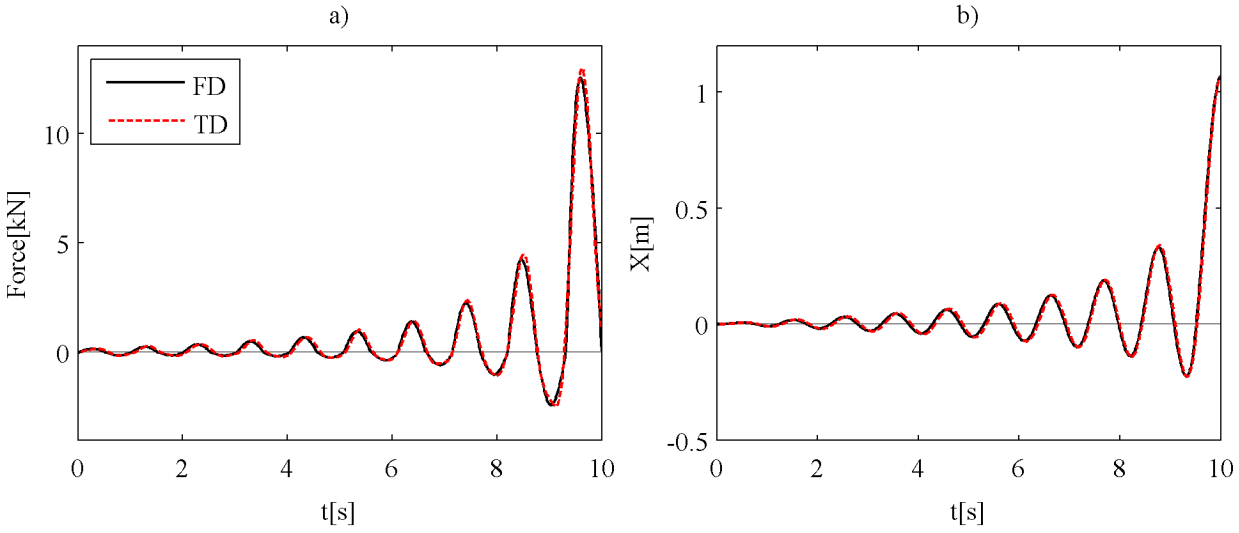

Figure 4.1: a) Design point excitation, b) Design point response for $x = 3\sigma_0$

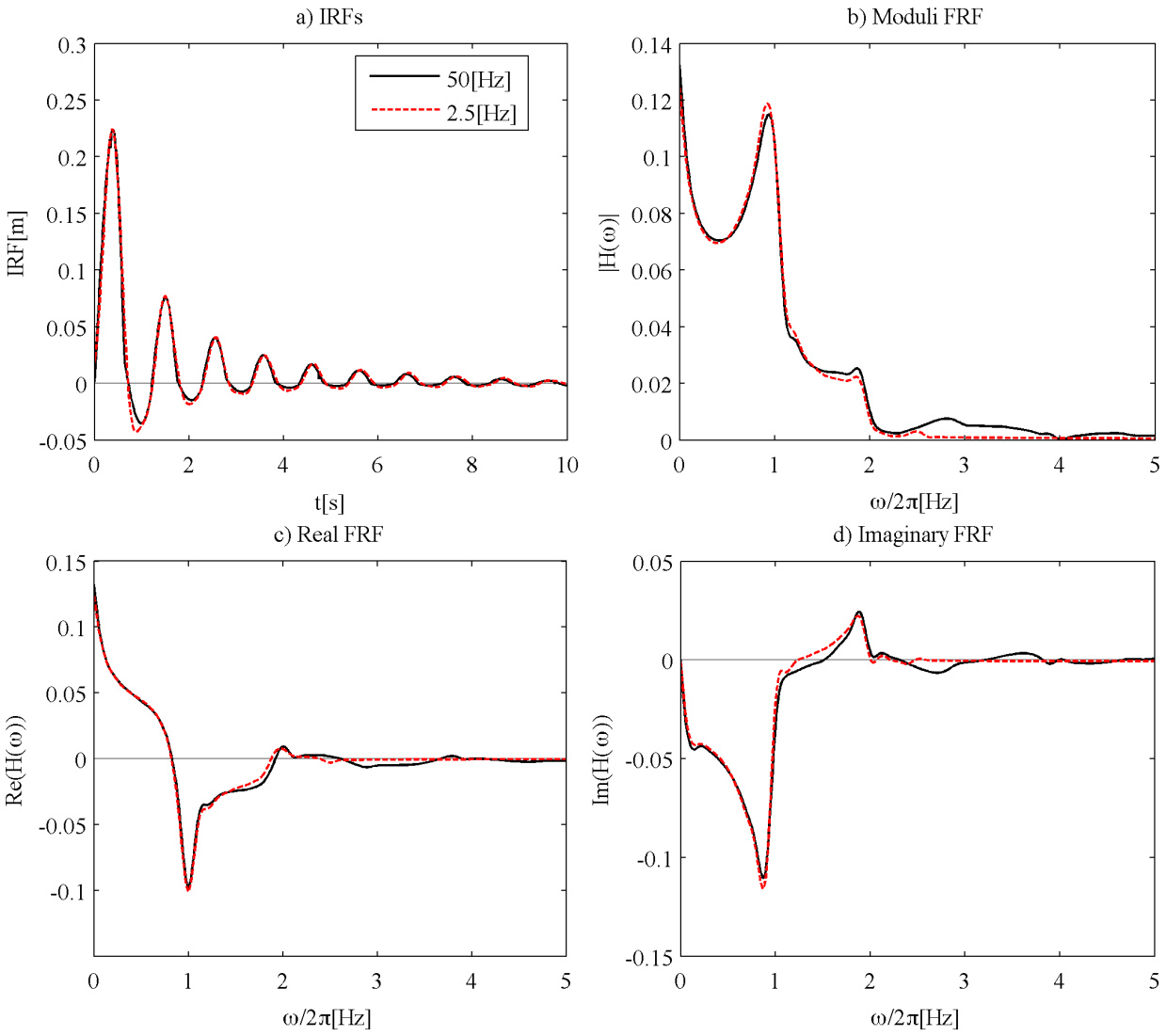

Figure 4.2: IRF and FRF of the nonlinear system for $x = 3\sigma_0$

Chapter 5

Multi-component TELM analysis

5.1 Introduction multi-component TELM at a glance

This chapter extends the TELM to the case of a nonlinear mechanical system subjected to multiple stochastic excitations. Following the original formulation, Chapter 2, the method employs a discrete representation of the stochastic inputs and the first-order reliability method, FORM. Each component of the Gaussian excitation is expressed as a linear function of standard normal random variables. For a specified response threshold of the nonlinear system, the TELS, is defined in an augmented standard normal space by matching the augmented design point of the equivalent linear and nonlinear responses. This leads to the identification of the TELS in terms of a frequency-response function or, equivalently, an impulse-response function for the response of interest with respect to each component of the input excitation. The method is demonstrated through its application to an asymmetric one-story building with hysteretic behavior. The degree of asymmetry is controlled by the eccentricity of the center of stiffness with respect to the center of mass. The relation between the probability of failure and the degree of asymmetry is studied in detail. The statistics of the response for stationary excitation obtained by TELM are in close agreement with Monte Carlo simulation results.

Part of the material covered in this chapter has been published in [18].

5.2 Stochastic representation of input excitations

As shown in Chapter 2, a fundamental requirement in TELM is discrete representation of the stochastic excitation in terms of a finite set of standard normal random variables $\boldsymbol{u} = [u_1, \ldots, u_N]^\intercal$ and a set of basis functions $\boldsymbol{s}(t) = [s_1(t), \ldots, s_N(t)]$. In the case of multiple components of zero-mean Gaussian excitation, assuming statistical independence between the components, each component is modeled as in (2.1) and collected in a vector form

$$\hat{\boldsymbol{F}}(t) = \begin{bmatrix} \hat{F}_1(t) \\ \vdots \\ \hat{F}_J(t) \end{bmatrix} = \begin{bmatrix} \boldsymbol{s}_1(t)\boldsymbol{u}_1 \\ \vdots \\ \boldsymbol{s}_J(t)\boldsymbol{u}_J \end{bmatrix}. \tag{5.1}$$

where J denotes the number of components and $\boldsymbol{s}_j$ and $\boldsymbol{u}_j$ respectively denote the vectors of basis functions and standard normal random variables for the j^{th} component of the excitation. In the following, we present the time- and frequency-domain discretization methods for multi-component excitations.

Time-domain discretization

Following the formulation described in Chapter 2, we define the j^{th} component of the zero-mean Gaussian excitation as

$$F_j(t) = [\eta_j(t) * W_j(t)]U(t) = \int_0^t \eta_j(t-\tau|\boldsymbol{\theta}_j)W_j(\tau)d\tau, \tag{5.2}$$

where $W_j(t)$ is a white-noise process and $\eta_j(t|\boldsymbol{\theta}_j)$ is a parametric impulse-response function of a stable linear filter with $\boldsymbol{\theta}_j$ as its parameters. Note that $F_j(t)$ asymptotically approaches a stationary process with increasing time. As we have seen in Chapter 2, TELM implementation of (5.2) requires discretization along the time axis. For a set of equally spaced time points $t_n = n\Delta t$, $n \in [0, \ldots, N]$, with time step Δt and initial time $t_0 = 0$, we approximate $W_j(t)$ with the rectangular wave process introduced in (2.5), i.e.

$$\hat{W}_j(t) = \frac{1}{\Delta t}\int_{t_{n-1}}^{t_n} W_j(\tau)d\tau, \quad t_{n-1} < t \le t_n, \quad n \in [1, \ldots, N]. \tag{5.3}$$

This process is band-limited at frequency $\Omega = \pi/\Delta t$ [rad/s] and, for a given white-noise spectral density S_j, has variance $\sigma_j^2 = 2\pi S_j/\Delta t$. Defining the standard normal random variables $u_{j,n} = \hat{W}_j(t_n)/\sigma_j$, (5.3) can be written in the form

$$\begin{aligned}
\hat{W}_j(t) &= \boldsymbol{\sigma}_j(t)\boldsymbol{u}_j, && (5.4)\\
\boldsymbol{\sigma}(t) &= [\sigma_{j,1}(t), \ldots, \sigma_{j,N}(t)], && (5.5)\\
\sigma_{j,n}(t) &= \sigma_j, \quad t_{n-1} < t < t_n && (5.6)\\
&= 0 \ \text{ otherwise,} &&\\
\boldsymbol{u}_j &= [u_{j,1}, \ldots, u_{j,N}]. && (5.7)
\end{aligned}$$

The discrete version of (5.2), $\hat{F}_j$, is obtained by replacing $W_j(t)$ with $\hat{W}_j(t)$, i.e.,

$$\begin{aligned}
\hat{F}_j(t) &= [\eta_j(t) * \hat{W}_j(t)]U(t) = \boldsymbol{s}_j(t)\boldsymbol{u}_j, && (5.8)\\
s_{j,n}(t) &= \sigma_j \int_{t_{n-1}}^{t_n} \eta_j(t-\tau|\boldsymbol{\theta}_j)d\tau, \quad t_{n-1} < t \le t_N, \quad n \in [1, \ldots, N], && (5.9)\\
&= 0 \quad t \le t_{n-1}.
\end{aligned}$$

In the time-domain formulation, the total number of random variables for the J excitation component is NJ. Thus, we introduce an augmented standard normal space of dimension NJ. The statistical independence condition between the J different components implies that there are J orthogonal subspaces in the new augmented space.

Discretization by use of sinc functions

Following the method described in Chapter 4, we can use sinc functions to describe a band-limited white noise in the discretized form

$$\hat{W}_j(t) = \sigma_j \sum_{n=1}^{N} u_{j,n} \mathrm{sinc}_{\Delta t}(t - n\Delta t). \tag{5.10}$$

Using this in (5.8), we obtain

$$s_{j,n}(t) = \sigma_j \int_0^t \eta_j(t - \tau|\boldsymbol{\theta}_j) \mathrm{sinc}_{\Delta t}(\tau - n\Delta t) d\tau. \tag{5.11}$$

Recall that this formulation has the advantage of decoupling the time step Δt used in discretizing the white noise process from the time step needed for numerical integration of the response.

Frequency-domain discretization

As we have seen in Chapter 2, an alternative representation in the frequency domain is obtained by selecting the basis functions to be the sine and the cosine functions. For a selected frequency discretization $k\Delta\omega$, $k \in [1, \ldots, K]$ with $\Delta\omega = \Omega/K$, the discretized excitation is written as

$$\hat{F}_j(t) = \sum_{k=0}^{K} \sigma_{j,k}[u_{j,k} \sin(\omega_k t) + u_{j,K+k} \cos(\omega_k t)] = \boldsymbol{s}_j(t)\boldsymbol{u}_j, \tag{5.12}$$

$$\boldsymbol{s}_j(t) = [s_{j,1}(t), \ldots, s_{j,K}(t), s_{j,K+1}(t), \ldots, s_{j,2K}(t)], \tag{5.13}$$

$$s_{j,k}(t) = \sigma_{j,k} \sin(\omega_k t), \tag{5.14}$$

$$s_{j,K+k}(t) = \sigma_{j,k} \cos(\omega_k t), \tag{5.15}$$

$$\sigma_{j,k} = \sqrt{2S_j(\omega_k|\boldsymbol{\theta}_j)\Delta\omega}, \tag{5.16}$$

$$\boldsymbol{u}_j = [u_{j,1}, \ldots, u_{j,K}, u_{j,K+1}, \ldots, u_{j,2K}], \tag{5.17}$$

in which $S_j(\omega|\boldsymbol{\theta}_j)$ is a parametric PSD and $\boldsymbol{\theta}_j$ is a set of shape parameters. As described in Chapter 2, the frequency-domain discretization leads to a periodic process having the period $T = 2\pi/\Delta\omega$.

5.3 Multi-component TELM analysis

In this section we extend the single-component, time- and frequency-domain TELM to the case of a nonlinear structure subjected to multi-component excitations. We assume the excitation processes are zero-mean, statistically independent and Gaussian so that they can be discretized in the manner described in Section 5.2. In the two subsections we describe identification of the tail-equivalent linear system (TELS) for time- and frequency-domain analyses. This is done by identifying the IRS (for time-domain analysis) and the FRF (for frequency-domain analysis) for the response quantity of interest with respect to each input excitation component for a given threshold x and time point t_x. Once the TELS is identified, methods of linear random vibration analysis are used to compute the response statistics of interest.

Multi-component time-domain TELM

Let $X(t,\boldsymbol{u})$ denote a generic response quantity of interest and $g(\boldsymbol{u},x,t_x)=x-X(t_x,\boldsymbol{u})$ denote the associated limit-state function for a selected threshold x and time point $t_x\equiv t_N$. For a linear system, let $h_j(t)$ denote the IRF of the response quantity with respect to the j^{th} excitation component. Using superposition over the input components in the time domain, the response of interest is given by

$$X(t,\boldsymbol{u}) = \sum_{j=1}^{J}[h_j(t)*F_j(t)]U(t). \tag{5.18}$$

Using the discretization (5.8)-(5.9),

$$X(t,\boldsymbol{u}) = \sum_{j=1}^{J}\sum_{n=1}^{N}\int_0^t h_j(t-\tau)s_{j,n}(\tau)d\tau u_{j,n} = \boldsymbol{a}(t)\boldsymbol{u}, \tag{5.19}$$

where

$$\boldsymbol{a}(t) = [a_{1,1}(t),\ldots,a_{1,N},\ldots,a_{J,1}(t)\ldots,a_{J,N}], \tag{5.20}$$
$$a_{j,n} = \int_0^t h_j(t-\tau)s_{j,n}(\tau)d\tau, \tag{5.21}$$
$$\boldsymbol{u} = [u_{1,1},\ldots,u_{1,N},\ldots,u_{J,1},\ldots,u_{J,N}]^\intercal, \tag{5.22}$$

or in compact form

$$\boldsymbol{a}(t) = [\boldsymbol{a}_1(t),\ldots,\boldsymbol{a}_J(t)], \tag{5.23}$$
$$\boldsymbol{a}_j(t) = [a_{j,1}(t),\ldots,a_{j,N}(t)], \tag{5.24}$$
$$\boldsymbol{u} = [\boldsymbol{u}_1^\intercal,\ldots,\boldsymbol{u}_J^\intercal]^\intercal. \tag{5.25}$$

where $\boldsymbol{u}_j$ is the same as in (5.7).

If the system is linear, the limit-state surface $g(\boldsymbol{u},x,t_x)=x-X(t_x,\boldsymbol{u})=x-\boldsymbol{a}(t_x)\boldsymbol{u}=0$ is still a hyperplane but in a new augmented standard normal space of dimension NJ. Given the augmented gradient vector in (5.20) and the augmented design point and the corresponding reliability index are given in closed form as in (2.15)-(2.16).

In the nonlinear case, given x and t_x, the design point $\boldsymbol{u}^*$ is obtained as the solution to the new augmented constrained optimization problem (2.19) with $\boldsymbol{u}\in\mathbb{R}^{JN}$. Given the augmented design point $\boldsymbol{u}^*$, the augmented $\boldsymbol{a}(t_x)$ is computed from (2.17) in the standard normal space of dimension NJ. This completely defines the TELS for the nonlinear case in the new augmented space. The IRF with respect to the j^{th} input component is computed by solving the set of equations

$$\sum_{m=1}^{M} h_j(t_x-t_m)s_{j,n}(t_m)\Delta t = a_{j,n}(t_x), \quad n\in[1,\ldots,N], \quad m\in[1,\ldots,M], \tag{5.26}$$

where M denotes the number of integration time steps and $t_M \equiv t_x$. Here, $M \equiv N$ since the time steps for the numerical integration and for the discretization of the input process are one and the same. The above set of equations can be written in a matrix form as in (4.53)

$$\boldsymbol{S}_j \boldsymbol{h}_j = \boldsymbol{a}_j^{\intercal}(t_M), \tag{5.27}$$

with

$$\boldsymbol{S}_j = \Delta t \begin{bmatrix} s_{j,1}(t_1) & \dots & s_{j,1}(t_M) \\ \vdots & \ddots & \vdots \\ 0 & \dots & s_{j,N}(t_M) \end{bmatrix}, \tag{5.28}$$

$$\boldsymbol{h} = \begin{bmatrix} h_j(t_M - t_1) \\ \vdots \\ h_j(t_M - t_M) \end{bmatrix}, \quad \boldsymbol{a}_j(t_M) = \begin{bmatrix} a_{j,n}(t_M) \\ \vdots \\ a_{j,N}(t_M) \end{bmatrix}. \tag{5.29}$$

However in different type of discretizations, based on different basis functions such as the sinc functions, the time resolution M can be selected independently from the number of random variables N. In particular for each j, the system of equations (5.28) is rectangular in form. As we stated in section (4.5), the solution of each j system can be found as the min-norm solution, or better by considering the j IRF as a band limited function that can be expressed in terms of sinc expansion. Then, it is sufficient to compute the samples of the j IRF and to reconstruct the continuous function by the sinc expansion. In other words, we enforce $M' \equiv N$, where M' is the minimum sufficient number of time points to describe the IRF with the sinc expansion. This leads to a system of N equations with N unknowns, which is solved by inversion as before. The size of this new j systems is much smaller than in the original formulation. Once the N samples of the j IRF are computed, the IRF is completely determined by the sinc expansion i.e.

$$h_j(t) \simeq \sum_{n=0}^{N} h_j(n\Delta t)\mathrm{sinc}_{\Delta t}(t - n\Delta t). \tag{5.30}$$

Multi-component frequency-domain TELM

In the frequency domain, the Fourier transform of the steady-state response of a linear system is is given by the superposition rule

$$\bar{X}(\omega) \quad = \quad \sum_{j=1}^{J} H_j(\omega)\bar{F}_j(\omega), \tag{5.31}$$

where $H_j(\omega)$ denotes the FRF relative to the j^{th} excitation component. Given the frequency-domain discretization of the input described in (5.12), the steady-state response of the linear system is given

by

$$X(t,\boldsymbol{u}) = \sum_{j=1}^{J}\sum_{k=1}^{K}\sigma_{j,k}|H_j(\omega_k)|[u_{j,k}\sin(\omega_k t-\varphi_{j,k})+u_{j,K+k}\cos(\omega_k t-\varphi_{j,k})] \quad (5.32)$$

$$= \boldsymbol{a}(t)\boldsymbol{u}, \quad (5.33)$$

where

$$\boldsymbol{a}(t) = [a_{1,1}(t),\ldots,a_{1,2K}(t),\ldots,a_{J,1}(t),\ldots,a_{J,2K}(t)], \quad (5.34)$$

$$a_{j,k}(t) = \sigma_{j,k}|H_j(\omega_k)|\sin(\omega_k t-\varphi_{j,k}), \quad (5.35)$$

$$a_{j,K+k}(t) = \sigma_{j,k}|H_j(\omega_k)|\cos(\omega_k t-\varphi_{j,k}), \quad (5.36)$$

$$\boldsymbol{u} = [u_{1,1},\ldots,u_{1,2K},\ldots,u_{J,1},\ldots,u_{J,2K}]^\intercal, \quad (5.37)$$

or written in a more compact form

$$\boldsymbol{a}(t) = [\boldsymbol{a}_1(t),\ldots,\boldsymbol{a}_J(t)], \quad (5.38)$$

$$\boldsymbol{a}_j(t) = [a_{j,1}(t),\ldots,a_{j,2K}], \quad (5.39)$$

$$\boldsymbol{u} = [\boldsymbol{u}_1^\intercal,\ldots,\boldsymbol{u}_J^\intercal]^\intercal, \quad (5.40)$$

in which $\varphi_{j,k}=\tan^{-1}\left[\mathrm{Im}(H_j(\omega_k))/\mathrm{Re}(H_j(\omega_k))\right]$ is the phase angle of the FRF and $\boldsymbol{u}_j$ is as in (5.17). In the nonlinear case, the augmented $\boldsymbol{u}^*$ is obtained by solving the optimization problem in the augmented space of dimension $2KJ$. This gives the augmented gradient vector $\boldsymbol{a}(t_x)$ according to (2.17). The modulus and phase angle of the FRF with respect to the j^{th} input component are then computed as

$$|H_j(\omega_k)| = \frac{\sqrt{a_{j,k}(t_x)^2+a_{j,K+k}(t_x)^2}}{\sigma_{j,k}}, \quad (5.41)$$

$$\varphi_{j,k} = \omega_k t_x - \tan^{-1}\left[\frac{a_{j,k}}{a_{j,K+k}}\right] k\in[1,\ldots,K], \text{ and } \varphi_{j,k}\in[-\pi,\pi]. \quad (5.42)$$

5.4 Direct differentiation method in multi-component TELM analysis

In our implementation of TELM analysis, the solution of the optimization problem (2.19), either in its original or augmented version, is obtained by using a gradient-based constrained optimization algorithm, such as the improved HLRF algorithm by Zhang and Der Kiureghian [112]. The computational cost of this solution method is related to the number of gradient computations. In Chapter 2 we have mentioned that an efficient scheme to compute the gradient is the direct differentiation method (DDM) proposed by by Zhang and Der Kiureghian [111]. In this section we formulate the DDM in the context of multi-component analysis. We discuss the use of this formulation in conjunction with the time-, and frequency-domain TELM, and sinc interpolation functions.

In finite-element formulation of the stochastic dynamic problem, a selected response quantity of interest, $X(t, \boldsymbol{u})$, is generally obtained as a function of the global response vector $\boldsymbol{U}(t)$ and, when the response is path-dependent, of its time derivative $\dot{\boldsymbol{U}}(t)$. Here, $\boldsymbol{U}(t)$ denotes the vector of displacements at the global degrees of freedom of the structure. Thus, we can write

$$X(t, \boldsymbol{u}) \quad = Q(\boldsymbol{U}(t), \dot{\boldsymbol{U}}(t)). \tag{5.43}$$

The quantities $\boldsymbol{U}(t)$ and $\dot{\boldsymbol{U}}(t)$ are of course implicit functions of $\boldsymbol{u}$, but for simplicity of the notation we have not indicated this. Taking derivative with respect to a generic parameter h, we have

$$\frac{\partial X(t, \boldsymbol{u})}{\partial h} = \frac{\partial Q(\cdot)}{\partial \boldsymbol{U}(t)} \frac{\partial \boldsymbol{U}(t)}{\partial h} + \frac{\partial Q(\cdot)}{\partial \dot{\boldsymbol{U}}(t)} \frac{\partial \dot{\boldsymbol{U}}(t)}{\partial h} + \frac{\partial Q(\cdot)}{\partial h}\Big|_{(\boldsymbol{U}(t), \dot{\boldsymbol{U}}(t) fixed}. \tag{5.44}$$

Given $Q(\cdot)$, $\partial \boldsymbol{U}(t)/\partial h$ and $\partial \dot{\boldsymbol{U}}(t)/\partial h$ need to be computed by sensitivity analysis [46, 47]. The algorithm for finding the design point requires computation of the gradient of the response of interest with respect to the vector of random variables defining the reliability problem. In the present case, the random variables are the standard normal variables $\boldsymbol{u}$ used in defining the input excitation(s) in a discrete form. Let $\nabla_{\boldsymbol{u}} X(t, \boldsymbol{u})$ denote the gradient vector; $\partial X(t, \boldsymbol{u})/\partial h$ is an element of this vector, where $h \equiv u_{j,n}$ for the discretization in the time domain and sinc interpolation formula. In the frequency-domain formulation since the index k belongs to the set $[1 \dots K]$ while the total number of random variables for each j is $2K$, we need to introduce a dummy index to write the complete gradient. Defining this dummy index as $\kappa \in [1 \dots 2K]$, we can define $h \equiv u_{j,\kappa}$. Although, more generally, h in DDM can be any material or load parameter, in the present application it only represents load parameters.

Following [46], consider the general equation of motion of a multi-degree-of-freedom (MDOF) nonlinear system defined by

$$\boldsymbol{M}\ddot{\boldsymbol{U}}(t) + \boldsymbol{C}\dot{\boldsymbol{U}}(t) + \boldsymbol{R}(\boldsymbol{U}(t), \dot{\boldsymbol{U}}(t)) \quad = \quad \boldsymbol{P}\boldsymbol{F}(t), \tag{5.45}$$

where $\boldsymbol{M}$ is the mass matrix, $\boldsymbol{C}$ is the damping matrix, $\boldsymbol{R}(\cdot)$ the restoring force vector, and $\boldsymbol{P}$ is the load-distribution matrix. Taking derivative of this equation with respect to h, we have

$$\boldsymbol{M}\frac{\partial \ddot{\boldsymbol{U}}(t)}{\partial h} + \boldsymbol{C}\frac{\partial \dot{\boldsymbol{U}}(t)}{\partial h} + \frac{\partial \boldsymbol{R}(\boldsymbol{U}(t), \dot{\boldsymbol{U}}(t))}{\partial h} \quad = \quad \boldsymbol{P}\frac{\partial \boldsymbol{F}(t)}{\partial h}. \tag{5.46}$$

Introducing the vector $\mathfrak{U}(t) = \partial \boldsymbol{U}(t)/\partial h$, we have

$$\boldsymbol{M}\ddot{\mathfrak{U}}(t) + \boldsymbol{C}\dot{\mathfrak{U}}(t) + \frac{\partial \boldsymbol{R}(\boldsymbol{U}(t), \dot{\boldsymbol{U}}(t))}{\partial h} \quad = \quad \boldsymbol{P}\frac{\partial \boldsymbol{F}(t)}{\partial h}. \tag{5.47}$$

Two terms must be evaluated in (5.47): the sensitivity of the restoring force term $\partial \boldsymbol{R}(\boldsymbol{U}(t), \dot{\boldsymbol{U}}(t))/\partial h$, and the sensitivity of the input term $\partial \boldsymbol{F}(t)/\partial h$. We start with the latter one which depends from the selected discretization scheme.

Sensitivity of the input term

In this subsection we examine the load sensitivity $\partial \boldsymbol{F}(t)/\partial h$, which depends on the discretization scheme used. In a time-domain discretization scheme with $h = u_{j,n}$, $n \in [1, \ldots, N]$, $j \in [1, \ldots, J]$, we can write

$$\frac{\partial \hat{\boldsymbol{F}}(t)}{\partial u_{j,n}} = \left[\frac{\partial \hat{F}_1(t)}{\partial u_{j,n}}, \ldots, \frac{\partial \hat{F}_J(t)}{\partial u_{j,n}}\right]^\intercal = \left[\frac{\partial \boldsymbol{s}_1(t)\boldsymbol{u}_1}{\partial u_{j,n}}, \ldots, \frac{\partial \boldsymbol{s}_J(t)\boldsymbol{u}_J}{\partial u_{j,n}}\right]^\intercal \tag{5.48}$$

$$= [0, \ldots, 0, s_{j,n}(t), 0, \ldots 0]^\intercal, \tag{5.49}$$

where $s_{j,n}(t)$ has the form in (5.9) for the original time-domain formulation or (5.11) for the formulation in terms of sinc functions. In the former case, $s_{j,n}(t) = 0$ for $t < t_n$. This means that (5.48), (5.49) at time t depends only on the past history of loading and not on the future loading. This is not the case when we use the sinc basis functions or as we will see in the frequency domain. Equation (5.49) can be written in compact notation by introducing the vector $\boldsymbol{\mathcal{S}}(t)$ as

$$\boldsymbol{\mathcal{S}}_{j,n}(t) \triangleq [0 \ldots s_{j,n} \ldots 0]^\intercal, \tag{5.50}$$

which is a vector of dimension $J \times 1$ collecting all zeros with the exception of the single base function $s_{j,n}$ located at position j. We adopt the symbol $\boldsymbol{\mathcal{S}}$ to underline the fact that the sensitivity of the load parameter is essentially a base function of a particular discretization scheme.

In the frequency-domain formulation with $h = u_{j,\kappa}$ the gradient of the load vector is given by

$$\frac{\partial \hat{\boldsymbol{F}}(t)}{\partial u_{j,\kappa}} = \left[\frac{\partial \hat{F}_1(t)}{\partial u_{j,\kappa}} \cdots \frac{\partial \hat{F}_J(t)}{\partial u_{j,\kappa}}\right]^\intercal = \left[\frac{\partial \boldsymbol{s}_1(t)\boldsymbol{u}_1}{\partial u_{j,\kappa}} \cdots \frac{\partial \boldsymbol{s}_J(t)\boldsymbol{u}_J}{\partial u_{j,\kappa}}\right]^\intercal \tag{5.51}$$

$$= [0 \ldots s_{j,\kappa}(t) \ldots 0]^\intercal \tag{5.52}$$

$$= [0 \ldots \sigma_{j,k} \sin(\omega_k t) \ldots 0]^\intercal \text{ for } \kappa \in [1, \ldots, K] \tag{5.53}$$

$$= [0 \ldots \sigma_{j,k} \cos(\omega_k t) \ldots 0]^\intercal \text{ for } \kappa \in [K+1, \ldots, 2K]. \tag{5.54}$$

As we have done in the time-domain context we define the vector $\boldsymbol{\mathcal{S}}(t)$ as

$$\boldsymbol{\mathcal{S}}_{j,\kappa}(t) \triangleq \begin{array}{l} [0 \ldots \sigma_{j,k} \sin(\omega_k t) \ldots 0]^\intercal \text{ for } \kappa \in [1, \ldots, K] \\ [0 \ldots \sigma_{j,k} \cos(\omega_k t) \ldots 0]^\intercal \text{ for } \kappa \in [K+1, \ldots, 2K]. \end{array} \tag{5.55}$$

In this case the sensitivity is computed as response to an harmonic load with frequency ω_k. Hereafter, for simplicity of notation we drop the subscripts of on $\boldsymbol{\mathcal{S}}_{j,n}(t)$ and $\boldsymbol{\mathcal{S}}_{j,\kappa}(t)$.

Sensitivity of the restoring force term

In this section we examine the sensitivity of the restoring force vector, $\partial \boldsymbol{R}(\boldsymbol{U}(t), \dot{\boldsymbol{U}}(t))/\partial h$, which is independent from the discretization employed. Before employing the derivative over the parameter h, it is crucial to discretize the variable t. In fact, the space of the continuous solution $\boldsymbol{\mathcal{U}}(t)$ is different from the space of the discrete solution $\boldsymbol{\mathcal{U}}(t_m)$. Introducing the "computational" discretization t_m with $m \in [1, \ldots, M]$ and $\Delta t_M = T/M$,[1] we define: $\boldsymbol{U}_{m+1} = \boldsymbol{U}(t_{m+1})$, $\boldsymbol{\mathcal{U}}_{m+1} = \boldsymbol{\mathcal{U}}(t_{m+1})$, and

[1] The time discretization is the same used to solve (5.45)

$\boldsymbol{\mathcal{S}}_{m+1} = \boldsymbol{\mathcal{S}}(t_{m+1})$ and write the (5.47) as

$$\boldsymbol{M}\ddot{\mathfrak{U}}_{m+1} + \boldsymbol{C}\dot{\mathfrak{U}}_{m+1} + \frac{\partial \boldsymbol{R}(\boldsymbol{U}_{m+1}, \dot{\boldsymbol{U}}_{m+1})}{\partial h} = \boldsymbol{P}\boldsymbol{\mathcal{S}}_{m+1}, \tag{5.56}$$

where

$$\frac{\partial \boldsymbol{R}(\boldsymbol{U}_{m+1}, \dot{\boldsymbol{U}}_{m+1})}{\partial h} = \frac{\partial \boldsymbol{R}(\boldsymbol{U}_{m+1}, \dot{\boldsymbol{U}}_{m+1})}{\partial \boldsymbol{U}_{m+1}}\mathfrak{U}_{m+1} + \tag{5.57}$$

$$\frac{\partial \boldsymbol{R}(\boldsymbol{U}_{m+1}, \dot{\boldsymbol{U}}_{m+1})}{\partial \dot{\boldsymbol{U}}_{m+1}}\dot{\mathfrak{U}}_{m+1} + \tag{5.58}$$

$$\frac{\partial \boldsymbol{R}(\boldsymbol{U}_{m+1}, \dot{\boldsymbol{U}}_{m+1})}{\partial h}\Big|_{\boldsymbol{U}_{m+1}, \dot{\boldsymbol{U}}_{m+1}}. \tag{5.59}$$

The differential term in (5.57) is defined as the consistent tangent stiffness matrix $\boldsymbol{K}_{m+1}$ [100], and analogously the differential term in (5.58) is defined as the consistent tangent damping matrix due to material viscosity $\boldsymbol{C}^{visc}_{m+1}$, i.e.

$$\boldsymbol{K}_{m+1} = \frac{\partial \boldsymbol{R}(\boldsymbol{U}_{m+1}, \dot{\boldsymbol{U}}_{m+1})}{\partial \boldsymbol{U}_{m+1}}, \tag{5.60}$$

$$\boldsymbol{C}^{visc}_{m+1} = \frac{\partial \boldsymbol{R}(\boldsymbol{U}_{m+1}, \dot{\boldsymbol{U}}_{m+1})}{\partial \dot{\boldsymbol{U}}_{m+1}}. \tag{5.61}$$

For an exhaustive discussion on the nature of $\boldsymbol{K}_{m+1}$ and $\boldsymbol{C}^{visc}_{m+1}$, the reader should consult a standard nonlinear finite element text, such as [9, 115]. Here we limit our discussion by noticing that $\boldsymbol{K}_{m+1}$ is in its general form and indeed it is composed by a geometrical term and a material term, i.e. $\boldsymbol{K}_{m+1} = \boldsymbol{K}^{G}_{m+1} + \boldsymbol{K}^{mat}_{m+1}$, where $\boldsymbol{K}^{G}_{m+1}$ is the geometrical stiffness and $\boldsymbol{K}^{mat}_{m+1}$ is the material stiffness. Moreover, in this dissertation we do not consider material viscosity, hence consequently (5.61) is neglected.

For problems involving inelasticity at the material level, computation of (5.59) is particularly subtle; thus, we will devote special attention to it later. For now, we define the vector $\boldsymbol{\mathcal{R}}_{m+1}$ as

$$\boldsymbol{\mathcal{R}}_{m+1} \triangleq -\frac{\partial \boldsymbol{R}(\boldsymbol{U}_{m+1}, \dot{\boldsymbol{U}}_{m+1})}{\partial h}\Big|_{\boldsymbol{U}_{m+1}, \dot{\boldsymbol{U}}_{m+1}}, \tag{5.62}$$

so that we can write (5.56) as

$$\boldsymbol{M}\ddot{\mathfrak{U}}_{m+1} + \boldsymbol{C}\dot{\mathfrak{U}}_{m+1} + \boldsymbol{K}_{m+1}\mathfrak{U}_{m+1} = \boldsymbol{P}\boldsymbol{\mathcal{S}}_{m+1} + \boldsymbol{\mathcal{R}}_{m+1}. \tag{5.63}$$

Two observations must be made. First, the inverse of the consistent tangent is already available at each discrete point m from the solution of the discretize version of the general equation of motion (5.45). Second, (5.63) is a linear equation. The linearity of (5.63) is a cornerstone of the DDM scheme and the essence of its efficiency. The reader, however, should recognize that in TELM analysis we need to solve NJM or $2KJM$ of these linear systems.

It is time now to come back to the definition of $\boldsymbol{\mathcal{R}}_{m+1}$. Problems involving inelasticity in the material model depend upon the previous loading history, consequently special considerations need

to be made for this term. An inelastic material model is defined by a set of constitutive history variables, which are time dependent and denoted with the vector $\boldsymbol{\theta}^{mat}(t)$ [2]. In problems with inelasticity at the material level, (5.62) is not only a function of $\boldsymbol{\theta}^{mat}(t)$ but also of the sensitivity of $\boldsymbol{\theta}^{mat}(t)$, [111] i.e.

$$\boldsymbol{\mathcal{R}}_{m+1} = f\left(\ldots, \frac{\partial \boldsymbol{\theta}^{mat}_{m+1}}{\partial h}\Big|_{\substack{\boldsymbol{U}_{m+1} \\ \dot{\boldsymbol{U}}_{m+1}}}, \frac{\partial \boldsymbol{\theta}^{mat}_{m}}{\partial h}\right). \tag{5.64}$$

As we can see from (5.64), $\boldsymbol{\mathcal{R}_{m+1}}$ is computed with the assumption of fixed *current* displacement and velocity. No assumptions however are made for *previous* time steps; to underline this difference the term $\partial \boldsymbol{\theta}^{mat}_{m}/\partial h$ is written explicitly with no "fixed" assumptions. Consequently we cannot store directly the variable $\partial \boldsymbol{\theta}^{mat}_{m+1}/\partial h\Big|_{\substack{\boldsymbol{U}_{m+1} \\ \dot{\boldsymbol{U}}_{m+1}}}$ otherwise in the next time step (5.64) will be computed incorrectly. To address this problem, the sensitivity analysis must be split in two phases:

Phase 1 The derivatives of the material parameters, $\partial \boldsymbol{\theta}^{mat}_{m+1}/\partial h\Big|_{\substack{\boldsymbol{U}_{m+1} \\ \dot{\boldsymbol{U}}_{m+1}}}$, are computed with assumption of fixed displacements and velocities; then (5.64) is assembled and then the sensitivities variables $\boldsymbol{\mathcal{U}}_{m+1}(t)$ and $\dot{\boldsymbol{\mathcal{U}}}_{m+1}(t)$ are computed by solving (5.63).

Phase 2 Once the the sensitivities variables $\boldsymbol{\mathcal{U}}_{m+1}(t)$ and $\dot{\boldsymbol{\mathcal{U}}}_{m+1}(t)$ are available, the derivatives of the material parameters, $\partial \boldsymbol{\theta}^{mat}_{m+1}/\partial h$, are computed with no assumption of fixed displacements or velocities. This is used in the next step for computing $\boldsymbol{\mathcal{R}}$.

A concrete example involving sensitivity of a Bouc-Wen model is described in [46]. The computation of (5.64) depends on the material model adopted. However, this selection must be made under the condition of differentiability of the limit state surface $g(\boldsymbol{u}, x, t_x)$. This translates into selecting material models that have smooth behavior in the loading path. For a comprehensive discussion in this topic and for a list of "smoothed" material models the reader should consult [46, 47].

DDM Summary

In this subsection we provide a step by step procedure to compute the gradient of the response in TELM analysis.

Computation of the gradient of the selected response by DDM

1. Select initial conditions $\boldsymbol{U}_{in}$, $\dot{\boldsymbol{U}}_{in}$, $\ddot{\boldsymbol{U}}_{in}$ and $\boldsymbol{\theta}^{mat}_{in}$ and a time discretization t_m with $m \in [1, \ldots, M]$ and $\Delta t_M = T/M$.

[2] For readers familiar with problems involving inelasticity at the material level, these material history variables are for example the internal hardening, and the back stress in the classical $J2$ plasticity mode [99].

2. Solve

$$\boldsymbol{M}\ddot{\boldsymbol{U}}_{m+1} + \boldsymbol{C}\dot{\boldsymbol{U}}_{m+1} + \boldsymbol{R}(\boldsymbol{U}_{m+1}, \dot{\boldsymbol{U}}_{m+1} | \boldsymbol{\theta}^{mat}_{m+1}) \;=\; \boldsymbol{P}\boldsymbol{F}_{m+1}. \tag{5.65}$$

To solve (5.65) classical time-stepping schemes such as the well-known Newmark and Wilson scheme can be used.

- $M \equiv N$ in the classical time domain analysis.
- $M \not\equiv N$ if basis function such as the sinc are adopted. Usually $M > N$ to guarantee convergence in solving (5.65).
- M is selected to guarantee convergence of (5.65), in frequency domain analysis.

3. For a given time step $m+1$, $\boldsymbol{U}_{m+1}$, $\dot{\boldsymbol{U}}_{m+1}$, $\ddot{\boldsymbol{U}}_{m+1}$, $\boldsymbol{K}^{-1}_{m+1}$ and $\boldsymbol{\theta}^{mat}_{m+1}$ are available from the solution of (5.65) and $\boldsymbol{U}_m$, $\dot{\boldsymbol{U}}_m$, $\ddot{\boldsymbol{U}}_m$, $\boldsymbol{\theta}^{mat}_m$ and $\partial\boldsymbol{\theta}^{mat}_m/\partial h$ from the previous time step m. Call DDM scheme.

   a) Select the random variable $u_{j,n}$ or $u_{j,\kappa}$ for $n \in [1, \ldots, N]$ and $\kappa \in [1, \ldots, 2K]$.

   b) Assemble $\boldsymbol{\mathcal{S}}_{m+1}$ according to (5.50) or (5.55).

   c) Compute the sensitivity of the restoring force term:

      a) **Phase 1**

      - Compute the derivatives of the material parameters according to the selected material model
      $$\left.\frac{\partial\boldsymbol{\theta}^{mat}_{m+1}}{\partial h}\right|_{\substack{\boldsymbol{U}_{m+1}\\ \dot{\boldsymbol{U}}_{m+1}}}.$$
      - Assemble $\boldsymbol{\mathcal{R}}_{m+1}$ according to the selected material model.
      - Solve (5.63) with the same scheme used to solve (5.65).

      a) **Phase 2**

      - Given $\ddot{\boldsymbol{\mathcal{U}}}_{m+1}$, $\dot{\boldsymbol{\mathcal{U}}}_{m+1}$ and $\boldsymbol{\mathcal{U}}_{m+1}$ from phase 1, compute
      $$\frac{\partial\boldsymbol{\theta}^{mat}_{m+1}}{\partial h},$$
      and store it for the next time step iteration.

   d) Repeat steps 3.1-3.3 until $n = N$ or $\kappa = 2K$ and $j = J$.

4. Repeat points 2-3 until $m+1 = M$ and $\nabla_{\boldsymbol{u}} X(t_M, \boldsymbol{u})$ is available.

5.5 Random vibration analysis

A we have seen in Chapter 2, once the TELS is obtained for a given combination of threshold x and time t_x the statistics of the nonlinear responses for the specified threshold are obtained by linear random vibration analysis. By repeated TELM analysis, a sequence of design points for an ordered set of thresholds $x_1 < \ldots < x_p$ is obtained and from this sequence it is possible to directly compute the first-order approximation of the point in time CDF by use of the (2.48) and the first order approximation of the PDF by use of the (2.50). In fact in the multi-component case, (2.48) and (2.50) are still valid by considering the augmented $\boldsymbol{u}^*$ and $\boldsymbol{a}(t_x)$.

Moreover, the IRFs and/or FRFs of each TELS can be used for time- or frequency-domain analysis to compute other statistics of interest, such as the mean up-crossing rate and the first-passage probability. For stationary excitations, a convenient approach is to compute these statistics in the frequency-domain, either by directly employing the frequency-domain discretization and identifying the FRFs, or by discrete Fourier transformations of the IRFs computed by the time domain approach. For each threshold of interest, the q^{th} spectral moment of the response is obtained as a combination of the single FRFs, i.e.

$$\lambda_q(x) = 2\int_0^\infty \omega^q \left(\sum_{j=1}^{J} |H_j(\omega, x)|^2 S_j(\omega|\boldsymbol{\theta}_j) \right) d\omega, \tag{5.66}$$

which using the discrete frequency can be written as

$$\lambda_q(x) = 2\Delta\omega \sum_{k=1}^{K}\sum_{j=1}^{J} \omega_k^q |H_j(\omega_k, x)|^2 S_j(\omega_k|\boldsymbol{\theta}_j), \tag{5.67}$$

where $S_j(\omega|\boldsymbol{\theta}_j)$ is the PSD of the j^{th} excitation component. Once the spectral moments are known for each threshold of interest, classical solutions can be used. For example, for the mean rate of up-crossing of the response of interest, we can use (2.51) and for the CDF of the maximum of the absolute response over an interval $[0, \bar{t}]$ we can make use of (2.53)-(2.54). In this dissertation we limit our analysis to the solution of these statistics by the frequency-domain approach and classical random vibration results. Solutions obtained using structural reliability methods can be found in [37, 38].

5.6 Multi-component TELM analysis, summary

A step-by-step summary to implement the multi-component TELM analysis for a general system is as follow:

1. Select one of the "stochastic" discretization by using one of the (5.8), (5.11) or (5.12). For stationary excitations, the focus of this chapter, one only need to select the appropriate filter for each excitation by choosing $\eta_j(t|\boldsymbol{\theta}_j)$ or $S_j(\omega_k|\boldsymbol{\theta}_j)$.

2. Select the response of interest $X(t_x, \boldsymbol{u})$ and the point in time t_x. For time-domain analysis t_x should be chosen sufficiently large to guarantee the stationarity of the response. This selection depends on the type of structure, load, damping, and material behavior. Define the limit state function(s) by defining the threshold(s) of interest i.e. $g(\boldsymbol{u}, x, t_x) = x - X(t_x, \boldsymbol{u})$.

3. Find the design point $\boldsymbol{u}^*$ for the nonlinear system. This requires repeated solutions of the nonlinear response and its gradient for values of $\boldsymbol{u}$ selected according to an optimization algorithm, such as the improved HLRF. The gradient computation is carried out by using the DDM scheme. Partition $\boldsymbol{u}^*$ to obtain the design point $\boldsymbol{u}_j^*$ for the j^{th} component. Each j partition represents the design point for the j^{th} input component.

4. Define the TELS by computing the augmented $\boldsymbol{a}(t_x)$. In the time domain, the IRF for the j^{th} input component is computed by solving (5.27) for each j. In the frequency domain, the FRF associated with the j^{th} input component is computed by solving (5.41)-(5.42).

5. Determine the statistic of the response. Compute the spectral moments of the response of interest by (5.67) and apply the classical solution of linear random vibration (2.51)-(2.53)-(2.54) for each TELS defined by the threshold of interest. A sequence of thresholds determines the statistical distribution of interest.

5.7 Numerical example

An asymmetric three-degree-of-freedom, one one-story, one-bay frame structure system with non-degrading hysteretic structural members is considered. The lateral force-resisting system consists of two shear walls in the x direction positioned symmetrically and one shear wall in the y direction with eccentricity e relative to the center of mass, see Figure 5.1. The in-plane inelastic behavior of each frames shear wall is described through a non-degrading Bouc-Wen model [8, 14, 109], which is governed by the following set of local differential equations:

$$k[\alpha v(t) + (1-\alpha)z(t)] = q(t), \tag{5.68}$$

$$\dot{z}(t) = -\gamma|\dot{v}(t)||z(t)|^{\hat{n}-1}z(t) - \eta|z(t)|^{\hat{n}}\dot{v}(t) + A\dot{v}(t), \tag{5.69}$$

in which $v(t)$ denotes the deformation (drift) of the shear wall, $q(t)$ denotes the applied shear force, $z(t)$ is the hysteretic response, and parameter α controls the degree of nonlinearity of the model (see 5.69). For the model parameters k, α, γ, η, $\hat{n}$ and A, the values listed in Table 5.1 are employed. The assumed values for the mass m, damping c, and dimensions terms a, b and e are also listed in Table 5.1. Figure 5.2 shows the hysteretic behavior of the frames for the assumed parameter values. Frames are assumed to have negligible out-of-plane stiffness. For the linear case (i.e., for $\alpha = 1$), the natural frequencies of the structure and the mode shapes are depicted in Figure 5.1.

The excitation is a bi-directional base motion, i.e. $J = 2$, described by $F_1 = \ddot{U}_{gx}$ and $F_2 = \ddot{U}_{gy}$, where $\ddot{U}_{gx}$, $\ddot{U}_{gy}$ are statistically independent components of ground acceleration processes in directions x and y, respectively. Two cases of stationary Gaussian excitations are considered: bi-component band-limited white noise having spectral densities $S_1 = S_2 = S$, and a bi-component filtered white noise process. The selected filter for the latter is the canonical Kanai-Tajimi PSD with a central frequency of $\omega_g = 3$[Hz] and bandwidth $\zeta_g = 0.6$ in each direction. In principle the independence condition between the components is not restrictive because for bi-directional input we can always apply a rotational transformation for which the two principal components are uncorrelated. In the Gaussian framework uncorrelation implies statistical independence. However, while we can always make the two components uncorrelated at the same time, we may not be able to make them uncorrelated at different times. In fact there are applications for which the independence assumption can be restrictive. One example in earthquake engineering is the response of a multiply-supported structure to partially coherent support motions. Other examples include wave or wind loading at different locations of a large structure. For this reason further development is needed to extend TELM to these classes of problems.

The load distribution matrix is given by $\boldsymbol{P} = -\boldsymbol{M}\boldsymbol{\iota}$, where the influence matrix, $\boldsymbol{\iota}$, represents the displacements of the mass resulting from static application of unit ground displacements along each degree of freedom (translations in x and y direction and rotation around the center of mass) [24]. Figure 5.3 shows the PSDs for the two cases of excitation and Table 5.1 summarizes the scale parameters, the discretization rules used, and the selected time point t_x at which reliability analysis is performed.

We select as response quantity of interest the horizontal displacement of shear wall 1, i.e., $X(t) = v_1(t)$, and the time $t_x = 12$[s]. We have verified that the duration $[0, 12]$[s] is sufficient to achieve near stationarity condition of the response. Small deformations is assumed so that (5.43) is a linear relationship. Specifically,

$$\boldsymbol{v}(t) = \boldsymbol{A}_f \boldsymbol{U}(t), \tag{5.70}$$

where $\boldsymbol{A}_f$ is the kinematic (compatibility) matrix relating the element deformation with the displacements at the free degrees of freedom of the structure [34]. Finally, the limit-state function is defined by selecting the threshold(s) x, i.e. $g(x, t_x, \boldsymbol{u}) = x - v_1(t_x, \boldsymbol{u})$. We consider failure events occurring during a period T of stationary response, representing the strong-motion phase of the earthquake ground motion. This condition is usually met in far field ground motions. We employ both time- and frequency-domain discretizations for the case of white-noise excitation and only frequency-domain discretization for the case of filtered white-noise excitation. Once the design point is obtained, the TELS is identified in the manner described in the step 4 of the summary procedure described in section 5.6.

It is of interest to examine the so-called design-point excitation and design-point response, which respectively represent realizations of the excitation and response with the highest probability density for a specific response threshold x and time t_x. For $x = 0.12$[m], which corresponds to a 3% drift, and $t_x = 12$[s], fig(5.4) shows the design-point excitation for the bi-directional white-noise input and fig(5.5) shows the same for the bi-directional Kanai-Tajimi colored noise . For the frequency-domain discretization approach, the design point is not only the point with the highest probability density function to achieve the response threshold, but it also represents the vector collecting the coefficients of the Fourier series representing the excitation. Thus, the constrained minimization

problem describes the physical task of finding the orbit of the input with the minimum energy so that the mechanical system is guided into the frontier of the failure domain. TELM analysis gives the opportunity to study the orbit of the excitation and the response under this condition. These orbits are paramount in elastic systems and with this approach we can study their shape for an inelastic structure to gain insight into its behavior. For example, it is of interest to observe that in the case of the white-noise excitation, which contains no predominant frequency, both input components achieve zero acceleration at time t_x, which suggest that the "exact" amount of energy is injected into the system to achieve the target failure event. In the case of color noise, this is not longer valid because the phase between input and response depend from the relationship between the "natural frequencies" and the input predominant frequency. The reader should note that the use of "natural frequencies" is not very appropriate (from here the justification of "·") since we are dealing with nonlinear problems, however the definition of TELS allows to use the vocabulary of linear systems. We have seen in Chapter 2, and we will see soon the same for multi-component TELM, that even for highly softening nonlinear problems, the system tends to preserve "memory" of the natural frequencies.

The design-point response and the orbit of the global response to the design-point excitation is shown in Figure 5.6 for the case of the white-noise input and in Figure 5.7 for the case of the Kanai-Tajimi colored noise. In the white-noise case, the response achieves the prescribed threshold with a zero slope (bottom curve in Figure 5.6). This suggests the velocity response is zero at this time, which also implies zero kinetic energy. In the colored noise case, this is no longer valid due to the presence of memory in the input process. The system achieves the prescribed response threshold with a non-zero velocity and non-zero kinetic energy. The relationship between predominant frequency of the input and natural frequency, determine the difference in phase between input and response. For example if the input frequency is significantly lower than the predominant frequency of the system the input and and the output are "close" in phase. This because the system is "slowly" loaded and the response is almost static. An alternative explanation is given by the fact that the white noise has no memory. Hence, the random variable value at t_x is independent of past and future values. Since it has no effect on the response at the same time, the most likely value of the random pulse there is zero. The Kanai-Tajimi model has memory. Thus, the pulse at t_x is correlated with the earlier and later pulses. As a result, the most likely value of the pulse at t_x for achieving the target response at t_x is not zero, as it also depends on the previous pulses.

For a particular discretization scheme, one can directly compute the IRFs and/or the FRFs of the TELS. For example, in the time-domain discretization, the IRFs are given by (5.27) and the FRFs can be computed by discrete Fourier transform. Likewise, in the frequency-domain discretization, FRFs are given by (5.41), (5.42) and the corresponding IRFs can be computed by discrete inverse Fourier transform. Three values of the threshold, $x = 0.01$[m], $x = 0.06$[m] and $x = 0.12$[m], are selected to examine the variation of the TELS with increasing level of inelasticity. Note that the lower threshold $x = 0.01$[m] corresponds essentially to the linear case. Figure 5.8 shows the IRFs, Figure 5.9 shows the moduli and phase angles of the FRFs, and Figure 5.10 shows the real and imaginary parts of the FRFs, all for the case of bi-component white-noise input. The FRFs are obtained by use of the frequency-domain discretization and the IRFs by discrete Fourier transform. Almost identical IRFs were obtained directly by time-domain discretization and are not displayed in Figure (5.8) to avoid making the graph too busy. Figure 5.11, 5.12 and 5.13 show the corresponding graphs for the case of the bi-component Kanai-Tajimi excitation. Several observations in these

figures are noteworthy. First note that the IRFs for higher threshold decay much faster than those for the lower threshold. Obviously this is due to the effect of hysteresis damping. As already observed in Chapter 2, as the system softens with increasing inelasticity to achieve a higher deformation threshold, the lower-frequency part of the FRF moduli become more pronounced. However, the peaks at the natural frequencies of the linear system are "imprinted" in the memory of the system, even at high thresholds. Also interesting is the contribution of the input component in the direction orthogonal to the response (noted as Component II in Figures 5.8, 5.9, 5.10, 5.11, 5.12 and 5.13). Of course this contribution is due to the coupling effect introduced by the eccentricity of the system. Note, however, that the effect of nonlinearity with increasing threshold is less pronounced in these IRSs and FRFs.

Once the TELS is obtained for a given combination of threshold x and time t_x, the statistics of the nonlinear response are obtained by linear random vibration analysis by following step 5 of the summary in section (5.6). By repeated TELM analysis, a sequence of design points for an ordered set of thresholds $x_1 < x_2 < \ldots < x_p$ is obtained, and from this sequence it is possible to directly compute the first-order approximation of the point-in-time distribution of the stationary response by using (2.50). Figures 5.14 and 5.15 show the reliability index and the complementary CDF of the response of interest as a function of the threshold for the white-noise and Kana-Tajimi bi-component inputs, respectively. The figure compares TELM results with the results of a crude Monte Carlo simulation (shown as one-standard deviation error bars) with a sample size of $100,000$. Also shown with dashed lines are the results of the linear ($\alpha = 1$) system. In the case of the white-noise excitation, the results obtained by time-domain and frequency-domain discretizations are nearly coincident and are shown here as a unique line under the label "TELM." We should note that thresholds higher then $x = 0.12$[m] have more an academic meaning rather then practical, however, they gives an interesting insight of the tail behavior of a highly nonlinear system. It is interesting observe that for this particular system the tail-probability distribution is not too different from that of the elastic system, although the physical behavior is entirely different. However, the distribution of the nonlinear system is clearly non-Gaussian, as the plot of the reliability index versus threshold deviates from a straight line. Finally, the FRFs of each TELS are used for frequency-domain random vibration analysis to compute the mean up-crossing rate and first-passage probability. Figures 5.16 and 5.17 respectively show the mean up-crossing rate and the complementary CDF of the maximum absolute response of the system over a duration $T = 12$[s] of stationary response to the bi-component white-noise and Kanai-Tajimi inputs. It interesting to observe that the system is less reliable for the Kanai-Tajimi excitation. This is because this colored noise excitation has higher spectral density values for lower values of frequencies and, thus, more energy is driven into the softening system, leading to a lower values of reliability index and higher probabilities of failure.

We have seen in Chapter 2 that an important property of TELS is its invariance relative to scaling of the excitation. Thus, the statistics of the response for any scaled version of the excitation is obtained by scaling down the reliability index by the same scale factor, i.e., the reliability index of the response to input $c\boldsymbol{F}(t)$ is simply β/c. This type of analysis is central to obtaining fragility curves in the context of the so-called "incremental dynamic analysis" [104]. Figures 5.18 and 5.19 show the tail probability of the maximum absolute response above threshold $x = 0.12$[m] for the scaled versions of the bi-components white-noise and Kanai-Tajimi excitations, respectively. The abscissa in these figures show the mean peak acceleration for each component of the input. Both excitation components are scaled by the same factor and the results are obtained using the single

design point computed for the original excitation case, which is marked in each figure.

It is of interest to investigate the behavior of the system with varying eccentricity. In all the above analysis, the eccentricity was assumed to be 9% of the lateral dimension of the system. Now, we conduct a parametric study for the fixed threshold $x = 0.12$[m] by varying the eccentricity from 0% up to 30%. Figure 5.20 shows the sequence of reliability index and the probability of failure as function of the relative eccentricity. The graph suggest a "penalty" factor in terms of structural safety that the designer is paying in selecting an eccentric system, or vice-versa it suggest the maximum eccentricity that the structure can be design, for a target reliability index or probability of failure.

5.8 Conclusion

The extension of the tail-equivalent linearization method for multiple stochastic excitations is developed. Following Chapter 2, the method is based on a discrete representation of each excitation component in terms of standard normal random variables. In the time domain discretization and sinc interpolation, the multi-component excitation and response belong to an augmented standard normal space of dimension NJ while in the frequency domain the dimension is $2KJ$. In these augmented spaces the equivalent linear system is defined by matching its design point with that of the nonlinear system for a specific threshold. For each TELS, the IRF or FRF for each component is determined. Once the IRFs or the FRFs are determined, linear random vibration analysis is employed to determine the statistics of interest.

The multi-component TELM analysis is a straightforward extension of the original TELM formulation, which offers a series of advantages to the simulation and ELM methods. First, TELM is able to capture the non-Gaussian distribution of the nonlinear response. Second, TELM is not a parametric method and does not require the selection of a linear model or a set of model parameters as in ELM. The advantage over the classical simulation methods lies in its efficiency. In fact TELM is able to accurately predict small tail probability values which are infeasible with classical simulation methods. The efficiency of TELM lies in efficient computation of the gradient in the improved HLRF algorithm. The number of random variables employed thus is crucial. Both versions, the time-domain and the frequency-domain, give similar and accurate results, even though, the two discretizations have different frequency contents. In particular, for time step $\Delta t = 0.01$[s], the time domain discretization has a cut off frequency of 50[Hz], while the frequency-domain has a cut off frequency of 15[Hz]. The almost identical results suggests that the influence of high-frequency content of the excitation is negligible in softening systems.

The drawbacks of multi-component TELM analysis are the same as those for the single component TELM analysis. In particular, TELM requires considerably more analysis than ELM if one is interested only in the first and second moments. For second-moment analysis, ELM is the appropriate method while TELM is effective for accurate estimation of tail probabilities. Moreover because TELM is based on FORM, there is no measure of the error due to the approximation and thus the accuracy of TELM cannot be estimated in advance. The numerical investigation shows the importance of considering both excitation components in computing the statistics of the response for coupled systems.

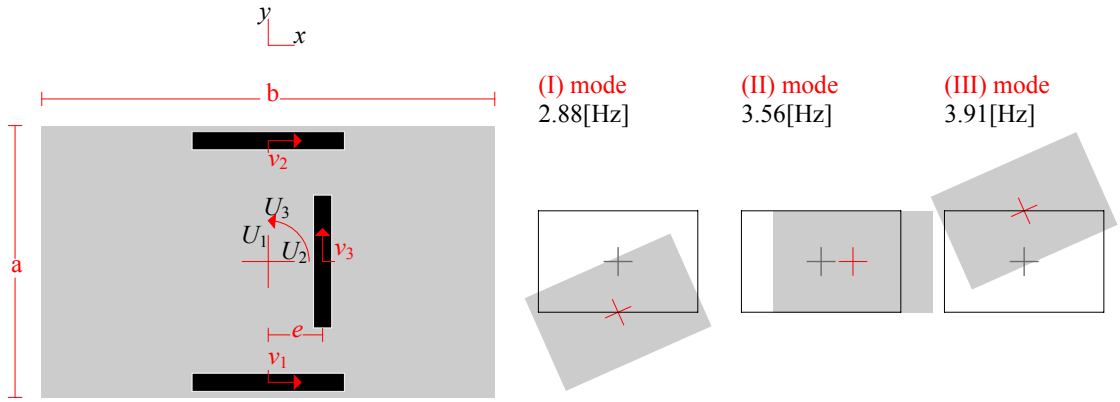

Figure 5.1: Structural archetype

Table 5.1: Structural and Excitation Properties

Structural Properties	a[m]	b[m]	e[m]	$\rho\left[\frac{\text{kg}}{m^2}\right]$				
	6.0	10.0	0.9	500				
Bouc-Wen Properties	α	$c\left[\frac{\text{kNs}}{\text{m}}\right]$	k[kN]	$\gamma\left[\frac{1}{\text{m}^{\hat{n}}}\right]$	$\eta\left[\frac{1}{\text{m}^{\hat{n}}}\right]$	$\hat{n}$	A	u_y
Frame 1 and 2	0.1	8.05E1	1.50E4	$1/2u_y^{\hat{n}}$	$1/2u_y^{\hat{n}}$	5	1	0.04
Frame 3	0.1	1.61E2	3.00E4	$1/2u_y^{\hat{n}}$	$1/2u_y^{\hat{n}}$	5	1	0.04
Excitation Properties	S_1	S_2	t_x	Δt	$\frac{\Delta\omega}{2\pi}$	$\frac{\bar{\omega}}{2\pi}$	N, K	
	$\left[\frac{\text{m}^2}{\text{s}^3}\right]$	$\left[\frac{\text{m}^2}{\text{s}^3}\right]$	[s]	[s]	[Hz]	[Hz]		
time-domain	0.25	0.25	12	0.02		50	2x600	
frequency-domain	0.25	0.25	12		0.1	10	4x200	

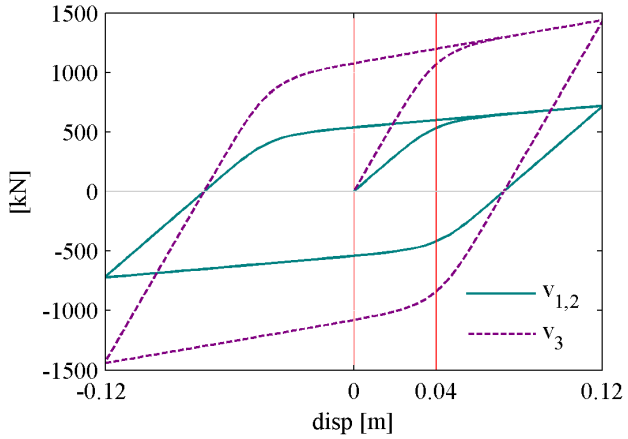

Figure 5.2: Hysteretic behavior of the frames

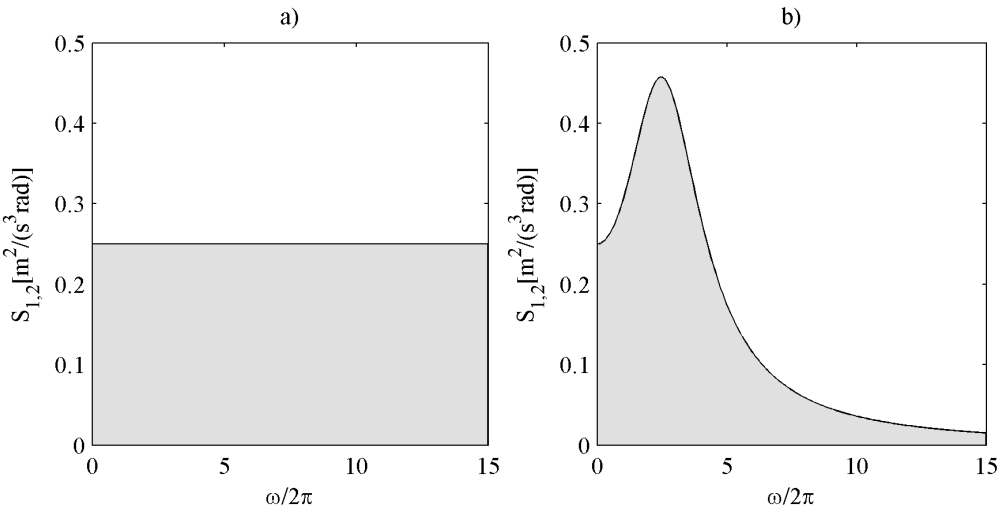

Figure 5.3: Power spectral densities: a) band-limit white noise, b) Kanai-Tajimi

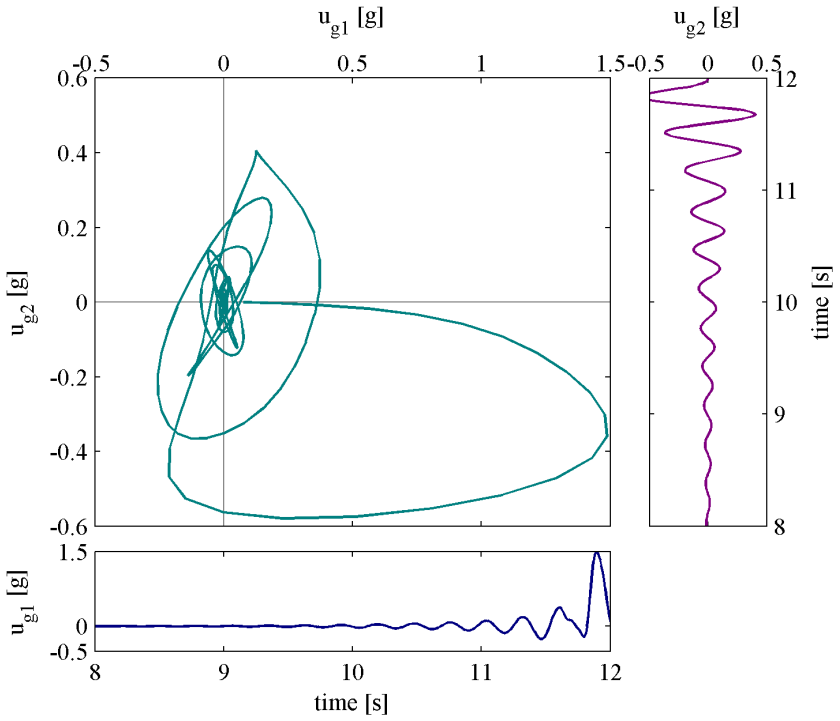

Figure 5.4: Design-point input, white noise input

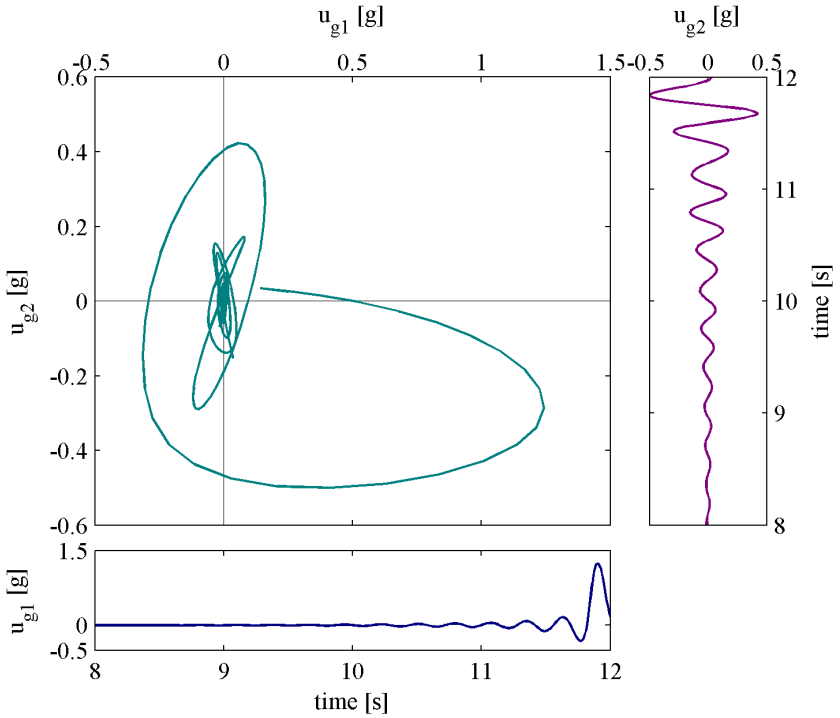

Figure 5.5: Design-point input, Kanai-Tajimi inputs

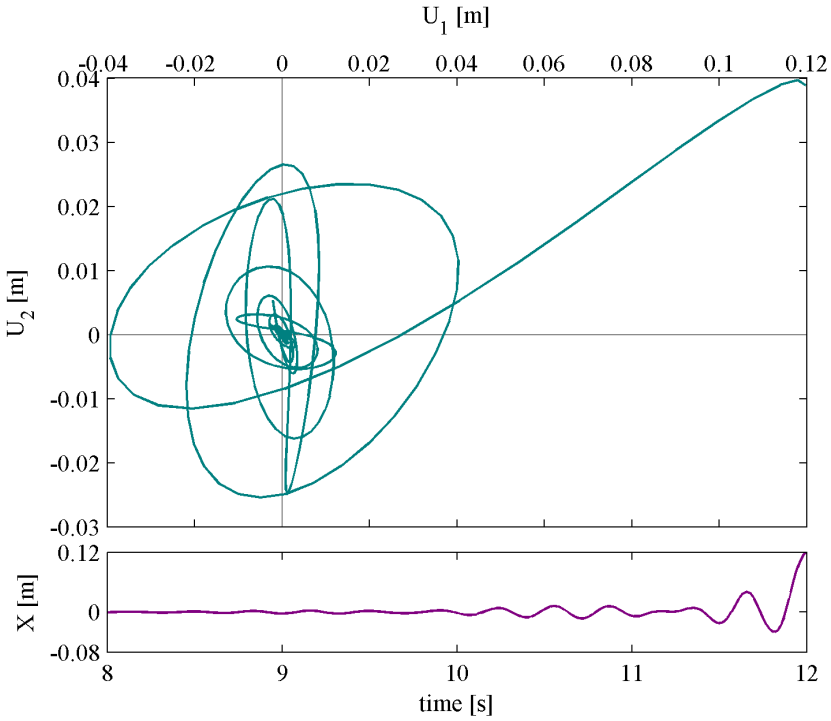

Figure 5.6: Global response to white noise design-point input and design-point response

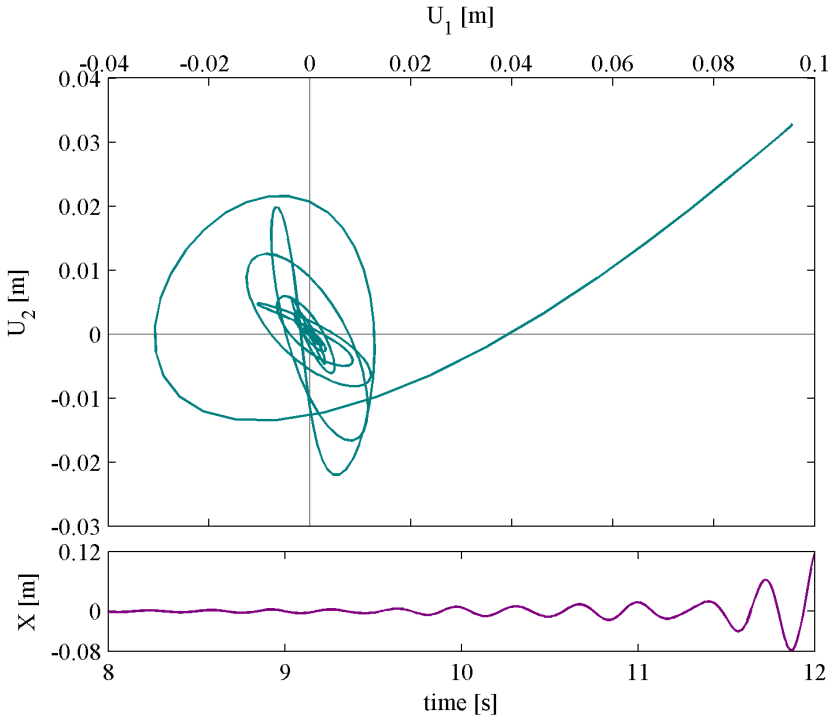

Figure 5.7: Global response to Kanai Tajimi design-point input and design-point response

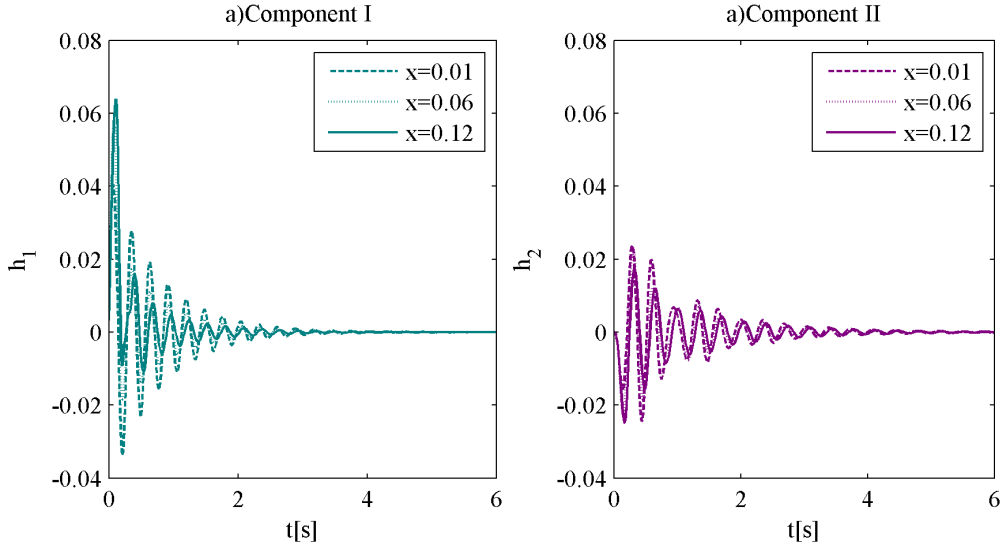

Figure 5.8: Impulse-response functions, white noise inputs

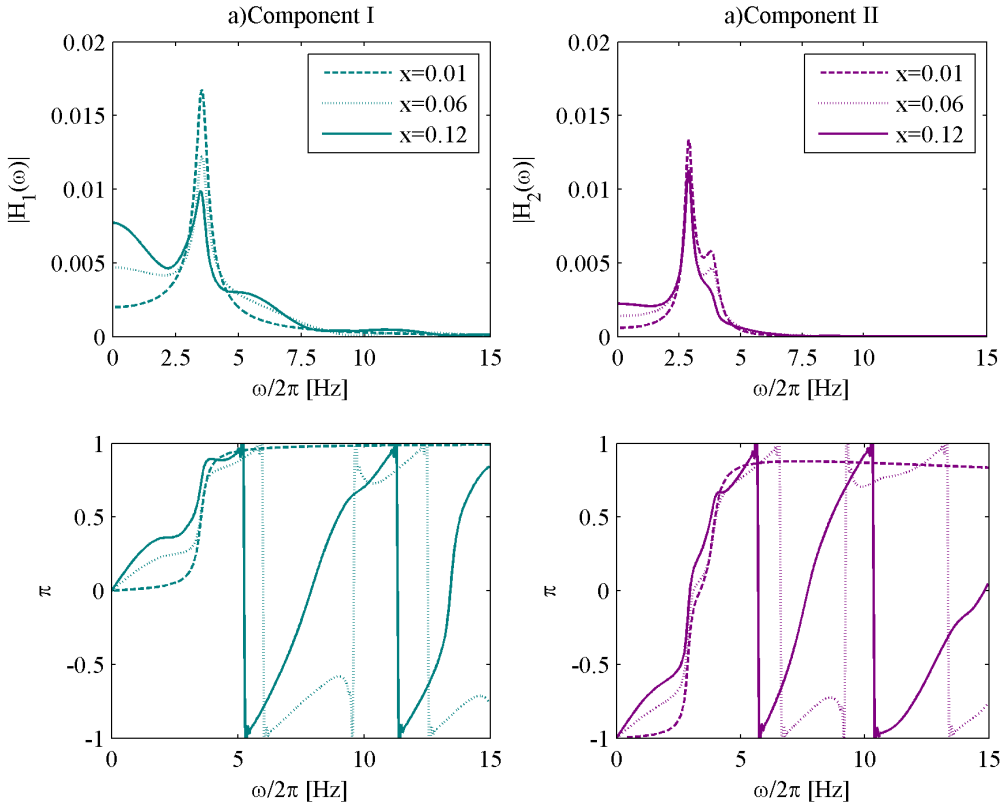

Figure 5.9: Frequency-response functions modulus and phase, white noise inputs

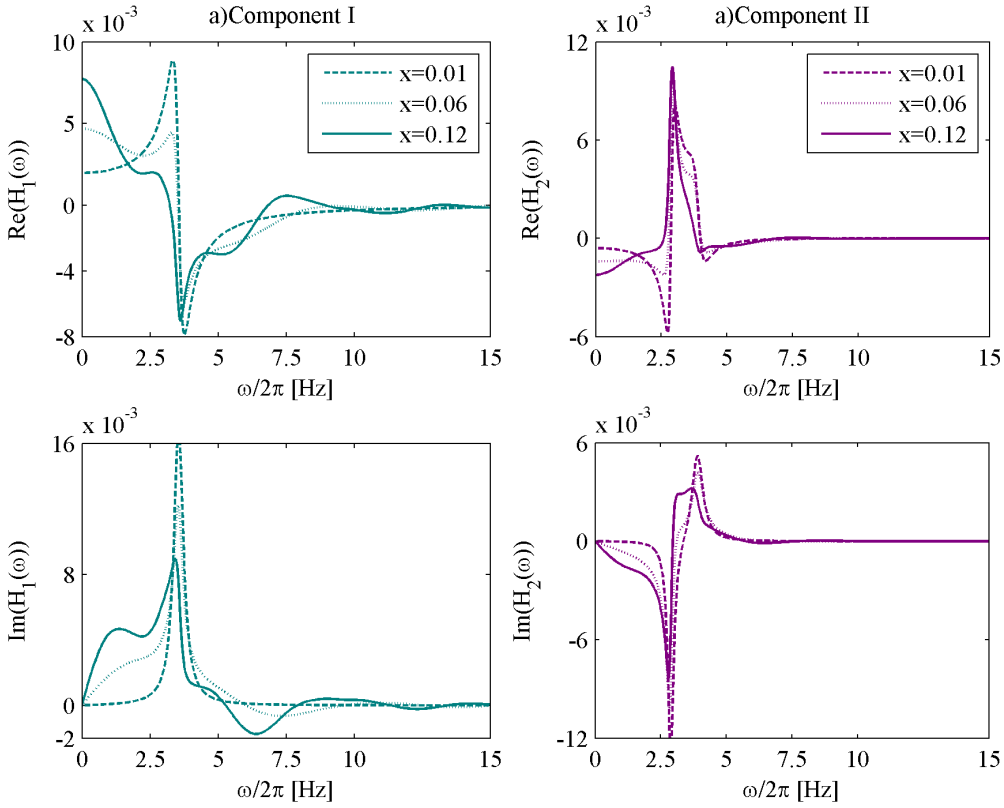

Figure 5.10: Frequency-response functions real and imaginary part, white noise inputs

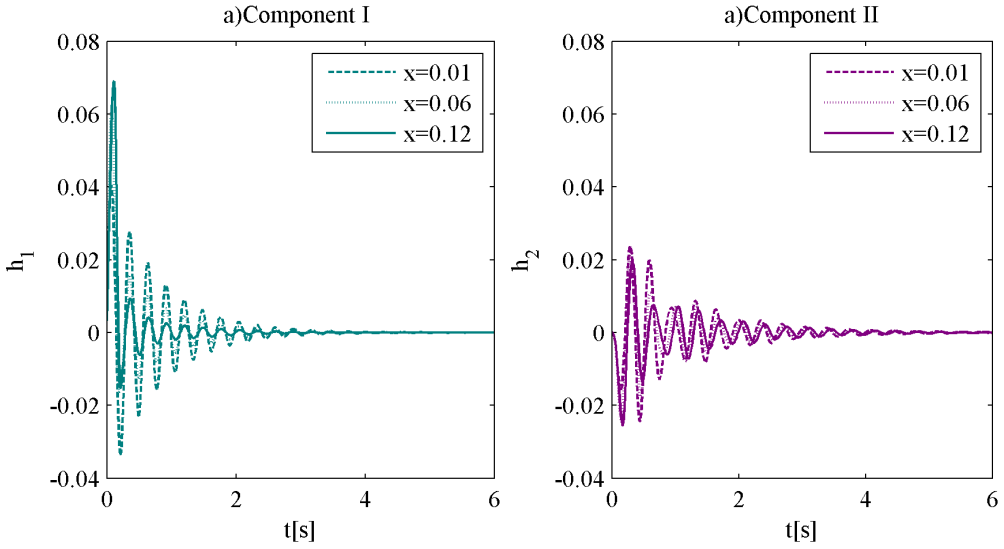

Figure 5.11: Impulse-response functions, Kanai-Tajimi inputs

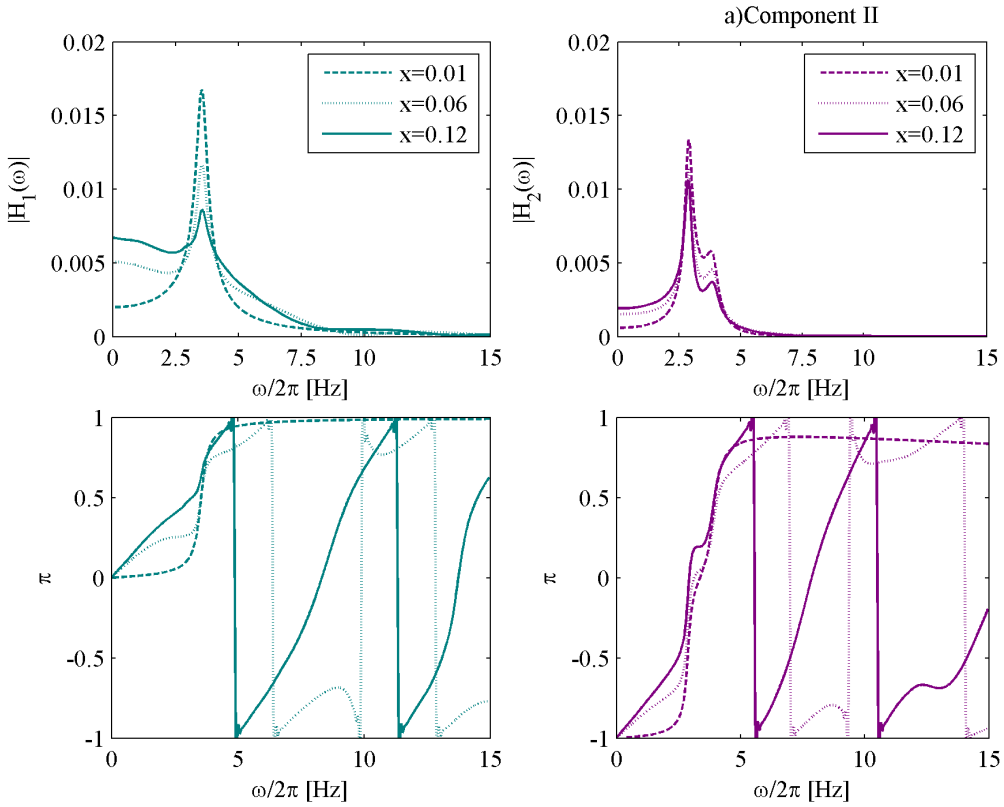

Figure 5.12: Frequency-response functions modulus and phase, Kanai-Tajimi inputs

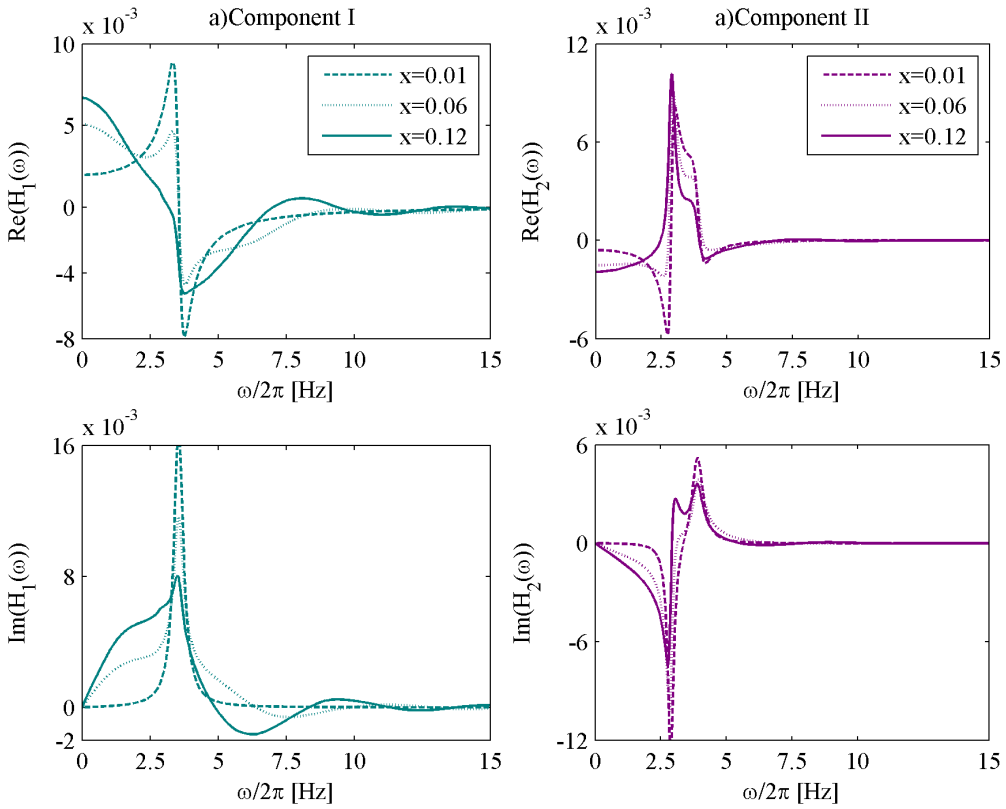

Figure 5.13: Frequency-response functions, real and imaginary part, Kanai-Tajimi inputs

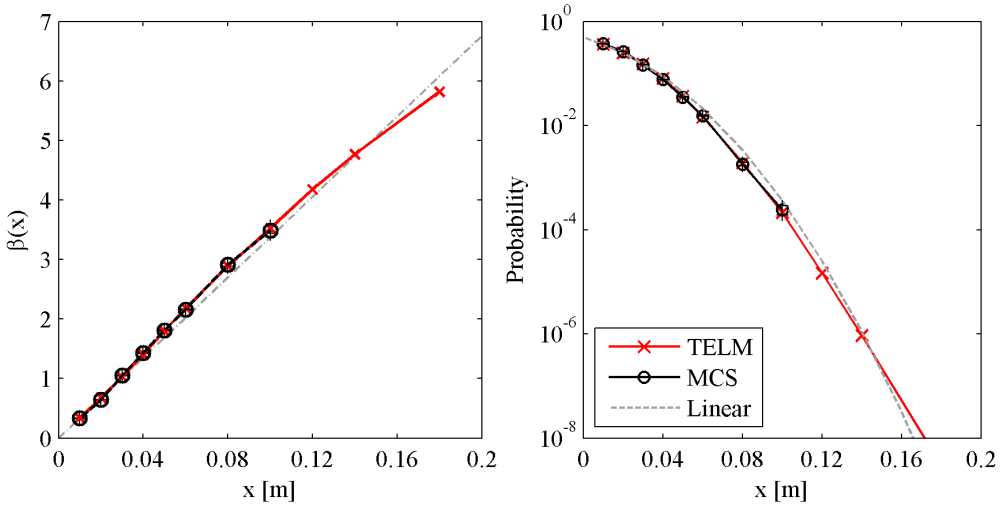

Figure 5.14: Reliability index and point in time probability, white noise inputs

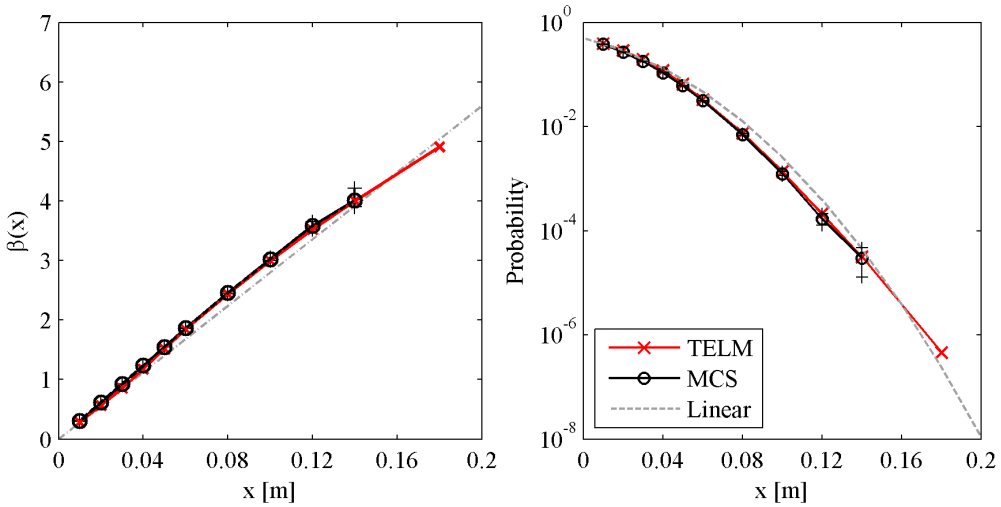

Figure 5.15: Reliability index and point in time probability, Kanai-Tajimi inputs

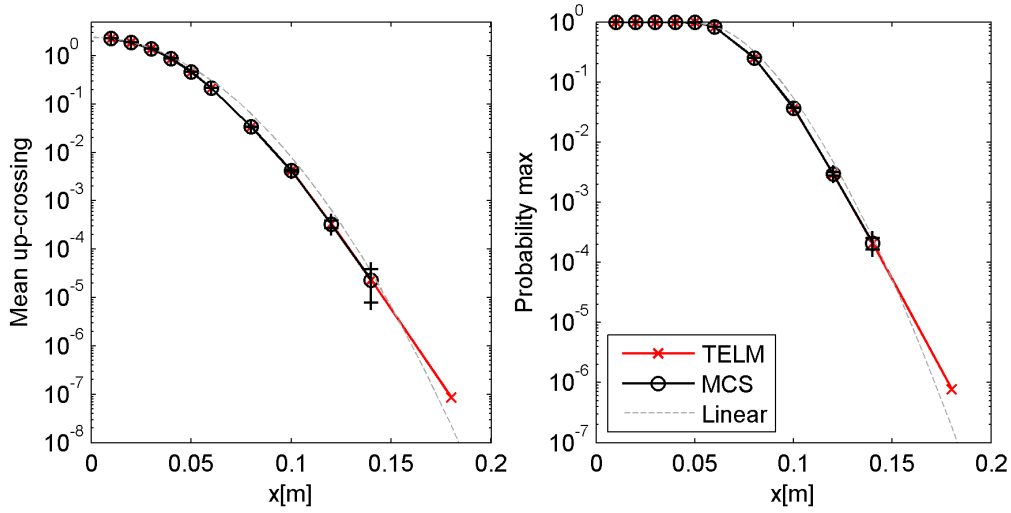

Figure 5.16: Mean up-crossing and Probability of maximum response, white noise inputs

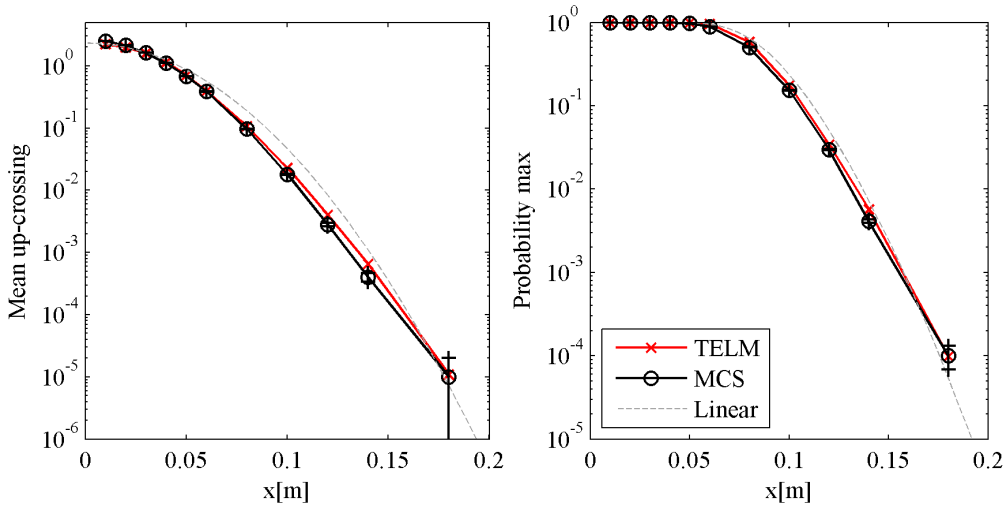

Figure 5.17: Mean up-crossing and probability of maximum response, Kanai-Tajimi inputs

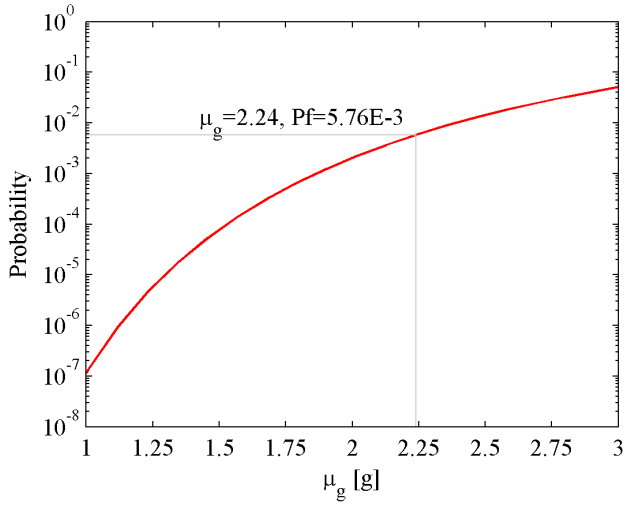

Figure 5.18: Tail-fragility curve of maximum response, white noise inputs

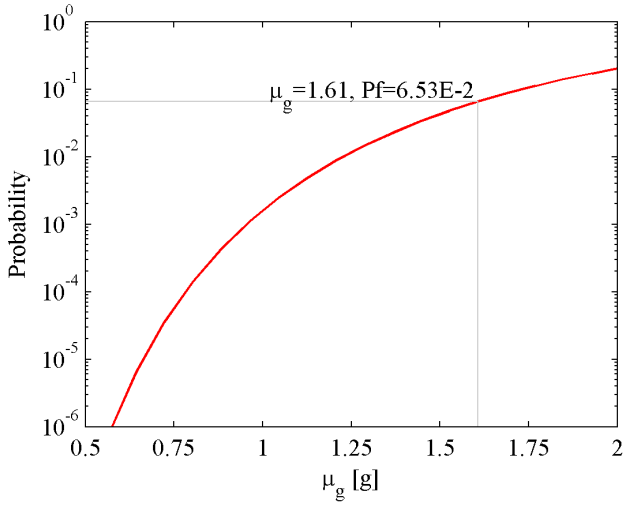

Figure 5.19: Tail-fragility curve of maximum response, Kanai-Tajimi inputs

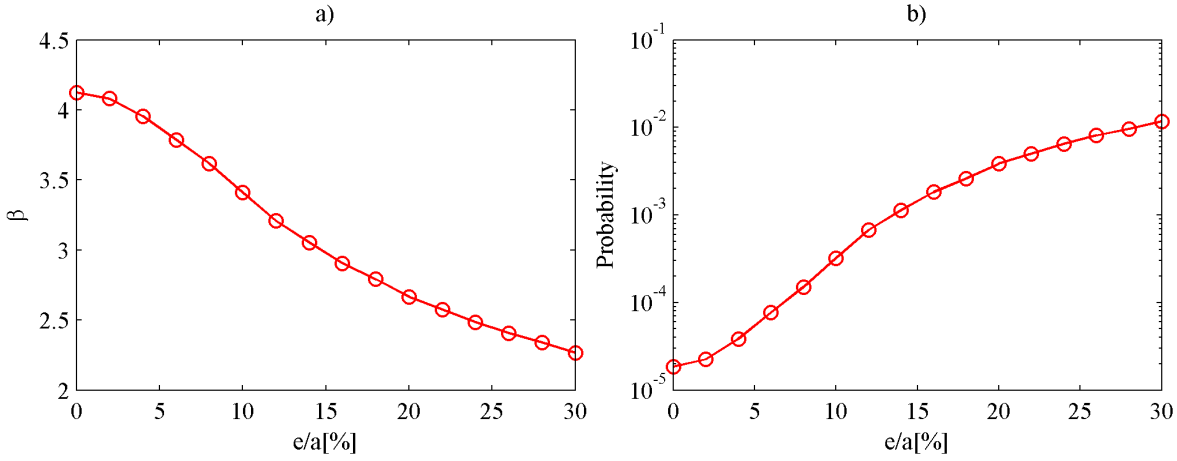

Figure 5.20: a) Reliability index b) Probability of failure for different eccentricities

Chapter 6

Non-stationary TELM analysis

6.1 Introduction non-stationary TELM at a glance

This chapter tackles the class of non-stationary problems. We have seen in the previous Chapters 2 and 5 that, for stationary problems, the TELS is time-independent and only one linear system needs to be defined to study the statistics of the response. However, for a transient input, the TELS also depends on the selected point in time. Thus, equivalent linear systems at multiple time points for one threshold must be defined to study the statistics of the non-stationary response. The definition of the TELS for a specified threshold and point in time requires knowledge of the design point, which in turn requires solution of a constrained nonlinear optimization problem. For non-stationary problems, the required multiple solutions can become computationally costly or even infeasible. Among the broad class of non-stationary processes, this chapter focuses on processes described by Priestley's evolutionary power spectral density (EPSD) [82], which is frequently used in engineering to model non-stationary excitation processes. The chapter introduces the definition of the evolutionary tail-equivalent linear system (ETELS) as an approximate alternative to conducting a series of point-in-time TELSs. Only one solution of the optimization problem is required to define the ETELS. An example is used to demonstrate the accuracy and effectiveness of the proposed method. Among the statistics of the non-stationary response, the first-passage probability is of particular interest. No closed form solution exists for this problem; often simulation methods are used to find an approximate solution. Au and Beck [4] proposed an efficient importance sampling method, which requires knowledge of the design points at a series of points in time. Given the ETELS, approximate design points of the non-stationary response are derived as a function of time and used in conjunction with the Au-Beck algorithm to obtain approximate solution of the first-passage probability for the non-stationary response.

6.2 Evolutionary TELM

Input representation

Evolutionary processes representing the non-stationary input and output are the focus of this work. It is convenient, in this case, to use the spectral representation of the input (2.28), rewritten here for convenience:

$$\hat{F}(t) = \sum_{k=1}^{K} \sigma_k [u_k \sin(\omega_k t) + u_{K+k} \cos(\omega_k t)]. \tag{6.1}$$

According to Priestley [82], the EPSD, $S_{FE}(\omega, t)$ is defined as

$$S_{FE}(\omega, t) = |A(\omega, t)|^2 S_0, \tag{6.2}$$

where $A(\omega, t)$ is a modulating function in both time and frequency and S_0 is the intensity of an underlying white-noise process. A subclass of the evolutionary processes is the uniformly modulated process. For this class, the modulating function can be written as the product of two separate functions as

$$A(\omega, t) = \Phi(\omega) q(t), \tag{6.3}$$

where $\Phi(\omega)$ defines the frequency-modulation function and $q(t)$ the time-modulation function. This formulation is equivalent to defining the non-stationary process as the product of a stationary process with PSD $S_F(\omega) = \Phi^2(\omega) S_0$ and the time-modulation function $q(t)$. The shape of the frequency content of this process remains invariant in time hence the name "uniformly" modulated process. For evolutionary processes, the representation in (6.1) is still valid; it only needs a small adjustment

$$\begin{aligned} \sigma_k(t) &= \sqrt{2 S_{FE}(\omega_k, t) \Delta\omega}, & (6.4)\\ &= |A(\omega_k, t)| \sqrt{2 S_0 \Delta\omega} & (6.5)\\ &= |A(\omega_k, t)| \sigma_0 & (6.6) \end{aligned}$$

where $\sigma_0 = \sqrt{2 S_0 \Delta\omega}$. Hence (6.1) can be rewritten as

$$\begin{aligned} \hat{F}_E(t) &= \sigma_0 \sum_{k=1}^{K} |A(\omega_k, t)| [u_k \sin(\omega_k t) + u_{K+k} \cos(\omega_k t)], & (6.7)\\ &= \boldsymbol{s}(t) \boldsymbol{u}, & (6.8) \end{aligned}$$

where

$$\begin{aligned} \boldsymbol{s}(t) &= [s_1(t), \ldots, s_K(t), s_{K+k}(t), \ldots, s_{2K}(t)], & (6.9)\\ s_k(t) &= \sigma_0 |A(\omega_k, t)| \sin(\omega_k t), & (6.10)\\ s_{K+k}(t) &= \sigma_0 |A(\omega_k, t)| \cos(\omega_k t), & (6.11) \end{aligned}$$

and $\boldsymbol{u}$ defined as (2.30). In the in the case of uniformly modulated process we can write for convenience (6.6) as

$$\begin{aligned} \sigma_k(t) &= \sqrt{2S_{FE}(\omega_k,t)\Delta\omega} && (6.12)\\ &= q(t)\sqrt{2\Phi^2(\omega_k)S_0\Delta\omega} && (6.13)\\ &= q(t)\sqrt{2S_F(\omega_k)\Delta\omega} && (6.14)\\ &= q(t)\sigma_k, && (6.15) \end{aligned}$$

and (6.16) as

$$\begin{aligned} \hat{F}(t) &= \sum_{k=1}^{K} q(t)\sigma_k[u_k\sin(\omega_k t) + u_{K+k}\cos(\omega_k t)] && (6.16)\\ &= \boldsymbol{s}(t)\boldsymbol{u}, && (6.17) \end{aligned}$$

where

$$\begin{aligned} s_k(t) &= q(t)\sigma_k\sin(\omega_k t), && (6.18)\\ s_{K+k}(t) &= q(t)\sigma_k\cos(\omega_k t). && (6.19) \end{aligned}$$

Evolutionary frequency-response function

Given the spectral representation of the input in (6.2), the EPSD of the response of a linear system is given by:

$$S_{XE}(\omega,t) = |M(\omega,t)|^2 S_0, \tag{6.20}$$

where $M(\omega,t)$ is the evolutionary frequency-response function (EFRF) of the linear system defined as

$$M(\omega,t) = \int_0^t A(\omega,t-\tau)h(\tau)e^{(-i\omega\tau)}d\tau. \tag{6.21}$$

One important difference to observe between the FRF and the EFRF is that the second one is not only a characteristic of the system but also of the input excitation. The response of a linear system

to an evolutionary excitation can be obtained as:

$$
\begin{aligned}
X(t) &= \hat{F}(t) * h(t)U(t), && (6.22)\\
&= \mathscr{F}^{-1}[\bar{\mathrm{F}}(\omega)](t) * h(t)]U(t) && (6.23)\\
&= \mathscr{F}^{-1}[A(\omega,t)\bar{\mathrm{W}}(\omega)](t) * h(t)U(t) && (6.24)\\
&= \int_0^t \left(\int_{-\infty}^{\infty} A(\omega,t)\bar{\mathrm{W}}(\omega)e^{i\omega\tau}d\omega \right) h(t-\tau)d\tau && (6.25)\\
&= \int_0^t \left(\int_{-\infty}^{\infty} A(\omega,t)\bar{\mathrm{W}}(\omega)e^{i\omega\tau}d\omega \right) h(t-\tau)e^{i\omega t}e^{-i\omega t}d\tau && (6.26)\\
&= \int_{-\infty}^{\infty} \bar{\mathrm{W}}(\omega) \left(\int_0^t A(\omega,t)h(t-\tau)e^{-i\omega(t-\tau)}d\tau \right) e^{i\omega t}d\omega && (6.27)\\
&= \int_{-\infty}^{\infty} \bar{\mathrm{W}}(\omega) \left(\int_0^t A(\omega,t-\tau)h(\tau)e^{-i\omega\tau}d\tau \right) e^{i\omega t}d\omega && (6.28)\\
&= \int_{-\infty}^{\infty} \bar{\mathrm{W}}(\omega)M(\omega,t)e^{i\omega t}d\omega && (6.29)\\
&= \mathscr{F}^{-1}[M(\omega,t)\bar{\mathrm{W}}(\omega)](t), && (6.30)
\end{aligned}
$$

which implies $\bar{\mathrm{X}}(\omega,t) = M(\omega,t)\bar{\mathrm{W}}(\omega)$. The (6.30) can be written explicitly as

$$
\begin{aligned}
X(t) &= \sum_{k=1}^{K} \sigma_0|M(\omega_k,t)|[u_k \sin(\omega_k t - \vartheta_k(t)) + u_{K+k}\cos(\omega_k t - \vartheta_k(t))] && (6.31)\\
&= \boldsymbol{a}(t)\boldsymbol{u}, && (6.32)
\end{aligned}
$$

with

$$
\begin{aligned}
\boldsymbol{a}(t) &= [a_1(t),\ldots,a_K(t),a_{K+k}(t),\ldots,a_{2K}(t)], && (6.33)\\
a_k(t) &= \sigma_0|M(\omega_k,t)|\sin(\omega_k t - \vartheta_k(t)), && (6.34)\\
a_{K+k}(t) &= \sigma_0|M(\omega_k,t)|\cos(\omega_k t - \vartheta_k(t)), && (6.35)
\end{aligned}
$$

where $\vartheta_k(t) = \tan^{-1}[\mathrm{Im}(M(\omega_k,t))/\mathrm{Re}(M(\omega_k,t))]$ is the phase and $|M(\omega_k,t)|$ the modulus of the EFRF. Analogously to the original frequency domain TELM we can write

$$
\begin{aligned}
|M(\omega_k,t)| &= \frac{\sqrt{a_k(t)^2 + a_{K+k}(t)^2}}{\sigma_0}, && (6.36)\\
\vartheta_k(t) &= \omega_k t - \tan^{-1}\left[\frac{a_{j,k}(t)}{a_{j,K+k}(t)}\right] k \in [1,\ldots,K], \text{ and } \vartheta_{j,k} \in [-\pi,\pi]. && (6.37)
\end{aligned}
$$

In the case of the uniformly modulating function we can slightly modify the previous derivation as

$$\begin{aligned} X(t) &= \int_{-\infty}^{\infty} \bar{\mathrm{W}}(\omega)\Phi(\omega)\left(\int_0^t q(t-\tau)h(\tau)e^{-i\omega\tau}d\tau\right)e^{i\omega t}d\omega && (6.38)\\ &= \int_{-\infty}^{\infty} \bar{\mathrm{W}}(\omega)\Phi(\omega)M(\omega,t)e^{i\omega t}d\omega && (6.39)\\ &= \int_{-\infty}^{\infty} \bar{F}(\omega)M(\omega,t)e^{i\omega t}d\omega && (6.40)\\ &= \mathscr{F}^{-1}[M(\omega,t)\bar{F}(\omega)](t), && (6.41) \end{aligned}$$

where we have defined

$$M(\omega,t) = \int_0^t q(t-\tau)h(\tau)e^{(-i\omega\tau)}d\tau, \tag{6.42}$$

for the uniformly modulated process (6.3). The (6.41) implies $\bar{\mathrm{X}}(\omega,t) = M(\omega,t)\bar{F}(\omega)$, and it can be written explicitly as

$$\begin{aligned} X(t) &= \sum_{k=1}^{K}\sigma_k|M(\omega_k,t)|[u_k\sin(\omega_k t-\vartheta_k(t)) + u_{K+k}\cos(\omega_k t-\vartheta_k(t))] && (6.43)\\ &= \boldsymbol{a}(t)\boldsymbol{u}, && (6.44) \end{aligned}$$

with

$$\begin{aligned} a_k(t) &= \sigma_k|M(\omega_k,t)|\sin(\omega_k t-\vartheta_k(t)), && (6.45)\\ a_{K+k}(t) &= \sigma_k|M(\omega_k,t)|\cos(\omega_k t-\vartheta_k(t)), && (6.46) \end{aligned}$$

and

$$\begin{aligned} |M(\omega_k,t)| &= \frac{\sqrt{a_k(t)^2+a_{K+k}(t)^2}}{\sigma_k}, && (6.47)\\ \vartheta_k(t) &= \omega_k t - \tan^{-1}\left[\frac{a_{j,k}(t)}{a_{j,K+k}(t)}\right] k\in[1,\ldots,K], \text{ and } \vartheta_{j,k}\in[-\pi,\pi]. && (6.48) \end{aligned}$$

Indeed, given a linear system, the EFRF can be re-constructed in two ways: directly using (6.36), (6.37) (in the general case) or (6.47), (6.48) (in the case of uniformly modulated process), or deriving the IRF and applying (6.21) or (6.42). In the following, we use the second approach.

When the system is nonlinear, linearization of the limit-state surface at each instant of time is required to fully study the statistics of the non-stationary response. This requires repeated solutions of the design point and the determination of a series of FRFs according to (2.43) and (2.44). The computational cost can be prohibitive. As an alternative, we propose the use of the evolutionary tail-equivalent linear system (ETELS), as described below.

The evolutionary tail-equivalent linear system

In the previous section we showed that the EFRF for linear systems can be directly determined by TELM analysis. In this section we introduce approximate methods to analyze the temporal evolutionary problem in the case of nonlinear systems. We start first by analyzing the case for which the modulating function is of the type in (6.3). Given a general nonlinear system and a stochastic input described by (6.3), we first solve the problem for response to the underlying stationary colored noise, $S_F(\omega)$, by the standard TELM procedure. In this case it is convenient to compute the IRF of the TELS by inverse Fourier transform of the FRF obtained from a frequency-domain discretization. The ETELS is then defined through its EFRF which, using (6.42), is given by

$$M(\omega,t)=\int_0^t q(t-\tau)h_{\mathrm{TELS}}(\tau)e^{(-i\omega\tau)}d\tau. \tag{6.49}$$

in which $h_{\mathrm{TELS}}(t)$ denotes the IRF of the TELS for the underlying stationary colored noise excitation. This approximation includes the influence of the frequency content of the excitation on the response of the nonlinear system. It is indeed a suitable approximation for both broad- and narrow-band excitations. The approximation works well as long as the modulating function $q(t)$ is slowly varying.

Given a general nonlinear system and a stochastic input described by (6.2), we first solve the problem for response to white noise by the standard TELM procedure. The IRF of the TELS is computed either directly, if a time-domain discretization is employed, or by inverse Fourier transform of the FRF, if a frequency-domain discretization is used. The ETELS is then defined through its EFRF, which, using (6.21), is obtained as

$$M(\omega,t)=\int_0^t A(\omega,t-\tau)h_{\mathrm{TELS}}(\tau)e^{(-i\omega\tau)}d\tau, \tag{6.50}$$

in which $h_{\mathrm{TELS}}(t)$ denotes the IRF of the TELS for response to the to white-noise excitation. In this case the approximation can be crude and it may work only for broad-band excitation with slowly varying frequency content. The discrete versions of equations (6.49) and (6.50) are

$$M(\omega,t_m) = \sum_{l=1}^{m} q(t_m-t_l)h_{\ \mathrm{TELS}}(t_l)e^{(-i\omega t_l)}\Delta t, \quad m\in[1\ldots M], \tag{6.51}$$

$$M(\omega,t_m) = \sum_{l=1}^{m} A(\omega,t_m-t_l)h_{\ \mathrm{TELS}}(t_l)e^{(-i\omega t_l)}\Delta t, \quad m\in[1\ldots M]. \tag{6.52}$$

Once the EFRF is available, linear random vibration analysis is employed.

The proposed method is clearly an approximation, since it decouples the transient nature of the input excitation represented by the modulating functions $q(t)$ or $A(\omega,t)$ from the frequency characteristics of the equivalent linear system lumped in $h_{\mathrm{TELS}}(t)$. This implies superposition and we know that for nonlinear systems this is not valid. The purpose of this chapter is to demonstrate that the series of TELSs can be approximated by a time-variant linear system, for which the concept of superposition holds.

Time variant design point

Once the ETELS is computed according to (6.51) or (6.52), all the needed information to compute design points and reliability indices as functions of time are available. For a selected time t_m, we compute the gradient of the ETELS, $\boldsymbol{a}_{\mathrm{ETELS}}(t_m)$, by using (6.34)-(6.35) or (6.45)-(6.46). This is then used in (2.15) to compute the design point $\boldsymbol{u}^*_{\mathrm{ETELS}}(t_m)$ and in (2.16) to compute the corresponding reliability index $\beta_{\mathrm{TELS}}(t_m)$. Since these expressions are easy to compute, the complete set of $\boldsymbol{u}_{\mathrm{ETELS}}(t_m)$ and $\beta_{\mathrm{ETELS}}(t_m)$ for $m \in [1 \dots M]$ are readily available for the computational cost of only one TELM analysis. This is the major advantage of ETELM analysis: its computational efficiency compared to repeated TELM analyses for a series of points in time. Moreover, knowing the design points at all times completely defines the probabilistic structure of the Gaussian response of the equivalent linear system for the selected threshold, including the autocorrelation structure.

One important difference between TELM and ETELM is that, while the former is a completely non-parametric method, the form of the input process parameterizes ETELM. More specifically, the ETELS is split in two parts: a parametric part defined by the EPSD and a nonparametric part defined by the TELS. The combination of the two is given by superposition via (6.51) or (6.52).

Once the design points are given at discrete points in time, we can apply linear random vibration analysis to the series of TELSs for each instant of time. The most important response statistic of interest in transient problems is the first-passage probability, for which an exact analytical solution does not exist even for the linear systems. An efficient importance sampling method has been proposed by Au and Beck [4] to solve this problem for linear systems. The algorithm requires knowledge of the design points as a function of time. This formulation is indeed appealing for the present study, since the required information is readily available.

Summary of the ETELM analysis

The following steps summarize the key points of the ETELM;

1. Select the desired threshold and formulate the limit-state function.
2. Perform TELM analysis for the colored or white-noise excitation according to the type of the modulating function, (6.2) or (6.3), and the nature of the excitation.
3. Determine the EFRF by solving (6.51) or (6.52).
4. Determine the gradient vector function $\boldsymbol{a}_{\mathrm{TELS}}(t_m)$ for $m \in [1 \dots M]$ by use of (6.34)-(6.35) or (6.45)-(6.46).
5. Given $\boldsymbol{u}^*(t_m)$ and $\beta(t_m)$ apply the Au-Beck algorithm to obtain the first-passage probability, as described in the following section.

6.3 The Au-Beck algorithm in the ETELM context

An analytical solution to solve the first-passage probability does not exist even in the linear cases. Different authors, departing from the earlier works of Rice [86] have proposed approximate analytical solutions based on out-crossing theory. In this dissertation, so far we have used the approach proposed by Vanmarcke [106] for stationary processes. A classical alternative to analytical solutions is given by simulation methods. For highly reliable structures the classical Monte Carlo simulation method becomes infeasible. For this reason, Au and Beck [4] proposed an importance sampling method that is suitable for this class of problems, even for small probabilities. The algorithm is designed for linear dynamical systems subjected to stationary or non-stationary Gaussian colored noise excitations. This section reviews and adapts this algorithm for TELM analysis of nonlinear system response under non-stationary excitations.

The first-passage failure event of interest, denoted with F, can be written in a discrete form as

$$F = \bigcup_{m=1}^{M} \{|X(t_m)| > x\} = \bigcup_{m=1}^{M} F_m, \tag{6.53}$$

where F_m is the point-in-time failure event defined as

$$F_m = \{|X(t_m)| > x\} = \{\boldsymbol{u} : |\boldsymbol{a}(t_m)\boldsymbol{u}| > x\}. \tag{6.54}$$

Since the problem is perfectly symmetric and the up-crossing, $F_m^+ = \{X(t_m) > x\}$, and down-crossing, $F_m^- = \{X(t_m) < x\}$, events are mutually exclusive, we can write

$$P(F_m) = P(F_m^+) + P(F_m^-) = 2P(F_m^+). \tag{6.55}$$

We have seen that the point-in-time probability of failure for a linear system is given by

$$P(F_m^+) = \Phi[-||\boldsymbol{u}^*(t_m)||] = \Phi[-\beta(t_m)]. \tag{6.56}$$

In the case of a nonlinear system, (6.56) is the probability of failure of the TELS defined at the specific point in time t_m and it represents the first-order approximation of the tail probability of the nonlinear system. The reader should be aware that both $\boldsymbol{u}^*(x, t_m)$ and $\beta(x, t_m)$ depend on the threshold x. However, in this chapter we consider this dependence implicit and, for the sake of simplicity of the notation, do not explicitly show the dependence on x.

The conditional PDF of a random vector $\boldsymbol{u}$ given that it belongs to a point-in-time failure region F_m is given by

$$f(\boldsymbol{u}|F_m) = \frac{\phi(\boldsymbol{u})\Pi_{F_m}(\boldsymbol{u})}{P(F_m)} = \frac{\phi(\boldsymbol{u})\Pi_{F_m}(\boldsymbol{u})}{2\Phi[-\beta(t_m)]}, \tag{6.57}$$

where $\phi(\cdot)$ is the standard multi-normal PDF and $\Pi_{F_k}(\cdot)$ is the indicator function such that $\Pi_{F_m}(\boldsymbol{u}) = 1$ if $\boldsymbol{u} \in F_m$ and $\Pi_{F_m}(\boldsymbol{u}) = 0$ otherwise. The importance sampling density (ISD) proposed by Au and Beck is a weighted sum of the point-in-time conditional PDFs, i.e.,

$$f(\boldsymbol{u}) = \sum_{m=1}^{M} \pi_m f(\boldsymbol{u}|F_m) = \sum_{m=1}^{M} \pi_m \frac{\phi(\boldsymbol{u})\Pi_{F_m}(\boldsymbol{u})}{P(F_m)}, \tag{6.58}$$

where

$$\sum_{m=1}^{M} \pi_m = 1 \text{ and } \pi_m \geq 0. \tag{6.59}$$

The weights π_m reflect the relative importances of the point-in-time failure events to the final probability of failure, and they are simply chosen as

$$\pi_k = \frac{P(F_m)}{\sum_{m=1}^{M} P(F_m)} = \frac{P(F_m)}{\tilde{P}(F)}, \tag{6.60}$$

where

$$\tilde{P}(F) = \sum_{m=1}^{M} P(F_m) = 2 \sum_{m=1}^{M} \Phi[-\beta(t_m)] \tag{6.61}$$

is an upper bound of the true probability of failure $P(F)$. Introducing the definition (6.60), the ISD (6.58) is rewritten as

$$f(\boldsymbol{u}) = \frac{\phi(\boldsymbol{u})}{\tilde{P}(F)} \sum_{m=1}^{M} \Pi_{F_m}(\boldsymbol{u}). \tag{6.62}$$

Using (6.62), the first-passage probability is calculated as

$$P(F) = \int \frac{\Pi_F(\boldsymbol{u})\phi(\boldsymbol{u})}{f(\boldsymbol{u})} f(\boldsymbol{u}) d\boldsymbol{u} = E\left[\frac{\Pi_F(\boldsymbol{u})\phi(\boldsymbol{u})}{f(\boldsymbol{u})}\right]. \tag{6.63}$$

Substituting (6.62) we obtain

$$P(F) = \tilde{P}(F) \times E\left[\frac{\Pi_F(\boldsymbol{u})}{\sum_{m=1}^{M} \Pi_{F_m}(\boldsymbol{u})}\right] = \tilde{P}(F) \times E\left[\frac{1}{\sum_{m=1}^{M} \Pi_{F_m}(\boldsymbol{u})}\right]. \tag{6.64}$$

Thus, $P(F)$ is estimated as:

$$P(F) \approx \hat{P}(F) = \frac{1}{\bar{N}} \tilde{P}(F) \times \sum_{\bar{n}=1}^{\bar{N}} r(\boldsymbol{u}_{\bar{n}}), \tag{6.65}$$

where

$$r(\boldsymbol{u}_{\bar{n}}) = \frac{1}{\sum_{m=1}^{M} \Pi_{F_m}(\boldsymbol{u}_{\bar{n}})}, \tag{6.66}$$

and $\bar{N}$ is the number of sample points. The coefficient of variation, c.o.v., of the estimator $\hat{P}(F)$ is defined as

$$\delta = \sqrt{\frac{\mathrm{Var}[r(\boldsymbol{u}_{\bar{n}})]}{\bar{N}}} \frac{1}{P(F)}, \tag{6.67}$$

and can be estimated as

$$\delta \approx \hat{\delta} = \sqrt{\frac{\hat{\mathrm{Var}}[r(\boldsymbol{u}_{\bar{n}})]}{\bar{N}}} \frac{1}{\hat{P}(F)}, \tag{6.68}$$

where $\hat{\mathrm{Var}}[\cdot]$ is the sample variance. In (6.64) and (6.66), $\Pi_F(\boldsymbol{u}) = 1$ since the samples $\boldsymbol{u}_{\bar{n}}$, drawn from the ISD (6.62), are guaranteed to belong to the failure domain. In the context of ETELM, these samples lie on the failure domain induced by the TELS, which is the first-order approximation of the nonlinear system, but they may or may not belong to the true failure domain. Thus the ETELM-Au-Beck algorithm uses an approximation of the true failure frontier and its accuracy depends on the degree of nonlinearity of the system.

The following procedure is suggested to sample from (6.62). Considering that the failure boundary ∂F^+ of a linear system or of the TELS is an hyperplane, the conditional vector $\boldsymbol{u}^+(t_m)$ distributed accordingly to (2.15) can be written as a sum of a parallel and perpendicular component to the design point, i.e.,

$$\boldsymbol{u}^+(t_m) = \alpha \boldsymbol{e}^*(t_m) + \boldsymbol{u}^\perp(t_m), \tag{6.69}$$

where $\boldsymbol{u}^\perp(t_m)$ is the perpendicular component,

$$\boldsymbol{e}^*(t_m) = \boldsymbol{u}^*(t_m)/\beta(t_m), \tag{6.70}$$

and α is a standard normal random variable conditioned on $\alpha > \beta(t_m)$, i.e.,

$$f(\alpha) = \phi(\alpha) U(\alpha - \beta(t_m))/\Phi[-\beta(t_m)], \tag{6.71}$$

where $U(\cdot)$ is the unit step function. It is easy to see that the the vector $\boldsymbol{u}^\perp(t_m)$ can be written as

$$\boldsymbol{u}^\perp(t_m) = \boldsymbol{u} - \langle \boldsymbol{u}, \boldsymbol{e}^*(t_m) \rangle \, \boldsymbol{e}^*(t_m), \tag{6.72}$$

and by using this expression (6.69) can be rewritten as

$$\boldsymbol{u}^+(t_m) = \boldsymbol{u} + (\alpha - \langle \boldsymbol{u}, \boldsymbol{e}^*(t_m) \rangle) \boldsymbol{e}^*(t_m); \tag{6.73}$$

by the same procedure we can sample $\boldsymbol{u}^-(t_m)$ as

$$\boldsymbol{u}^-(t_m) = -\boldsymbol{u} - (\alpha - \langle \boldsymbol{u}, \boldsymbol{e}^*(t_m) \rangle) \boldsymbol{e}^*(t_m). \tag{6.74}$$

ETELM/Au-Beck algorithm, summary

The following steps summarize the key points of the Au-Beck algorithm applied to ETELM analysis.

1. Perform ETELM analysis according to summary (6.2). The gradient vectors $\boldsymbol{a}(t_m)$, the design points $\boldsymbol{u}(t_m)$ and the reliability indexes $\beta(t_m)$ of the ETELS are available after the analysis.

2. Compute the point in time probability by (6.55) and (6.56), the upper bound $\tilde{P}(F)$ according to (6.61), and the weights π_m according to (6.60).

3. Sample $\bar{N}$ i.i.d. $\boldsymbol{u}_{\bar{n}}$ generated from the ISD (6.62). To simulate samples from (6.62):

   a) Draw an index m from the set $[1 \dots M]$ with probabilities π_m.

   b) Simulate $\boldsymbol{u}$ as a standard normal vector with independent components.

   c) Simulate α from (6.71) by drawing a uniform random variable, U_1, on $[0, 1]$ and computing:

   $$\alpha = \Phi^{-1}[U_1 + (1 - U_1)\Phi[\beta(t_m)]]. \tag{6.75}$$

   d) Simulate $\boldsymbol{u}_{\bar{n}}$ drawing a uniform random variable, U_2, on $[0, 1]$ and computing:

   $$\boldsymbol{u}_{\bar{n}} = \begin{cases} \boldsymbol{u} + (\alpha - \langle \boldsymbol{u}, \boldsymbol{e}^*(t_m) \rangle)\boldsymbol{e}^*(t_m) \text{ for } U_2 \leq 0.5 \\ -\boldsymbol{u} - (\alpha - \langle \boldsymbol{u}, \boldsymbol{e}^*(t_m) \rangle)\boldsymbol{e}^*(t_m) \text{ otherwise} \end{cases} \tag{6.76}$$

   where is $\boldsymbol{e}^*(t_m)$ is defined according to (6.70).

4. Estimate $P(F)$ by computing $\hat{P}(F)$ according to (6.65), and the c.o.v. of the estimator by (6.68).

6.4 Example I, separable modulating function

As a first example, we consider a single-degree-of-freedom (SDOF) oscillator described by the non-degrading hysteretic Bouc-Wen material model [8, 14, 109]. The responses of the oscillator to three input excitations are considered: a time-modulated white-noise excitation (Excitation I), a time-modulated broad band excitation (Excitation II), and a time-modulated narrow band excitation (Excitation III). The following subsections describe the input excitations, the physical model, the results of ETELM analyses, and finally the first-passage probability computed by ETELM-Au-Beck algorithm.

The input excitation

Three different excitations are used to investigate the accuracy of the ETELM analysis. For all three excitations the time-modulating function is defined as

$$q(t) = \sqrt{\frac{1 + \sin\left[\pi\left(\frac{t}{t_x} - \frac{1}{2}\right)\right]}{2}}. \tag{6.77}$$

This function has only one parameter, the peak time t_x, at which the function has value 1. In this way we can directly control the variance of the process at the peak of the time-modulating function. Figure 6.1 shows the modulating function (6.77) while Figure 6.2 shows the EPSD of the time-modulated white noise.

The frequency-modulating function is selected as the square root of the Kanai-Tajimi PSD, which is widely used in earthquake engineering and here rewritten for convenience as

$$\Phi(\omega)^2 = \frac{\omega_f^4 + 4\zeta_f^2\omega_f^2\omega^2}{(\omega_f^2 - \omega^2)^2 + 4\zeta_f^2\omega_f^2\omega^2}, \tag{6.78}$$

where ω_f and ζ_f are parameters, the first controlling the central frequency and the second controlling the bandwidth of the process. The full modulating function is obtained by (6.3). Two sets of parameter values for the above model are selected to study the effect of the frequency content on ETELM analysis. The first set describes a broad-band process, the second set describes a relatively narrow-band process. Figures 6.3 and 6.4 respectively show the EPSDs for the time-modulated broad- band and narrow-band excitations. The three excitations are tuned so that they have the same value of the EPSD at the natural frequency of the oscillator for small-amplitude vibrations, ω_0, at time t_x, i.e. $S_{FE}^I(\omega_o, t_x) = S_{FE}^{II}(\omega_o, t_x) = S_{FE}^{III}(\omega_o, t_x)$. This allows a better understanding of the effect of the frequency content on the ETELM analysis. The processes, naturally, have different variances. Table 6.1 summarizes the input parameters.

The physical model

The considered hysteretic oscillator is defined by the differential equation:

$$m\ddot{X} + c\dot{X} + k[\alpha X(t) + (1-\alpha)Z(t)] = -m\ddot{U}_G(t), \tag{6.79}$$

Table 6.1: Excitation Properties

input	$S_0[\frac{\mathrm{m}^2}{\mathrm{s}^3}]$	$S_{FE}(\omega_0)$	t_x[s]	ω_f[Hz]	ζ_f	$\sigma_{FE}(t_x)$[g]
I	1.00	1.00	10.00			0.457
II	0.733	1.00	10.00	1.00	0.8	0.217
III	0.141	1.00	10.00	1.00	0.2	0.113

where the stochastic base input $\ddot{U}_G(t)$ has the EPSD defined in the previous subsection. The mass, m, and stiffness, k, are selected to produce $\omega_0/2\pi = 1$[Hz] as the natural frequency of the linear ($\alpha = 1$) oscillator and the damping, c, is set to match a viscous damping ratio of 5%. The term α controls the degree of hysteresis and $Z(t)$ follows the Bouc-Wen hysteresis law, here rewritten for convenience

$$\dot{Z}(t) = -\gamma|\dot{X}(t)||Z(t)|^{(n-1)}Z(t) - \eta|Z(t)|^n\dot{X}(t) + A\dot{X}(t). \tag{6.80}$$

The parameters γ and η are given in terms of the mean-square response of the linear oscillator ($\alpha = 1$) under white-noise excitation, $\bar{\sigma}^2 = \pi S_0 m^2/(ck)$. All system parameters are given in Table 6.2. The parameters are calibrated to have a softening system.

The ETELM analysis

As in the original TELM analysis, ETELM requires the definition of a threshold x. Here, we select $x = 3\sigma_0$, which is proven to be in the inelastic branch of the system. Figure 6.5 shows the hysteresis loop for the broad-and narrow-band excitation.

To test the ETELM, we compare the continuous trace of the reliability index $\beta_{ETELS}(t)$ obtained by the proposed method with reliability indices $\beta_{TELS}(t_i)$ computed at four instants of time with the original TELM analysis. Moreover, following the same logic, we compare the EFRF of the ETELS obtained by the proposed approximate method with the FRFs of TELSs obtained from the original TELM at selected points in time. Table 6.3 shows the values obtained by the two analyses. The results are satisfactory since $\beta_{ETELS}(t_i)$ closely agree with $\beta_{TELS}(t_i)$ at all selected time points. Moreover, the approximation is performing better around the peak of the excitation, which is the most important part of the analysis. Figures 6.6, 6.7 and 6.8 show the functions $\beta_{ETELS}(t)$ versus the four $\beta_{TELS}(t_i)$ values for the white-noise, wide- and narrow-band excitations, respectively. The advantage of ETELM is clear from these figures, since only one optimization problem needs to be solved to obtain a precise estimation of the complete time trajectory of $\beta(t)$.

Figures 6.9, 6.10 and 6.11 compare the EFRFs obtained with the proposed method with the FRFs of four TELSs obtained with the original TELM at the selected time points for the white-noise, broad- and narrow-band excitations, respectively. It can be seen that the EFRFs for the three different excitations at the four selected times are similar in shape, although different in intensity. ETELM implicitly uses this fact by convolving the shape of the IRF of the TELS with

Table 6.2: System Properties

System	$T_0[s]$	$\zeta[\%]$	$\bar{\sigma}$		
	1.00	5	$\frac{\pi S_0 m^2}{ck}$		
Bouc Wen	α	γ	η	n	A
	0.1	$1/(2\bar{\sigma})$	$1/(2\bar{\sigma})$	3	1

the modulating function. Comparing the EFRFs with the FRFs obtained by TELM analysis at the selected points, we find that the approximation is precise at the peak of the excitation, while it degrades (but remains acceptable) for times distant from the peak. The reader may also note that the reliability of the oscillator for the first two excitations is similar, while the input excitations have different variances. This is a consequence of the frequency contents of the EFRFs, which mainly involve low frequencies due to the softening of the system. High frequencies do not play a major role in this problem and that is the reason why a lower energy input such as excitation II, leads to similar reliability indices and similar EFRFs. This corroborates the idea of white-noise approximation for broad band processes. For excitation III, the reliability of the oscillator is significantly higher since most of energy is concentrated in the central frequency, which leads (due to the nature of the used normalization) to a significantly lower value of the variance of the excitation and significantly lower values of spectral components in the low frequency range. The shape of the EFRF for narrow-band process, Figure 6.11, shows that the white-noise approximation is inapplicable since ETELS strongly depends from the frequency content of the excitation. Finally the ETELM-Au-Beck algorithm is applied to the three systems for a duration of 15[s]. Table 6.4 reports the results compared to results obtained from a crude MCS analysis. Figures 6.12, 6.13 and 6.14 report the convergence to the target probability of failure as a function of the number of sample size. The discrepancy between MCS and ETELM-Au-Beck algorithm is due to the approximation involved in using the union of ETELSs as surrogate of the failure domain. We note that ETELM produces results that have order-of-magnitude accuracy, with somewhat better results for the white-noise and broad-band excitations. This level of accuracy is sufficient in many engineering applications.

Table 6.3: ETELM output

Input	$\beta(4)$		$\beta(6)$		$\beta(8)$	
	ETELS	TELS	ETELS	TELS	ETELS	TELS
I	6.030	6.095	4.149	4.160	3.410	3.411
II	6.227	6.278	4.290	4.302	3.530	3.534
III	9.215	9.175	6.355	6.360	5.251	5.250
Input	$\beta(10)$		$\beta(12)$			
	ETELS	TELS	ETELS	TELS		
I	3.154	3.154	3.225	3.218		
II	3.269	3.269	3.346	3.351		
III	4.880	4.880	5.015	5.016		

6.5 Example II, non-separable modulating function

In this second example, we report an excitation of the type (6.2) which is used in [20, 28, 84, 85] to simulate earthquake ground motions. We analyze two excitations: a fully non-stationary broad-band excitation and a fully non-stationary narrow-band excitation. Both are completely non-stationary models since the frequency modulating filter has time varying parameters. In particular, the EPSD of these models is written as

$$A(\omega, t) = \Phi(\omega|\boldsymbol{\theta}(t))q(t), \tag{6.81}$$

where $\Phi(\omega|\boldsymbol{\theta}(t))$ is a frequency modulated filter with time varying parameters, e.g.,

$$\Phi(\omega|\boldsymbol{\theta}(t))^2 = \frac{\omega_f(t)^4 + 4\zeta_f(t)^2\omega_f(t)^2\omega^2}{(\omega_f(t)^2 - \omega^2)^2 + 4\zeta_f(t)^2\omega_f(t)^2\omega^2}, \tag{6.82}$$

where $\boldsymbol{\theta}(t) = [\omega_f(t), \zeta_f(t)]$ is a set of time varying parameters. Following the work of [84, 85], these parameters are chosen as

$$\omega_f(t) = \omega_{mid} + \omega'(t - t_{mid}), \tag{6.83}$$

where ω_{mid} is the filter frequency at time t_{mid} and ω' is the rate of change of the filter frequency. We select $t_{mid} = t_{max}$, where t_max is the time at which the time-modulating function $q(t)$ takes its maximum. The bandwidth parameter is chosen as a constant

$$\zeta_f(t) = \bar{\zeta}. \tag{6.84}$$

Table 6.5 reports values of the parameters for the two excitations. For the fully non-stationary broad-band excitation, the white-noise approximation is applied, as illustrated in Section 6.2. For the fully non-stationary narrow-band process, since the previous approximation is inaccurate, we apply the following procedure: We compute the IRF of the TELS at the time of the peak of the modulating function $q(t)$, i.e., at t_{max}; then, using this IRF in (6.51), we compute the EFRF. In this linearization, the frequency content of the ETELS is time invariant and is fixed by the linearization at the peak of the excitation. It follows that the method can be applied only to an excitation process that has a "slowly varying" frequency content. Figures 6.15 and 6.16 show

Table 6.4: Estimates of first-passage probability by ETELM and MCS

Input	x	$\hat{P}(F)$	$P_{MC}(F)$	$\hat{\delta}$ [%]	δ_{MC} [%]	$\bar{N}$	$\bar{N}_{MC}$
I	$3\sigma_0$	2.459E-03	2.250E-03	4.32	6.66	500	10^5
II	$3\sigma_0$	1.685E-03	2.010E-03	4.12	7.04	500	10^5
III	$3\sigma_0$	1.776E-05	2.300E-05	3.98	20.85	500	10^6

the trajectory of the design point excitations for the fully non-stationary broad- and narrow-band excitations, respectively. As can be observed, both provide a fairly good level of "engineering" approximation, although for the fully non-stationary narrow-band excitation the proposed ETELM tends to overestimate the probability of failure. Figures 6.19 and 6.20 compare the EFRFs obtained with the proposed method with the FRFs of four TELSs obtained with the original TELM at the selected time points for the fully non-stationary broad- and narrow-band excitations, respectively. The comparison shows that the EFRFs at the selected times closely approximate the corresponding FRFs. Finally the ETELM-Au-Beck algorithm is applied to the two systems for a duration of 15[s]. Table 6.7 reports the results compared to results obtained from a crude MCS analysis. Figures 6.21 and 6.22 report the convergence to the target probability of failure as a function of the number of sample size. As we have seen before, ETELM produces results that have order-of-magnitude accuracy, which is sufficient in many engineering applications.

Table 6.5: Excitation Properties fully non-stationary excitation

Input	$S_0(t_x)[\frac{\mathrm{m}^2}{\mathrm{s}^3}]$	$S_{FE}(\omega_0, t_x)$	t_x[s]	ω_{mid}[Hz]	$\omega'[\frac{\mathrm{Hz}}{\mathrm{s}}]$	$\bar{\zeta}$	$\sigma_{FE}(t_x)$[g]
IV0.733	1.00	10.00	1.00	-0.06	0.8	0.217	
V	0.590	1.00	10.00	1.00	-0.06	0.2	0.113

Table 6.6: ETELM output fully non-stationary excitation

Input	$\beta(4)$		$\beta(6)$		$\beta(8)$	
	ETELS	TELS	ETELS	TELS	ETELS	TELS
IV	6.183	6.273	4.249	4.278	3.499	3.513
V	10.192	10.902	6.900	7.146	5.507	5.584
Input	$\beta(10)$		$\beta(12)$			
	ETELS	TELS	ETELS	TELS		
IV	3.256	3.256	3.387	3.367		
V	4.945	4.945	5.061	4.969		

6.6 Conclusion

This chapter investigates an alternative method for studying nonlinear random vibration for non-stationary excitations and highly reliable systems. The input excitation is described as an evolutionary process according to Priestley's definition [82]. The approach used is in the family of linearization methods and since small values of probability are of interest TELM is used as a framework. An evolutionary TELM, named ETELM, is proposed to efficiently solve this class of problems. The key aspect of ETELM versus the normal TELM analysis is that only one optimization problem is solved, significantly reducing the computational cost. The method has been tested for five types of excitations: a time modulated band-limited white noise, two Kanai-Tajimi EPSDs representing a broad-band and a narrow-band process and two Kanai-Tajimi EPSDs with time varying parameters representing fully non-stationary broad-band and narrow-band excitation. The results are encouraging and they show that ETELM analysis can be employed instead of a series of TELMs without losing a significant degree of accuracy. In general, ETELM shares the shortcomings of the original TELM. In particular, because ETELM is based on FORM, there is no measure of the error due to the first-order approximation and thus the accuracy cannot be estimated in advance.

Table 6.7: Estimates of first-passage probability by ETELM and MCS fully non-stationary excitation

Input	x	$\hat{P}(F)$	$P_{MC}(F)$	$\hat{\delta}$ [%]	δ_{MC} [%]	$\bar{N}$	$\bar{N}_{MC}$
IV	$3\sigma_0$	1.599E-03	1.980E-03	4.01	7.10	500	10^5
V	$3\sigma_0$	2.779E-05	1.600E-05	3.81	25.00	500	10^5

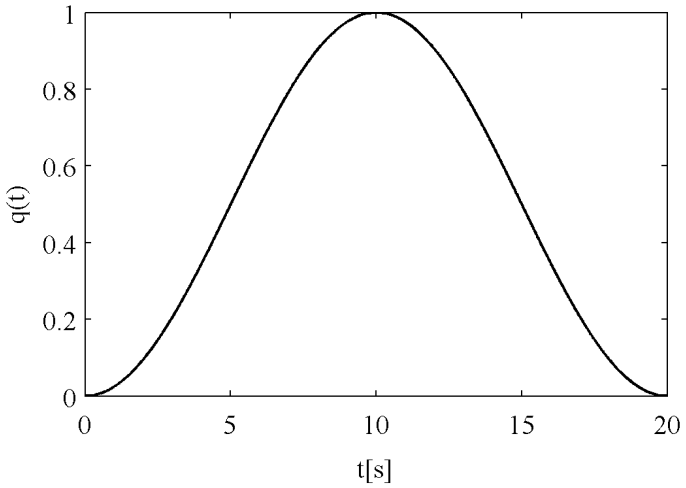

Figure 6.1: Time modulating function $q(t)$

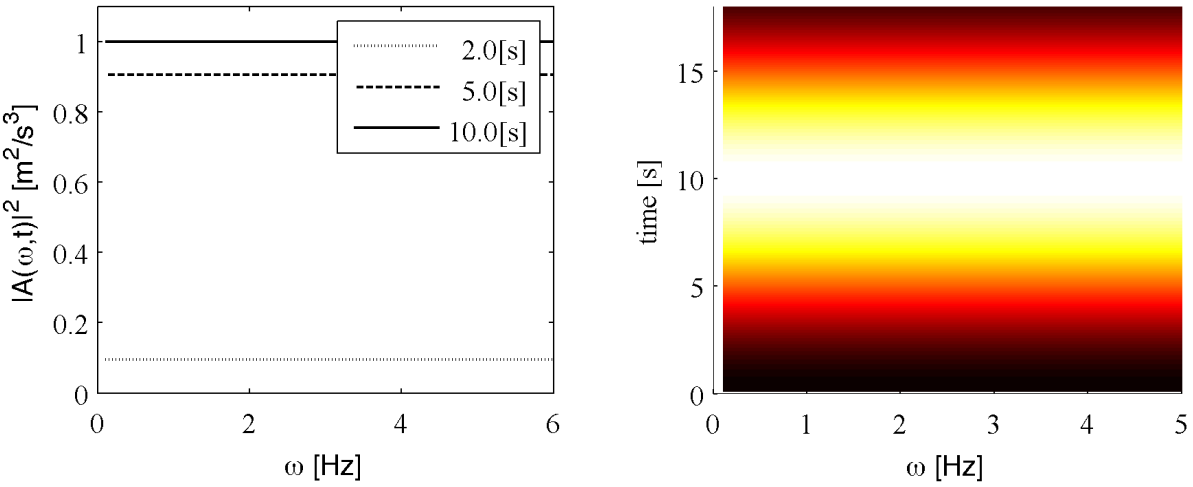

Figure 6.2: EPSD of modulated white noise excitation (excitation I)

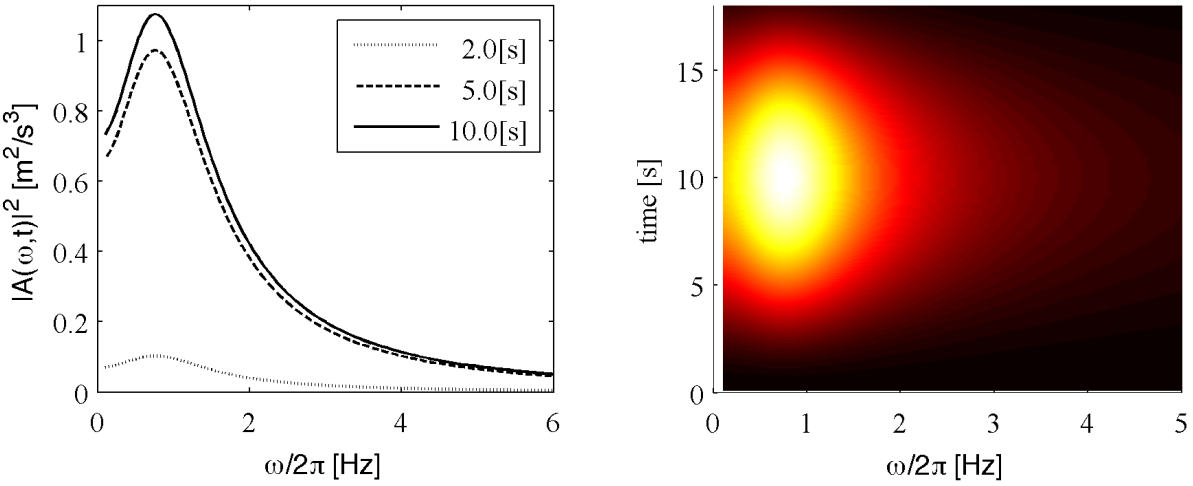

Figure 6.3: EPSD modulated broad-band excitation (excitation II)

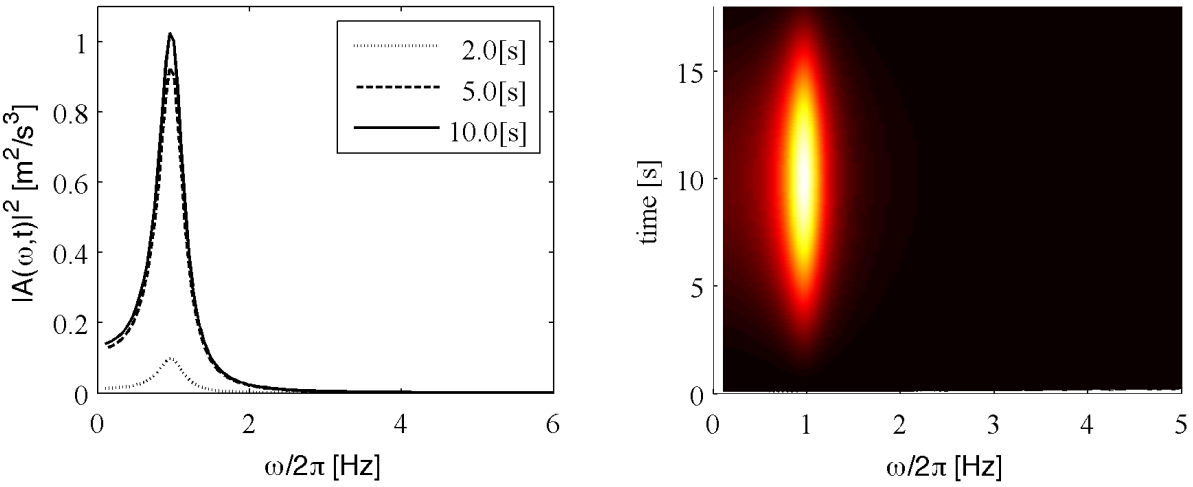

Figure 6.4: EPSD modulated narrow-band excitation (excitation III)

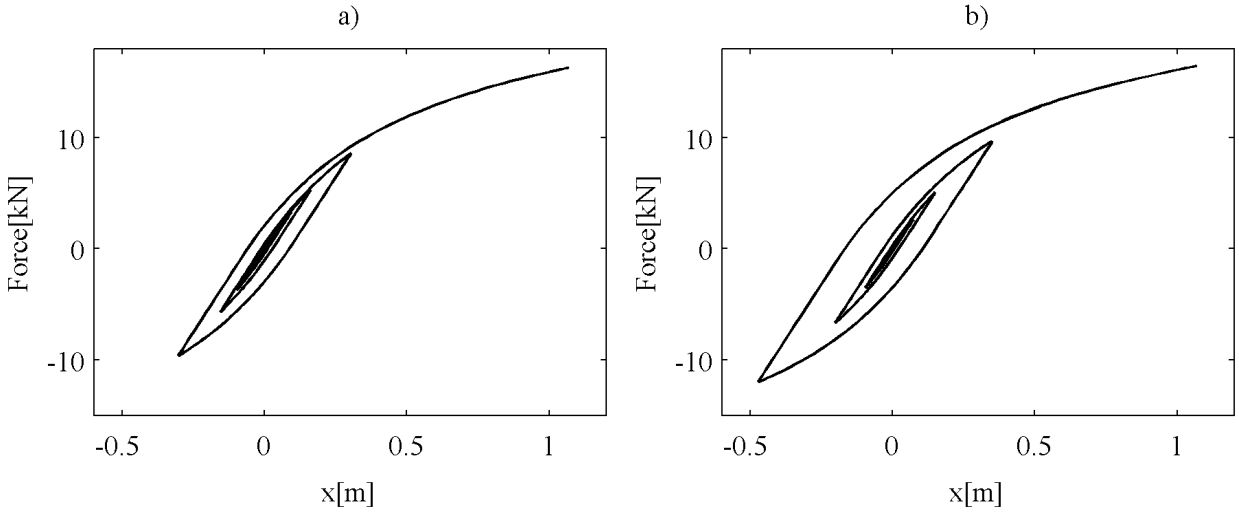

Figure 6.5: Hysteresis loop, for modulated broad-a) and narrow-b) band excitation

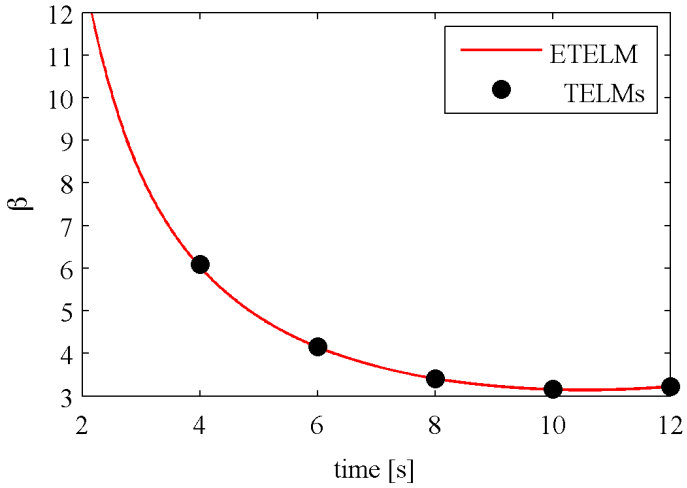

Figure 6.6: Reliability index for response to modulated white-noise (excitation I)

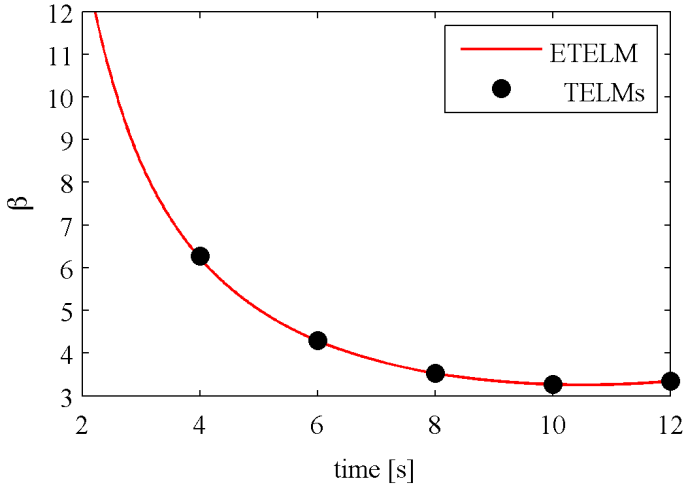

Figure 6.7: Reliability index for response to modulated broad-band excitation (excitation II)

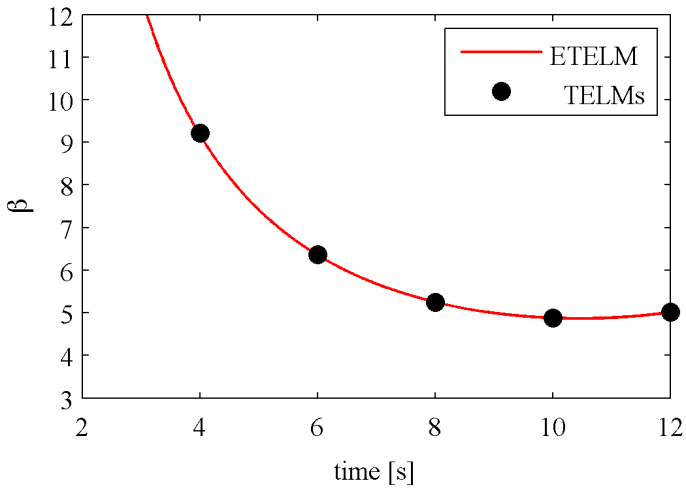

Figure 6.8: Reliability index for response to modulated narrow-band excitation (excitation III)

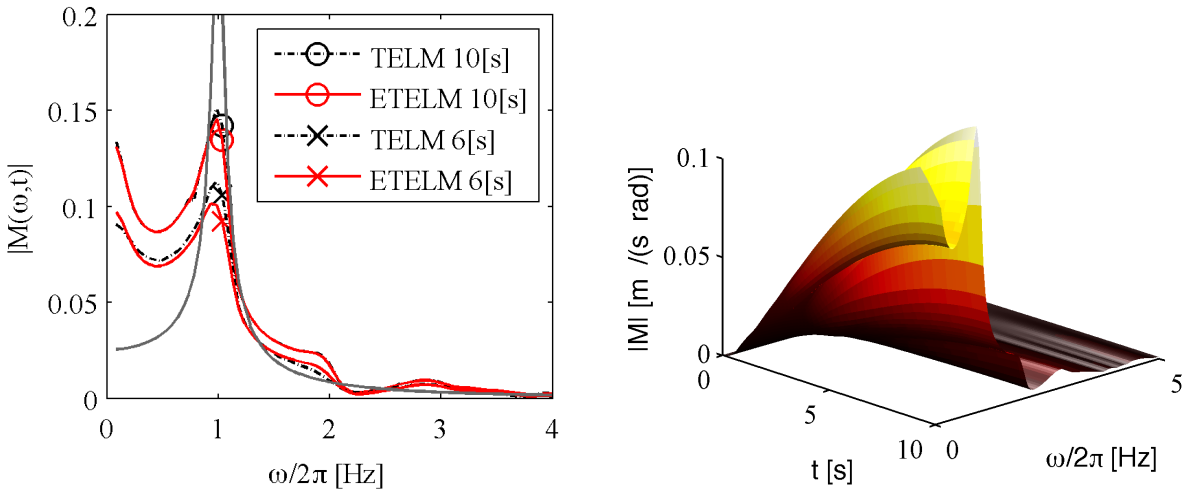

Figure 6.9: EFRF for response to modulated white-noise (excitation I), the grey line corresponds to the linear case

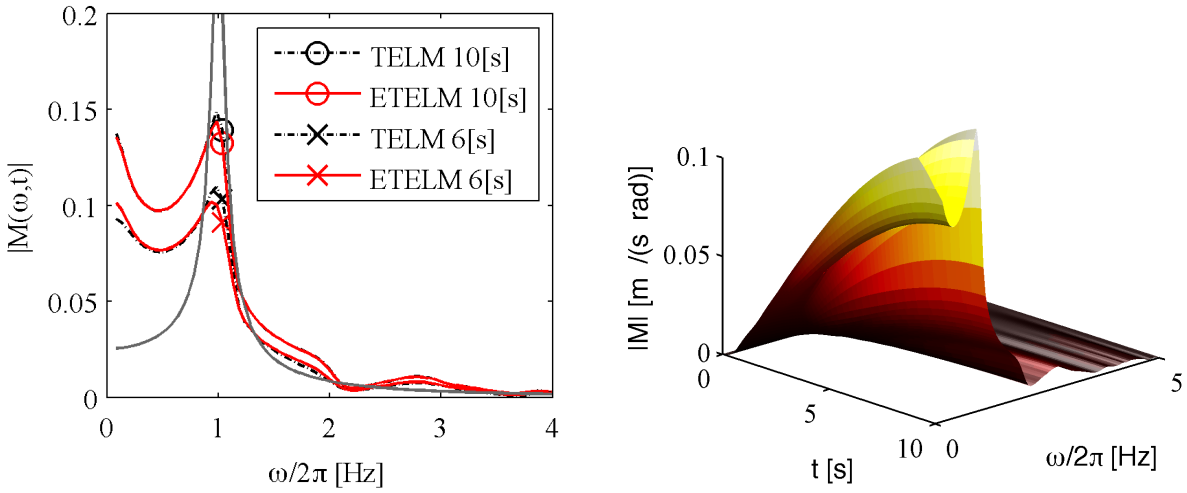

Figure 6.10: EFRF modulated broad-band excitation (excitation II), the grey line correspond to the linear case

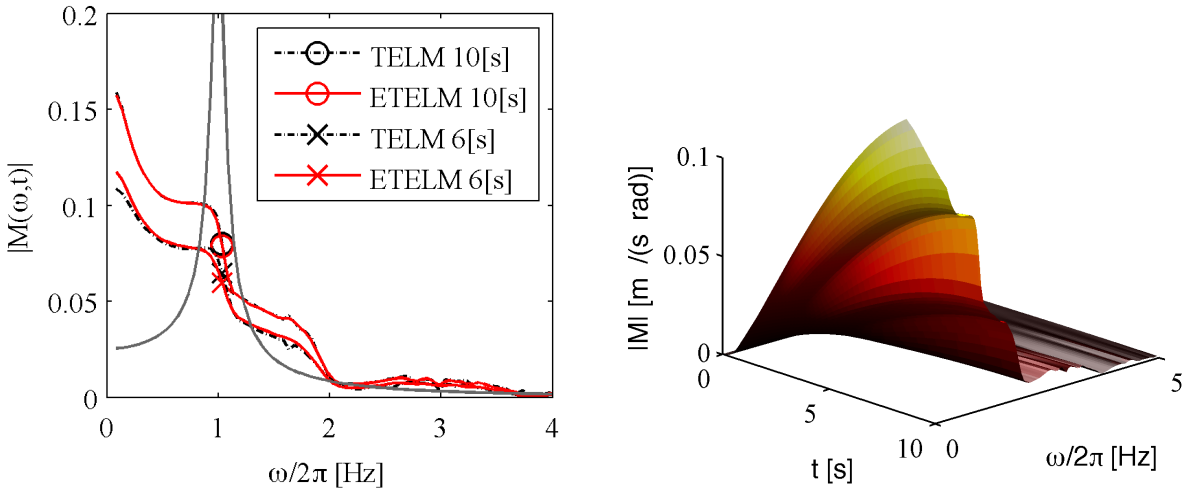

Figure 6.11: EFRF modulated narrow-band excitation (excitation II), the grey line correspond to the linear case

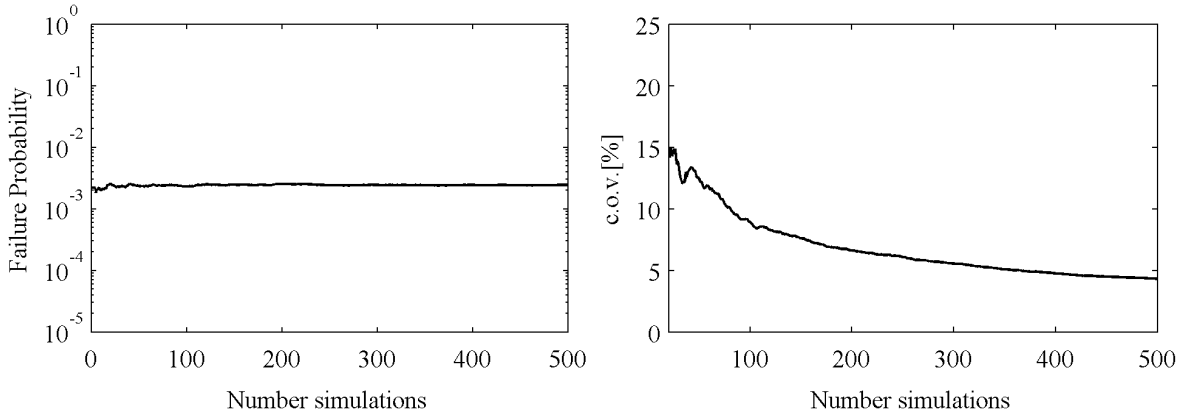

Figure 6.12: Convergence of $\hat{P}(F)$ for the case with modulated white-noise excitation (excitation I)

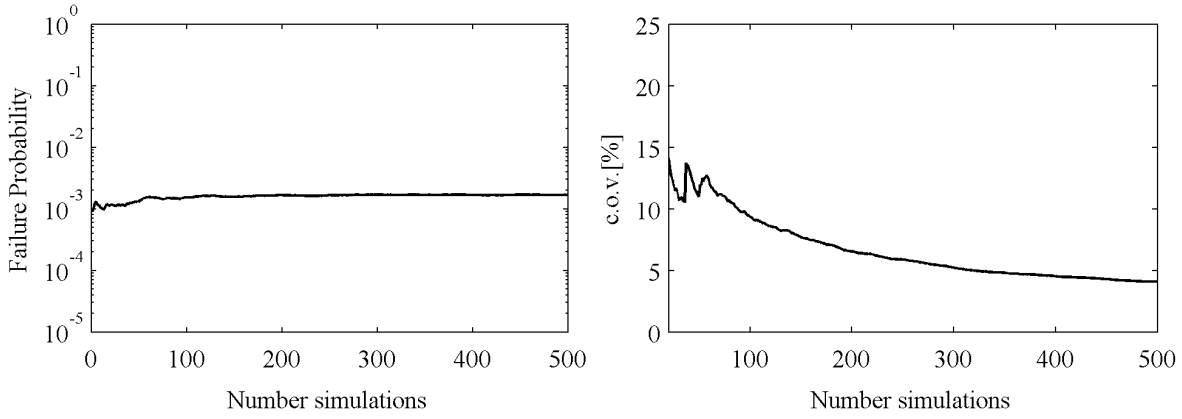

Figure 6.13: Convergence of $\hat{P}(F)$ for the case with modulated broad-band excitation (excitation II)

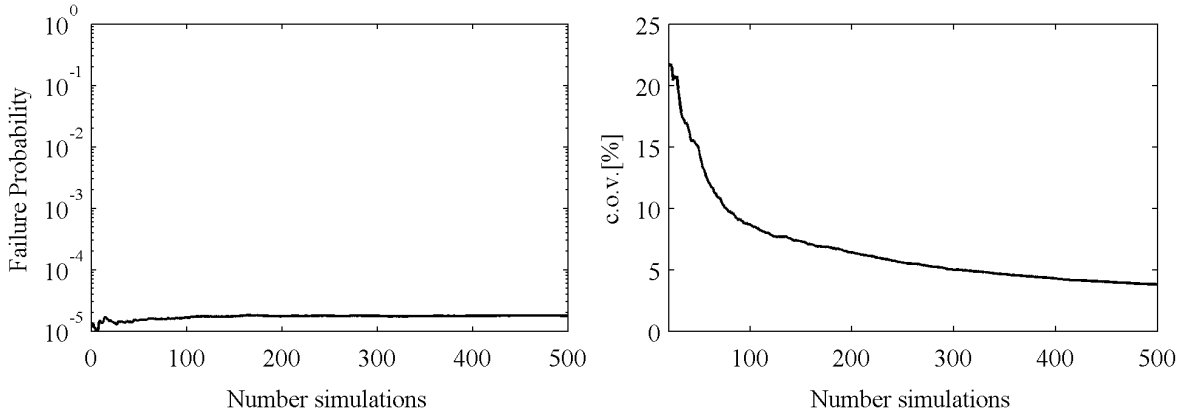

Figure 6.14: Convergence of $\hat{P}(F)$ for the case with modulated narrow-band excitation (excitation III)

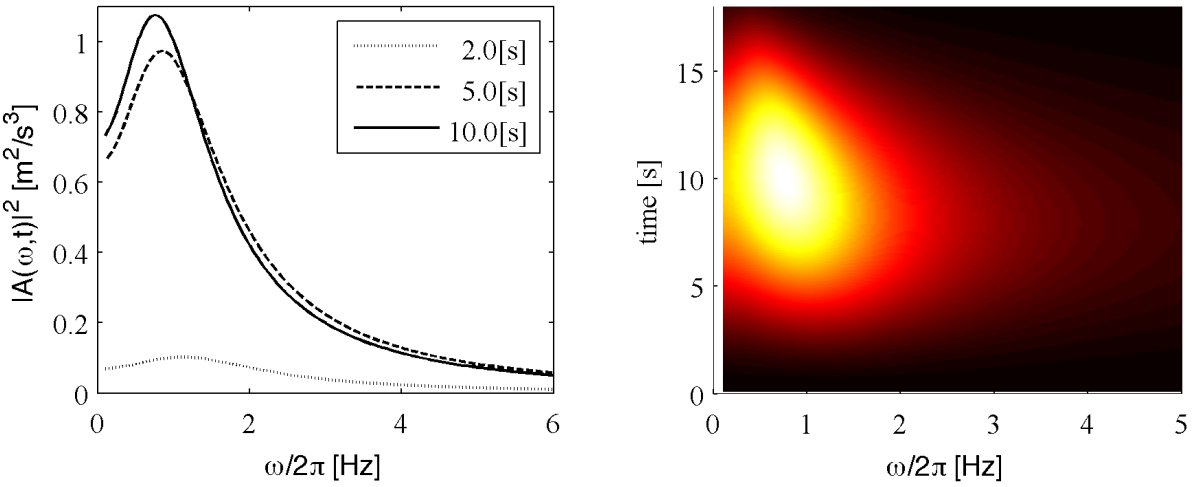

Figure 6.15: EPSD fully non stationary broad-band excitation (excitation IV)

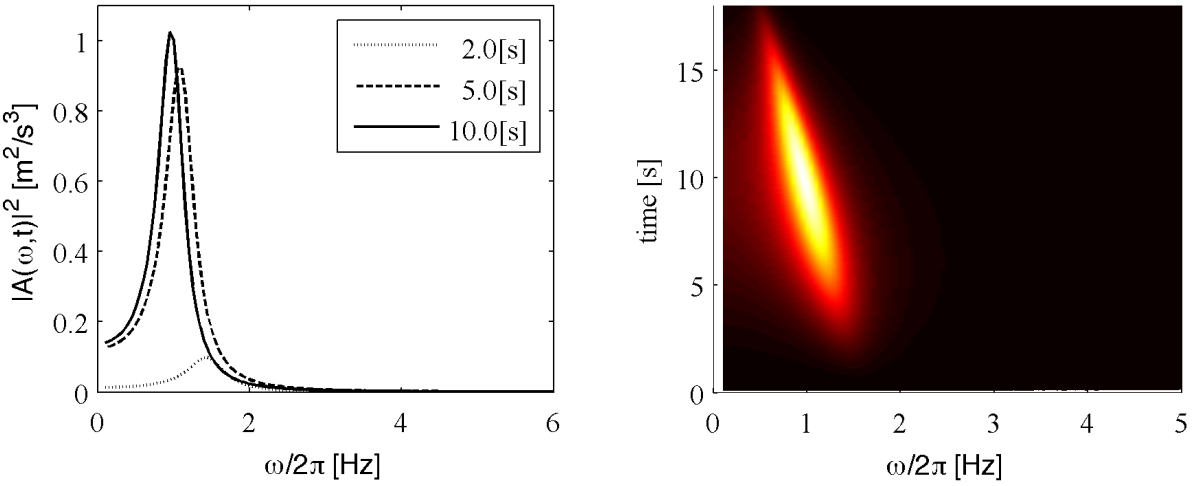

Figure 6.16: EPSD fully non stationary narrow-band excitation (excitation V)

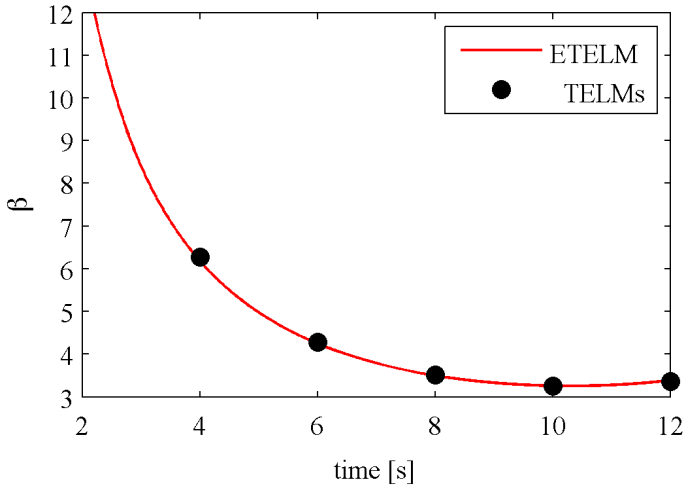

Figure 6.17: Reliability index for response to fully non-stationary broad-band excitation (excitation IV)

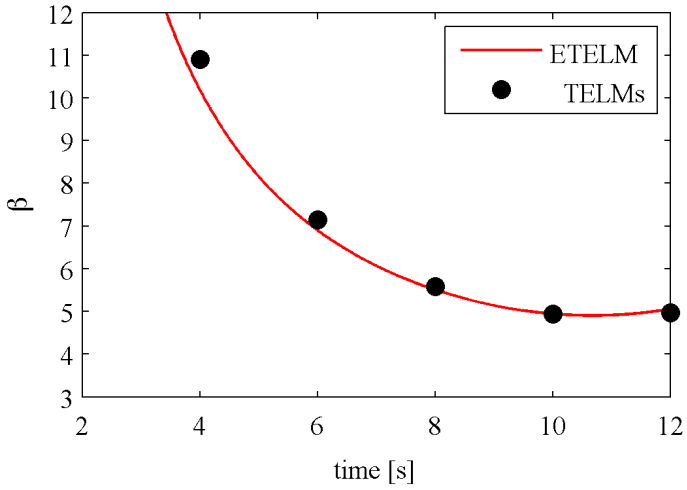

Figure 6.18: Reliability index for response to fully non-stationary narrow-band excitation (excitation V)

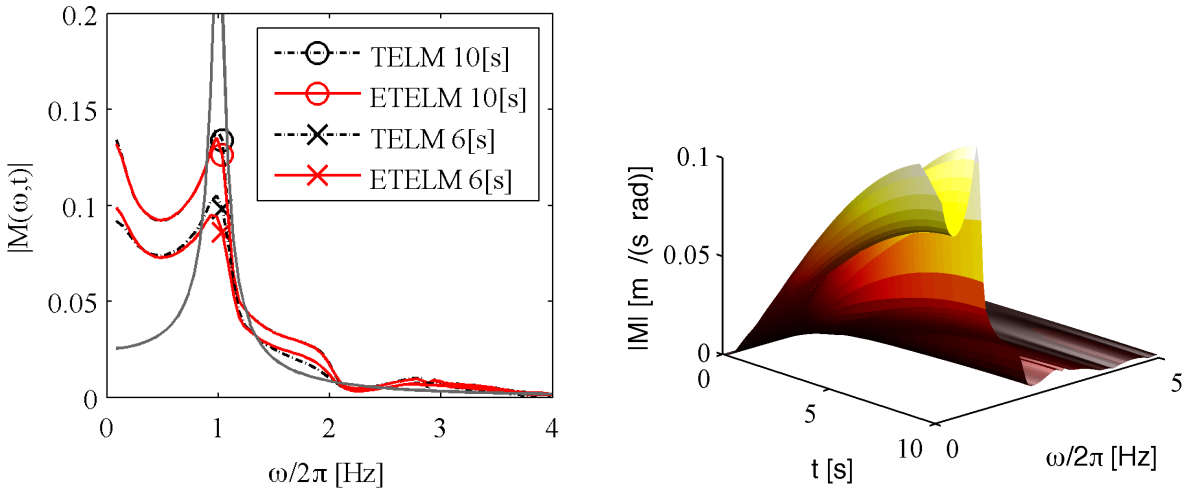

Figure 6.19: EFRF fully non-stationary broad-band excitation (excitation IV), the grey line correspond to the linear case

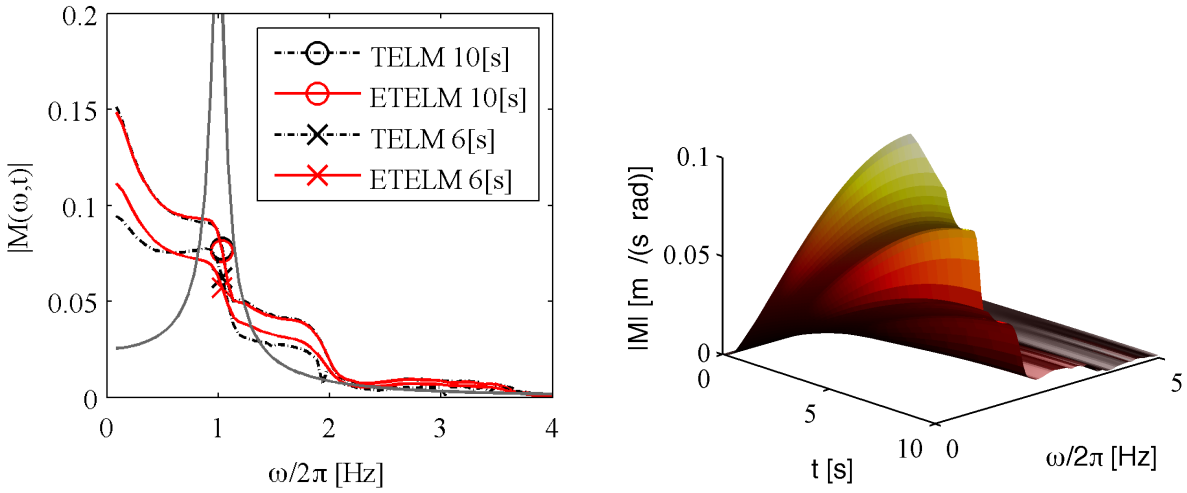

Figure 6.20: EFRF fully non-stationary narrow-band excitation (excitation V), the grey line correspond to the linear case

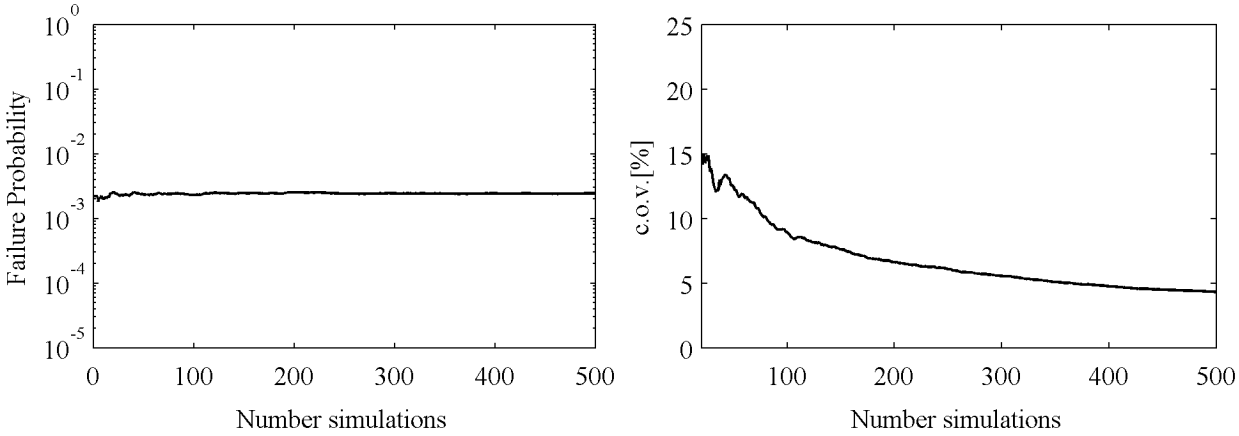

Figure 6.21: Convergence of $\hat{P}(F)$ for the case with fully non-stationary broad-band excitation (excitation IV)

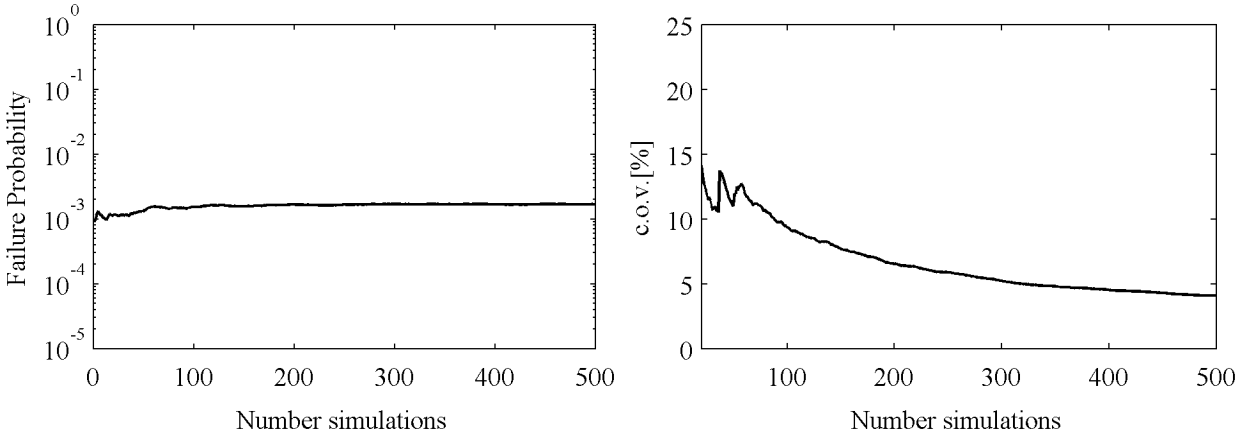

Figure 6.22: Convergence of $\hat{P}(F)$ for the case with fully non-stationary narrow-band excitation (excitation V)

Chapter 7

Conclusion

7.1 Introduction

In this last chapter, we conclude our journey by reviewing the contribution of this research to TELM and by consequently summarizing the past and current state-of-the-art of the method. We then dedicate a section on discussing the shortcomings of the first-order reliability method, FORM and thus indirectly of TELM in high dimensional spaces. The chapter ends with a description of recommended future studies.

7.2 State of art of TELM

This dissertation finds its roots in the previous works of Fujimura and Der Kiureghian [37, 38, 55] and Garrè and Der Kiureghian [40], which is summarized in the following subsection.

TELM: Previous research

The TELM is a novel linearization method that uses FORM to accurately estimate the tail of the response distribution for nonlinear systems under stochastic inputs. The following points summarize important characteristics of the method:

- The tail-equivalent linear system, TELS, is introduced and numerically identified in terms of its IRF and/or FRF for a specific response threshold. A one-to-one relationship exists between the design point of the tail distribution and the IRF/FRF of a linear system. In particular, the coordinates of the design point are sufficient to determine the IRF/FRF. In the nonlinear case, this one-to-one relationship completely characterizes the TELS when linearization is employed at the design point of the nonlinear system. Remarkably, TELS is a nonparametric linear system in the sense that no parameterized model needs to be defined. Even the order of the system need not be determined.

- The TELS is independent of a scaling of the excitation since the direction of the design point or the shape of the limit-state surface is invariant of this scaling. This characteristic is central in obtaining fragility curves and, hence, particularly useful in the context of PBEE.

- For broad-band excitations, the TELS is mildly dependent on the frequency content of the excitation. Hence, a white-noise approximation can be used to determine the IRF/FRF. For narrow-band excitations, this is no longer valid and the IRF/FRF must be determined for the specific input power spectral density.

- The TELS is strongly dependent on the response threshold that defines the limit-state function. Through this dependence, TELM is able to capture the non-Gaussian tail of the response distribution. By selecting a series of thresholds, one obtains a series of different TELSs. Statistics of the response of interest are obtained by applying linear stochastic dynamic theory to each of the identified TELSs.

Contribution of this dissertation to TELM and the current state of the method

After the introductory Chapter 2, where the frequency-domain application of TELM, originally proposed by Garrè and Der Kiureghian [40], has been extended to an inelastic system, the first part of this dissertation formalizes and extends TELM analysis with different types of discretization of the input process. Specifically, a general formulation for discrete representation of a Gaussian band-limited, white-noise process is introduced, which employs the sum of deterministic and orthogonal basis functions weighted by random coefficients. Representation of the band-limited white noise is essential in TELM since it serves as a building block for describing general stationary and non-stationary processes in frequency and time domains. It was shown that the selection of the basis functions completely defines the two types of discretizations used in the earlier works. In particular, a train of equally spaced time delta-Dirac functions leads to the current time-domain discretization, while harmonic functions, i.e., sine and cosine, with equally spaced frequencies lead to the current frequency-domain discretization. However, other types of orthogonal basis functions can be used with advantage to represent a Gaussian band-limited white noise. In this dissertation, we used sinc basis functions, which are at the base of the well-known sinc interpolation formula. More specifically, the sinc interpolation formula is used to generate band-limited Gaussian white noise by randomizing the coefficients of the series. It turns out that this representation is suitable for reducing the total number of random variables that are necessary to describe the process, since it decouples the computational-time discretization from the band-limit of the process. Through a numerical example, we showed that use of the sinc basis functions leads to significant computational savings in TELM. At the current stage, only sinc functions have been explored. Further research may consider other basis functions.

Next, we focused on the problem of a nonlinear system subjected to multi-component excitations. In its original version, TELM was developed for a single component of excitation. However, several practical problems require analysis for simultaneous excitations. A good example is a 3-dimensional structure subjected to earthquake ground motions. In this work, we tackled this class of problems by defining an augmented standard normal space composed of all the random variables that define

the multiple components of the excitation. We defined the limit-state function in this space and determined the augmented design point. The linearization then takes place at the augmented design point, which is determined by applying the iHLRF algorithm [112]. Special attention must be paid to the computation of the augmented gradient when using this algorithm. The TELS is identified in terms of the coordinates of the augmented design point, this leading to numerical determination of the IRF/FRF of the response quantity of interest, at the specified threshold, with each input component. Notably, the partition of the design point, induced by the components, is used to identify each particular IRF or FRF. Once the TELS is defined, response statistics of interest are determined by linear random vibration analysis by superposition of responses due to each component of excitation. The method is numerically examined for an asymmetric structure subjected to two statistically independent components of excitation. The example reported uses stationary excitations, but the non-stationary case can be studied with the method proposed in the last part of the dissertation.

In Chapter 6, we introduced a novel method to study the stochastic response of a nonlinear system under non-stationary excitation. For non-stationary excitations, the original TELM requires computation of TELSs for a series of points in time to study the evolution of response statistics. This procedure turns out to be computationally burdensome. As an approximate alternative, we proposed the evolutionary TELM, ETELM. Since TELM analysis requires the representation of the input as a filtered Gaussian white noise process, the evolutionary process theory introduced by Priestley [82] is of specific interest. In particular, we extended the concept of evolutionary FRF, EFRF, to TELM analysis. We started by showing that, for a linear system, TELM correctly represents the EFRF. Then, we use Priestley's theory to define an evolutionary TELS, ETELS, for a nonlinear system. This is done by first numerically determining the IRF, and then determining the EFRF as its incomplete Fourier transformation "weighted" by the modulating function. Different methods were proposed for obtaining the IRF, depending on the nature of the excitation. If the input excitation is uniformly modulated, the IRF is obtained by applying the classical TELM analysis to the underlying stationary process, and then the EFRF is obtained as discussed above. On the other hand, if the filter has a time varying frequency content, linearization is applied at the time of the peak variance of the excitation, and the EFRF is again obtained by the incomplete Fourier transform.

The ETELS accurately estimates the continuous time evolution of the design point by only one TELM analysis. This is the essence of its efficiency compared to the standard TELM analysis. The method has been investigated for five type of excitations: (I) uniformly modulated white noise, (II) uniformly modulated broad-band excitation, (III) uniformly modulated narrow-band excitation, (IV) fully non-stationary broad-band excitation, and (V) fully non-stationary narrow-band excitation. Once the ETELS is defined, linear random vibration is used to compute the design point as a function of time.

In reliability analysis of a structure subjected to a transient stochastic excitation, the most important statistic of interest is the first-passage probability, i.e., the probability that the response will exceed a specified threshold during the course of the excitation. An exact solution of this problem does not exist even for linear systems and, hence, approximate methods are used. In this dissertation, Chapter 2 and Chapter 5 have used the approximate formula proposed by Vanmarcke [105], which is not applicable to non-stationary excitations. For the last part of this dissertation, we make use of a simulation method in conjunction with ETELM to solve the first-passage probability.

An importance sampling method originally proposed by Au and Beck [4] for linear systems has been employed for this purpose. The algorithm principally requires knowledge of the evolution of the design point in time, which is readily given by ETELM analysis. The application to a nonlinear system, with the five proposed excitations, shows that the Au-Beck algorithm, together with ETELS, provides a good estimation of the first passage probability. Moreover, the methodology has been shown to be highly efficient in comparison to the original TELM analysis for non-stationary problems.

7.3 Limitations and shortcomings of TELM

The classical drawbacks of FORM also apply to TELM [37, 38]. In particular, there is no measure of the error due to the linearization approximation, which means that the accuracy of TELM cannot be estimated in advance. Moreover, TELM requires far more analysis than ELM, if one is interested only in the first and second moments of the nonlinear response. Thus, for second-moment analysis, ELM is the appropriate method, while TELM is the appropriate method to use for estimation of tail probabilities.

In the past few years, several authors [53, 93, 103] have raised concerns on use of FORM in high dimensional spaces, which also indirectly applies to TELM. In essence, the issue is related to the significance of the design point in high dimensional spaces. The design point represents the point in the standard normal space with the highest probability density in the failure domain. While in small dimensions this point and its neighborhood represent also the region with the highest contribution to the failure probability, in high dimensional spaces this is no longer the case. This problem is known as "the curse of dimensionality" and it is due to the geometrical properties of high-dimensional Gaussian spaces . This is elaborated on in the next subsection.

Some properties of standard normal space in high dimensions

It is well known that the square of the Euclidean norm of a vector $\boldsymbol{u} = [u_1, \ldots, u_N]$ in an N-dimensional standard normal space has the chi-square distribution with N degree of freedom, i.e.,

$$\|\boldsymbol{u}\|^2 \sim \chi^2_N. \tag{7.1}$$

When N tends to infinity (or for engineering purpose when N is sufficiently large), the distribution of the norm of $\|\boldsymbol{u}\|$, which has a χ distribution, can be approximated with a normal distribution of mean $\sqrt{N}$ and variance equal to $1/2$ [21, 35], i.e.,

$$\|\boldsymbol{u}\| \sim \chi_N \approx \mathcal{N}\left(\sqrt{N}, \frac{1}{2}\right), \text{ for } N \to \infty. \tag{7.2}$$

Figure 7.1 shows the evolution of χ_N distribution as N increases. This implies that most of the probability mass in the N-dimensional standard normal space belongs to an hyper-ring centered at distance $\sqrt{N}$ from the origin. We name the neighborhood of this ring as the important hyper-ring. In particular, we can define the important hyper ring by specifying its inner and outer radiuses by

$$\sqrt{N} - \bar{u} \leq \|\boldsymbol{u}\| \leq \sqrt{N} + \bar{u}, \tag{7.3}$$

where $\bar{u}$ is a scalar that determines the quantity of probability included in the ring. As an example, consider the problem introduced in Chapter 4, where the input excitation of the original TELM is defined using 1000 random variables. This leads to a standard normal space of dimension $N = 1000$. If we want to include, for example, $1-10^{-6}$ probability content in the important hyper-ring, we need to select $\bar{u} = 3.46$. In that case, virtually all the probability is inside the region $28.2\boldsymbol{e} \leq \boldsymbol{u} \leq 34.8\boldsymbol{e}$, where $\boldsymbol{e}$ is the unit normal along $\boldsymbol{u}$. In our example, we saw that the design point was $\beta = 3.1$, while the important hyper-ring is centered on an hyper-sphere of radius $\|\boldsymbol{u}\| = 31.6$. This means that, even though the design point has highest probability density in the failure domain, its neighborhood is insignificant since the bulk of the probability mass is located at the important hyper-ring, which is at distance of $\|\boldsymbol{u}\| = 31.6$ from the origin. This realization has led to criticism of using the design point as a statistical linearization point for high dimensional reliability problems. While the significance of the design point can be questioned in statistical terms, the point still preserves all the physical properties described in this dissertation. In particular, it remains as the realization point with the highest probability density function.

It is clear that in high dimensions, most of the failure probability is located in the intersection domain of the important hyper-ring and the failure domain, which depends on the shape of the limit-state surface. Of course the accuracy of FORM depends on the shape of limit-state surface, which inherently depends on the physics of the problem. In particular, the error in TELM in high dimensions is given by the volume of the segment of the important hyper-ring that is between the limit-state surface and the hyperplane at the design point that defines the TELS. Here, we denote this segment of the hyper-ring as the "volume error". Figure 7.2 shows schematically the concept of "volume error".

FORM accuracy vs shape of the limit state surface

While for a linear case the limit-state surface is a hyperplane and the design point preserves its significance, the nature of the nonlinear system strongly influences the shape of the limit-state surface. In particular, it has been shown [53, 56] that for stiffening systems the limit-state surface

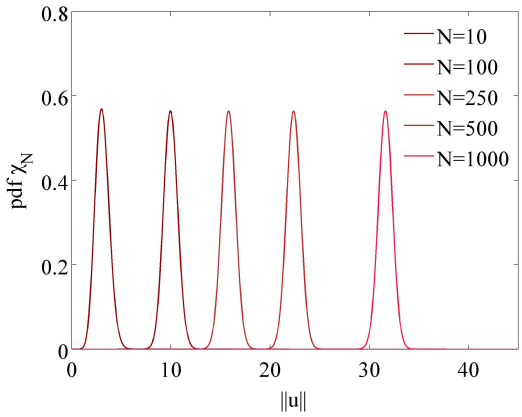

Figure 7.1: χ convergence for $N \to \infty$

becomes very irregular, often with safe and unsafe patches, and FORM cannot be applied. This is due to the fact that the high-frequency content in the response process becomes progressively more important as we advance to the nonlinear range.

On the other hand, we have seen that softening systems involve progressively lower frequency content, which leads to smooth limit state functions with saddle-shape limit-state surfaces. For this type of systems, which are most common in civil structures, FORM has been found to be fairly accurate [56]. Figure 7.3 illustrates limit-state surfaces for a linear, a stiffening and a softening system.

To understand the reason why TELM performs well for softening systems, we examine the geometry of the limit-state surface. Since the problem is defined in a high-dimensional space, we can only plot the shape of the limit-state surface in selected planes [53]. In particular, let us define the plane $\Pi(\boldsymbol{e}^*, \boldsymbol{e})$ as the subspace induced by the design point direction $\boldsymbol{e}^*$ and a selected perpendicular direction $\boldsymbol{e}$. In the case of softening systems, our experience shows that the limit-state surface always has a saddle shape, regardless of how we select the second direction (see Figure 7.4-c). For this type of limit-state surface, the TELM works properly since the volume error on the two sides of the surface is compensated. Figure 7.4-c illustrates this concept. For plots for different types of physical systems, the reader should consult [53, 56]. Our interpretation of this behavior is suggested by the physical nature of softening systems, where the contribution of high frequencies is negligible, since the important frequency content is on the low frequency range. A problem arises with negligible high frequency content in that the net "volume error" is approximately invariant to high frequencies. Since it is possible to increase the high frequency content by increasing the number of random variables, and consequently shifting away from the origin the important hyper-ring, the only way to keep the net volume error constant is to have a saddle-shape limit-state surface. As we have seen in Chapter 4, when we discretize a white noise on the time interval $[0, \bar{t}]$, the number of random variables controls the bandwidth of the input. We have seen that by decreasing this number, and hence by reducing the bandwidth, the design point and the approximation of the failure probability

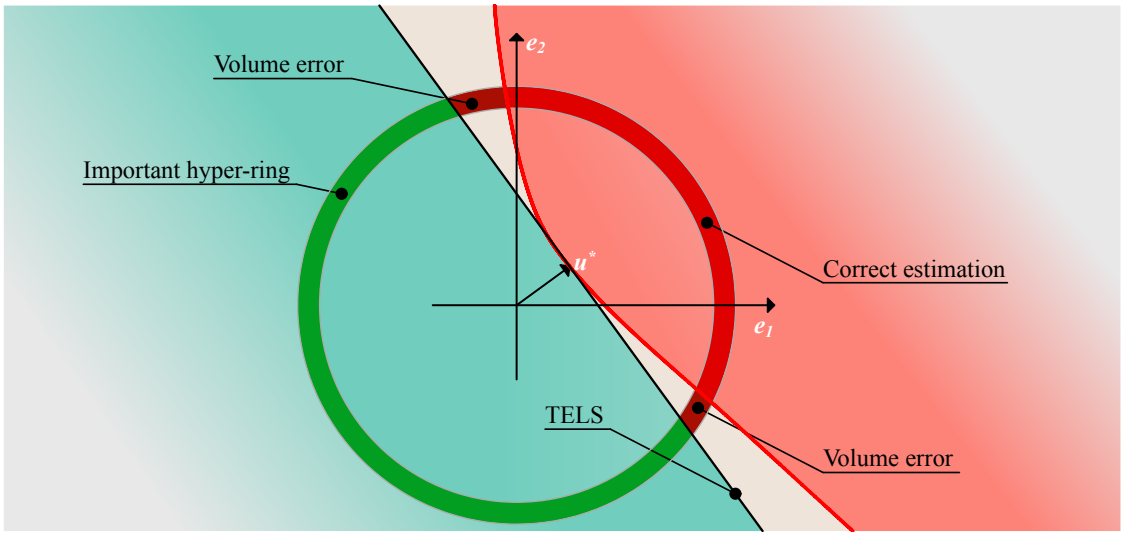

Figure 7.2: Volume error concept

do not change. These results are confirmed by MCS. This means that, physically, high-frequency components do not contribute to the failure of the system. A useful reliability interpretation then emerges, which argues that the error of the linearization is independent of the increasing number of random variables. This is because the underestimating and overestimating errors are compensating each other, and also because the limit-state surface is flat with respect to random variables that define high-frequency components in the excitation. It also follows that TELM must be used with caution for problems that are not physically based, or for problems where this physical interpretation cannot be applied. Because of the importance of the "volume error" in high dimensions, limit-state surfaces that are concave or convex (see Figure 7.4 a and b) may lead to a strong lack of accuracy of FORM [93]. Nevertheless, the direction of the design point in high dimensional spaces still preserves a high significance since it indicates the direction of the failure domain.

An ongoing work attempts at introducing a new concept of linearization based on a secant plane, which can be applied to more general limit-state surfaces. A recent works by Alibrandi *et al.* [1, 69] applies a correction to the original FORM, also employing a secant plane.

In conclusion, TELM is an efficient method that accurately estimates the tail distribution of responses of nonlinear systems, in particular for softening systems. In these cases, TELM is far more accurate than ELM in estimating the tail of the response distribution [37, 38], since it can capture the non-Gaussian nature of the distribution. It is also computationally more efficient than ELM when fragility curves are of interest, and it is generally much more efficient than the classical MCS method. However, TELM must be used with caution and with good understanding of the physical behavior of the system. In particular, further research needs to be conducted in studying the general reliability problem when system uncertainties are also included in the analysis as random variables. The influence of these random variables on the shape of the limit-state surface, and thus on the accuracy of TELM needs further investigation.

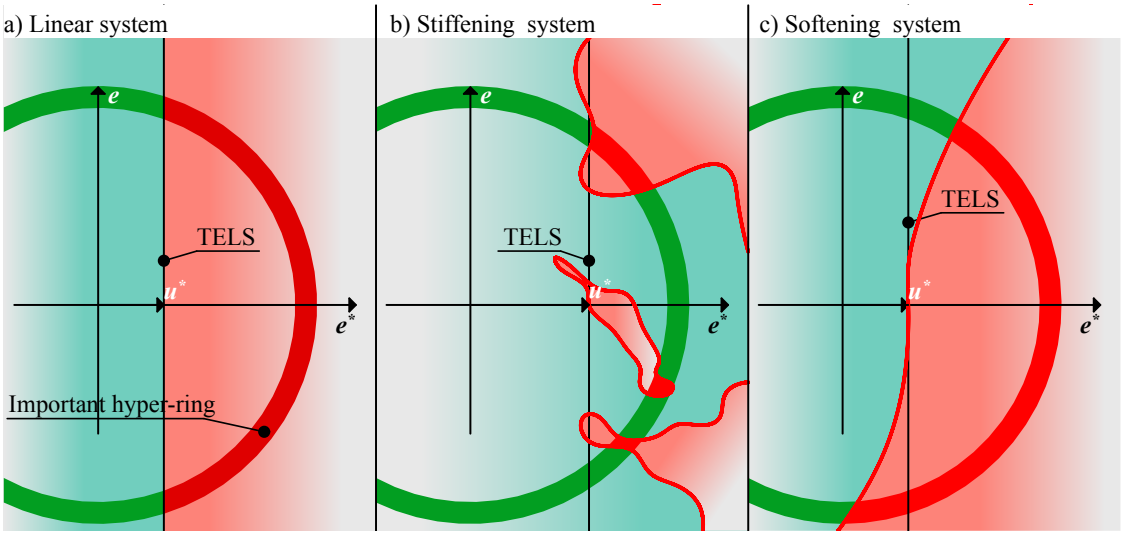

Figure 7.3: Limit state functions for different physical systems. a) FORM correct solution, b) FORM not applicable, c) FORM accurate solution

7.4 Further studies

Although TELM is approaching maturity, some open issues remain unsolved and require further analysis and development:

- For discrete representation of the input process(es), forms of basis functions other than sinc functions can be explored. Particularly appealing are Lagrange polynomials and spline basis functions. More generally, it is worth exploring the possibility of using wavelet theory, especially for non-stationary excitations. The path is drawn by the first part of this work. Starting from basic wavelet expansions, it is eventually possible to build a band-limit white noise by randomizing the coefficient of the series. From there, the theory of TELM can be applied as was done in Chapter 4.

- TELM has been successfully extended for analysis of nonlinear response to multiple components of statistically independent Gaussian excitations. The issue of correlated excitations remains open. In general, the independence assumption between different components of ground motion at a given site is not restrictive because uncorrelated principal components can be determined by a rotational transformation. But there are many applications that this assumption can be restrictive. One example in earthquake engineering is the response of a multiply-supported structure to partially coherent support motions. Other examples include wave or wind loading at different locations of a large structure. Additional development is needed to extend TELM to these classes of problems.

- The non-stationary case has been solved with good accuracy and computational efficiency; however, the problem of degrading systems still remains open. Responses of degrading systems are inherently non-stationary, even when the input excitation is stationary. Whether TELM or ETELM are applicable to these systems is not clear at the present time.

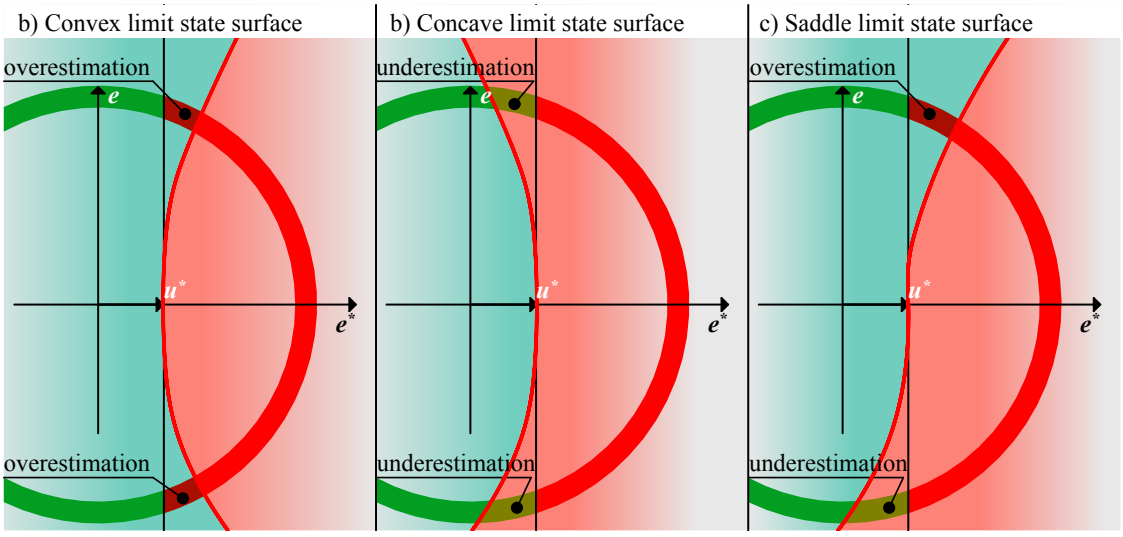

Figure 7.4: Limit state functions shapes a) FORM overestimates the response, b) FORM underestimates the response, c) FORM, the overestimation and underestimation error compensate

- This study considered the application of TELM to deterministic systems subjected to stochastic excitations. Earlier works by Koo *et al.* [57] investigated an application of FORM including system uncertainties and stochastic inputs. The coordinates of the design point obtained in the extended FORM, in theory, completely define the TELS. Statistics obtained with this TELS include also the effect of system uncertainties. Nevertheless, further investigation is necessary to understand the effect of these uncertainties on the shape of the limit-state surface. As we have seen in the preceding section, the shape of the limit-state surface can strongly influence the accuracy of FORM and thus of TELM analysis.

- The TELS is invariant of the scale of the excitation, and this property is used to efficiently derive fragility curves, as demonstrated in Chapter 2 and Chapter 5. However, further research is needed to establish to determine the ranges of validity of this approximation. In fact, our experience shows that for particular combinations of input intensities and parameters of the nonlinear model, this approximation may not provide sufficient accuracy. An ongoing investigation is attempting to shed further light on this problem.

- There is need for further investigation to address problems related to the FORM and TELM approximations in high dimensions, as described in the preceding section. In particular, an approximation that takes advantage of the knowledge of the important hyper-ring should be sought. Further effort along this line is currently underway.

Bibliography

[1] Umberto Alibrandi and Armen Der Kiureghian. "A gradient-free method for determining the design point in nonlinear stochastic dynamic analysis". In: *Probabilistic Engineering Mechanics* 28 (2012), pp. 2–10.

[2] T.S. Atalik and S. Utku. "Stochastic linearization of multi-degree-of-freedom nonlinear systems". In: *Earthquake Engineering & Structural Dynamics* 4.4 (1976), pp. 411–420.

[3] S.K. Au and J. L. Beck. "Estimation of small failure probabilities in high dimensions by subset simulation". In: *Probabilistic Engineering Mechanics* 16.4 (2001), pp. 263–277.

[4] S.K. Au and J. L. Beck. "First excursion probabilities for linear systems by very efficient importance sampling". In: *Probabilistic Engineering Mechanics* 16.3 (2001), pp. 193–207.

[5] S.K. Au and J.L. Beck. "Important sampling in high dimensions". In: *Structural Safety* 25.2 (2003), pp. 139–163.

[6] S.K. Au and J.L. Beck. "Subset simulation and its application to seismic risk based on dynamic analysis". In: *Journal of Engineering Mechanics* 129.8 (2003), pp. 901–917.

[7] S.K. Au, J. Ching, and J.L. Beck. "Application of subset simulation methods to reliability benchmark problems". In: *Structural Safety* 29.3 (2007), pp. 183–193.

[8] T.T. Baber and Y.K. Wen. "Random vibration hysteretic, degrading systems". In: *Journal of the Engineering Mechanics Division* 107.6 (1981), pp. 1069–1087.

[9] T. Belytschko et al. *Nonlinear finite elements for continua and structures*. John Wiley & Sons, 2013.

[10] C.M. Bender and S.A. Orszag. *Advanced mathematical methods for scientists and engineers I: Asymptotic methods and perturbation theory*. Vol. 1. Springer, 1999, pp. 545–551.

[11] P. Bjerager. "Probability integration by directional simulation". In: *Journal of Engineering Mechanics* 114.8 (1988), pp. 1285–1302.

[12] N.N. Bogolyubov and N.M. Krylov. "Fokker-Planck equations generated in perturbation theory by a method based on the spectral properties of a perturbed Hamiltonian". In: *Zapiski Kafedry Fiziki Akademii Nauk Ukrainian SSR* 4 (1939), pp. 81–157.

[13] N.N. Bogolyubov and D.P. Sankovich. "NN Bogolyubov and statistical mechanics". In: *Russian Mathematical Surveys* 49.5 (1994), pp. 19–49.

[14] R. Bouc. "Forced vibration of mechanical systems with hysteresis". In: *Proceedings of the fourth conference on non-linear oscillation, Prague, Czechoslovakia*. 1967.

[15] R.N. Bracewell. *The Fourier transform and its applications 3th edition*. Vol. 31999. McGraw-Hill New York, 1999.

[16] O. Brad. "The Fourier Transform and its Applications". In: *Lecture Notes for EE261, Stanford University* (2007).

[17] M. Broccardo and A. Der Kiureghian. "Discretization of stochastic processes in time domain by sinc basis function and application in TELM analysis". In: *Proceedings of the 16th conference of the International Federation of Information Processing (IFIP) Working Group 7.5 on Reliability and Optimization of Structural Systems*. Yerevan, Armenia, 2012.

[18] M. Broccardo and A. Der Kiureghian. "Multi-component nonlinear stochastic dynamic analysis using tail-equivalent linearization method". In: *Proceeding of 15th world conference on earthquake engineering*. Lisbon, Portugal, 2012.

[19] M. Broccardo and A. Der Kiureghian. "Non-stationary Stochastic Dynamic Analysis by Tail-Equivalent Linearization". In: *Proceeding of 11th International Conference on Structural Safety and Reliability*. New York, USA, 2013.

[20] M. Broccardo and A. Der Kiureghian. "Simulation of near-fault ground motions using frequency-domain discretization". In: *Proceedings of the 10th National Conference on Earthquake Engineering*. Anchorage, Alaska, 2014.

[21] L. Canal. "A normal approximation for the chi-square distribution". In: *Computational statistics & data analysis* 48.4 (2005), pp. 803–808.

[22] F. Casciati, L. Faravelli, and A.M. Hasofer. "A new philosophy for stochastic equivalent linearization". In: *Probabilistic engineering mechanics* 8.3 (1993), pp. 179–185.

[23] T.K. Caughey. "Equivalent linearization techniques". In: *The Journal of the Acoustical Society of America* 35.11 (1963), pp. 1706–1711.

[24] A.K. Chopra. *Dynamics of structures*. Vol. 3. Prentice Hall New Jersey, 1995. Chap. 9, p. 339.

[25] S. H. Crandall. "Non-Gaussian closure for random vibration of non-linear oscillators". In: *International Journal of Non-Linear Mechanics* 15.4 (1980), pp. 303–313.

[26] S.H. Crandall. "Non-Gaussianclosure techniques for stationary random vibration". In: *International journal of non-linear mechanics* 20.1 (1985), pp. 1–8.

[27] S.H. Crandall. "Perturbation techniques for random vibration of nonlinear systems". In: *The Journal of the Acoustical Society of America* 35.11 (1963), pp. 1700–1705.

[28] M. Dabaghi, S. Rezaeian, and A. Der Kiureghian. "Stochastic simulation of near-fault ground motions for specified earthquake and site characteristics". In: *Proceedings of the 11th International Conference on Applications of Statistics and Probability in Civil Engineering, Zürich, Switzerland*. Zürich, Switzerland, 2011, pp. 2498–2505.

[29] A. Der Kiureghian. "The geometry of random vibrations and solution by FORM and SORM." In: *Probabilistic Engeneering Mechanics* 23.3 (2010), pp. 322–338.

[30] O. Ditlevsen and H.O. Madsen. *Structural reliability methods*. Wiley, 1996.

[31] O. Ditlevsen, R.E. Melchers, and H. Gluver. "General multi-dimensional probability integration by directional simulation". In: *Computers & Structures* 36.2 (1990), pp. 355–368.

[32] I. Elishakoff and R. Zhang. "Comparison of the new energy-based versions of the stochastic linearization technique". In: *Nonlinear stochastic mechanics* (1992), pp. 201–212.

[33] S. Engelund and R. Rackwitz. "A benchmark study on importance sampling techniques in structural reliability". In: *Structural Safety* 12.4 (1993), pp. 255–276.

[34] F.C. Filippou. "Structural Analysis, theory and applications". In: *Lecture Notes for CE220, University of California Berkeley* (2009).

[35] R.A. Fisher. "On the interpretation of $\chi 2$ from contingency tables, and the calculation of P". In: *Journal of the Royal Statistical Society* (1922), pp. 87–94.

[36] P. Franchin. "Reliability of uncertain inelastic structures under earthquake excitation". In: *Journal of engineering mechanics* 130.2 (2004), pp. 180–191.

[37] K. Fujimura and A. Der Kiureghian. "Tail-equivalent linearization method for nonlinear random vibration". PhD thesis. University of California, Berkeley, 2006.

[38] K. Fujimura and A. Der Kiureghian. "Tail-equivalent linearization method for nonlinear random vibration". In: *Probabilistic Engineering Mechanics* 22.1 (2007), pp. 63–76.

[39] C.W. Gardiner. *Stochastic methods*. Springer-Verlag, Berlin–Heidelberg–New York–Tokyo, 1985.

[40] L. Garrè and A. Der Kiureghian. "Tail-Equivalent Linearization Method in frequency domain and application to marine structures". In: *Marine Structures* 23.3 (2010), pp. 322–338.

[41] A.E. Gelfand and A.F.M. Smith. "Sampling-based approaches to calculating marginal densities". In: *Journal of the American statistical association* 85.410 (1990), pp. 398–409.

[42] S. Geman and D. Geman. "Stochastic relaxation, Gibbs distributions, and the Bayesian restoration of images". In: *Pattern Analysis and Machine Intelligence, IEEE Transactions on* 6 (1984), pp. 721–741.

[43] W.R. Gilks. *Markov chain monte carlo*. Wiley Online Library, 2005.

[44] J. Goodman. *Introduction to Fourier optics*. McGraw-hill, 2008.

[45] M. Grigoriu and S. Balopoulou. "A simulation method for stationary Gaussian random functions based on the sampling theorem". In: *Probabilistic engineering mechanics* 8.3 (1993), pp. 239–254.

[46] T. Haukaas and A. Der Kiureghian. "Finite element reliability and sensitivity methods for performance-based earthquake engineering". In: *Pacific Earthquake Engineering Research Center, College of Engineering, University of California, Berkeley* (2004).

[47] T. Haukaas and A. Der Kiureghian. "Parameter sensitivity and importance measures in nonlinear finite element reliability analysis". In: *Journal of engineering mechanics* 131.10 (2005), pp. 1013–1026.

[48] M. Hohenbichler and R. Rackwitz. "Improvement of second-order reliability estimates by importance sampling". In: *Journal of Engineering Mechanics* 114.12 (1988), pp. 2195–2199.

[49] R.A. Ibrahim, A. Soundararajan, and H. Heo. "Stochastic response of nonlinear dynamic systems based on a non-Gaussian closure". In: *Journal of applied mechanics* 52.4 (1985), pp. 965–970.

[50] W.D. Iwan. "A generalization of the concept of equivalent linearization". In: *International Journal of Non-linear mechanics* 8.3 (1973), pp. 279–287.

[51] W.D. Iwan and I.M. Yang. "Application of statistical linearization techniques to nonlinear multidegree-of-freedom systems". In: *Journal of Applied Mechanics* 39.2 (1972), pp. 545–550.

[52] R.N. Iyengar and P.K. Dash. "Study of the random vibration of nonlinear systems by the Gaussian closure technique". In: *Journal of Applied Mechanics* 45.2 (1978), pp. 393–399.

[53] L.S. Katafygiotis and K.M. Zuev. "Geometric insight into the challenges of solving high-dimensional reliability problems". In: *Probabilistic Engineering Mechanics* 23.2 (2008), pp. 208–218.

[54] R.Z. Khasminskii. "A limit theorem for the solutions of differential equations with random right-hand sides". In: *Theory of Probability & Its Applications* 11.3 (1966), pp. 390–406.

[55] A. Der Kiureghian and K. Fujimura. "Nonlinear stochastic dynamic analysis for performance-based earthquake engineering". In: *Earthquake Engineering & Structural Dynamics* 38.5 (2009), pp. 719–738.

[56] S.D. Koduru and A. Der Kiureghian. "FORM in high dimensions for stochastic dynamic analysis". In: *Proceedings of the 16th conference of the International Federation of Information Processing (IFIP) Working Group 7.5 on Reliability and Optimization of Structural Systems*. Yerevan, Armenia, 2012.

[57] H. Koo, A. Der Kiureghian, and K. Fujimura. "Design-point excitation for non-linear random vibrations". In: *Probabilistic Engineering Mechanics* 20.2 (2005), pp. 136–147.

[58] P.S. Koutsourelakis. "Reliability of structures in high dimensions. Part II. Theoretical validation". In: *Probabilistic engineering mechanics* 19.4 (2004), pp. 419–423.

[59] P.S. Koutsourelakis, H.J. Pradlwarter, and G.I. Schuëller. "Reliability of structures in high dimensions, part I: algorithms and applications". In: *Probabilistic Engineering Mechanics* 19.4 (2004), pp. 409–417.

[60] F. Kozin. "The method of statistical linearization for non-linear stochastic vibrations". In: *Nonlinear Stochastic Dynamic Engineering Systems*. Springer, 1988, pp. 45–56.

[61] R.H. Kraichnan. "The closure problem of turbulence theory". In: (1961).

[62] E. Kreyszig. *Introductory functional analysis with applications*. Vol. 81. wiley New York, 1989.

[63] Bogoliubov N.N. Krylov N.M. "Introduction a la mechanique nonlineaire: Les methodes approaches et asymptotices". In: *Chaire de Phys. Math. Ann., Ukr. Akad. Nauk. Inst. de la Mecanique (1937) Translated by S. Lefshetz in Ann. Math. Studies (1947) Princeton, NJ* 11 (1937), pp. 419–423.

[64] C.D. Levermore. "Moment closure hierarchies for kinetic theories". In: *Journal of Statistical Physics* 83.5-6 (1996), pp. 1021–1065.

[65] C.C. Li and A. Der Kiureghian. "Mean out-crossing rate of nonlinear response to stochastic input". In: *Proceedings of ICASP-7, Balkema, Rotterdam* (1995), pp. 295–302.

[66] Y.K. Lin and G.Q. Cai. *Probabilistic structural dynamics: advanced theory and applications*. McGraw-Hill New York, 1995.

[67] P.L. Liu and A. Der Kiureghian. "Multivariate distribution models with prescribed marginals and covariances." In: *Probabilistic Engineering Mechanics* 1.2 (1986), pp. 105 –112.

[68] L.D. Lutes and S. Sarkani. *Random vibrations: analysis of structural and mechanical systems*. Butterworth-Heinemann, 2004.

[69] C.Y. Ma, U. Alibrandi, and C.G. Koh. "The Improved FORM for Stochastic Dynamic Analysis". In: *Vulnerability, Uncertainty, and Risk*. American Society of Civil Engineers, 2014. Chap. 255, pp. 2536–2545. DOI: 10.1061/9780784413609.255. eprint: http://ascelibrary.org/doi/pdf/10.1061/9780784413609.255. URL: http://ascelibrary.org/doi/abs/10.1061/9780784413609.255.

[70] I.I. Marks and J. Robert. *Introduction to Shannon sampling and interpolation theory*. Springer-Verlag New York, Inc., 1991.

[71] R.E. Melchers. "Importance sampling in structural systems". In: *Structural safety* 6.1 (1989), pp. 3–10.

[72] R.E. Melchers. "Radial importance sampling for structural reliability". In: *Journal of Engineering Mechanics* 116.1 (1990), pp. 189–203.

[73] R.E. Melchers. "Search-based importance sampling". In: *Structural Safety* 9.2 (1990), pp. 117–128.

[74] N. Metropolis and S. Ulam. "The monte carlo method". In: *Journal of the American statistical association* 44.247 (1949), pp. 335–341.

[75] N. Metropolis et al. "Equation of state calculations by fast computing machines". In: *The journal of chemical physics* 21.6 (1953), pp. 1087–1092.

[76] A.H. Nayfeh. *Perturbation methods*. John Wiley & Sons, 2008.

[77] D.E. Newland. *An introduction to random vibrations, spectral & wavelet analysis*. Courier Dover Publications, 2012.

[78] N.C. Nigam. *Introduction to random vibrations*. MIT press, 1983.

[79] G.C. Papanicolaou. "Some problems and methods for the analysis of stochastic equations". In: *Stochastic Differential Equations* 6 (1973), pp. 21–23.

[80] G.C. Papanicolaou and W. Kohler. "Asymptotic theory of mixing stochastic ordinary differential equations". In: *Communications on Pure and Applied Mathematics* 27.5 (1974), pp. 641–668.

[81] H.J. Pradlwarter, G.I. Schuëller, and C.A. Schenk. "A computational procedure to estimate the stochastic dynamic response of large non-linear FE-models". In: *Computer methods in applied mechanics and engineering* 192.7 (2003), pp. 777–801.

[82] M.B. Priestley. "Evolutionary spectra and non-stationary processes". In: *Journal of the Royal Statistical Society. Series B (Methodological)* (1965), pp. 204–237.

[83] R. Rackwitz. "Reliability analysis a review and some perspectives". In: *Structural safety* 23.4 (2001), pp. 365–395.

[84] S. Rezaeian and A. Der Kiureghian. "A stochastic ground motion model with separable temporal and spectral nonstationarities". In: *Earthquake Engineering & Structural Dynamics* 37.13 (2008), pp. 1565–1584.

[85] S. Rezaeian and A. Der Kiureghian. "Simulation of synthetic ground motions for specified earthquake and site characteristics". In: *Earthquake Engineering & Structural Dynamics* 39.10 (2010), pp. 1155–1180.

[86] S.O. Rice. "Mathematical analysis of random noise". In: *Bell System Technical Journal* 23.3 (1944), pp. 282–332.

[87] H. Risken. "The Fokker-Planck Equation. Methods of Solution and Applications, vol. 18 of". In: *Springer Series in Synergetics* (1989).

[88] J.B. Roberts and P.D. Spanos. *Random vibration and statistical linearization.* Courier Dover Publications, 2003.

[89] J.B. Roberts and P.D. Spanos. "Stochastic averaging: an approximate method of solving random vibration problems". In: *International Journal of Non-Linear Mechanics* 21.2 (1986), pp. 111–134.

[90] S.M. Ross. *Simulation.* Elsevier Science, 2012. ISBN: 9780124159716. URL: `http://books.google.com/books?id=sZjDT6MQGF4C`.

[91] C.A. Schenk, H.J. Pradlwarter, and G.I. Schuëller. "Non-stationary response of large, non-linear finite element systems under stochastic loading". In: *Computers & structures* 83.14 (2005), pp. 1086–1102.

[92] M.N. Schmidt and M. Morup. "Nonparametric Bayesian modeling of complex networks: an introduction". In: *Signal Processing Magazine, IEEE* 30.3 (2013), pp. 110–128.

[93] G.I. Schuëller, H.J. Pradlwarter, and P.S. Koutsourelakis. "A critical appraisal of reliability estimation procedures for high dimensions". In: *Probabilistic Engineering Mechanics* 19.4 (2004), pp. 463–474.

[94] C.E. Shannon. "A mathematical theory of communication". In: *ACM SIGMOBILE Mobile Computing and Communications Review* 5.1 (2001), pp. 3–55.

[95] M. Shinozuka. "Digital simulation of random processes". In: *Journal of Sounds and Vibration* 25 (1972), pp. 111–128.

[96] M. Shinozuka. "Monte Carlo solution of structural dynamics". In: *Computers & Structures* 2.5 (1972), pp. 855–874.

[97] M. Shinozuka and G. Deodatis. "Simulation of the stochastic process by spectral rappresentation". In: *American Society of Mechanical Engineering* 25 (1991), pp. 191–204.

[98] M. Shinozuka and C.M. Jan. "Digital simulation of random processes and its applications". In: *Journal of sound and vibration* 25.1 (1972), pp. 111–128.

[99] J.C. Simo and T.J.R. Hughes. *Computational Inelasticity.* Interdisciplinary Applied Mathematics Series. Springer, 2000. ISBN: 9783540975205. URL: `http://books.google.com/books?id=MNN3PwAACAAJ`.

[100] J.C. Simo and R.L. Taylor. "Consistent tangent operators for rate-independent elastoplasticity". In: *Computer methods in applied mechanics and engineering* 48.1 (1985), pp. 101–118.

[101] T.T. Soong and M. Grigoriu. "Random vibration of mechanical and structural systems". In: *NASA STI/Recon Technical Report A* 93 (1993), p. 14690.

[102] M.A. Tanner. *Tools for statistical inference*. Vol. 3. Springer, 1991.

[103] M.A. Valdebenito, H.J. Pradlwarter, and G.I. Schuëller. "The role of the design point for calculating failure probabilities in view of dimensionality and structural nonlinearities". In: *Structural Safety* 32.2 (2010), pp. 101–111.

[104] D. Vamvatsikos and C.A. Cornell. "Incremental dynamic analysis". In: *Earthquake Engineering & Structural Dynamics* 31.3 (2002), pp. 491–514.

[105] E. H. Vanmarcke. "On the distribution of the first-passage time for normal stationary random processes". In: *Journal of Applied Mechanics, ASME* 42.1 (1975), pp. 215–220.

[106] E.H. Vanmarcke. "On the distribution of the first-passage time for normal stationary random processes". In: *Journal of applied mechanics* 42.1 (1975), pp. 215–220.

[107] B. Walsh. "Markov Chain Monte Carlo and Gibbs Sampling". In: *Lecture Notes for EEB 581, version 26, Massachusetts Institute of Technology* (2004).

[108] Y.K. Wen. "Equivalent linearization for hysteretic systems under random excitation". In: *Journal of Applied Mechanics* 47.1 (1980), pp. 150–154.

[109] Y.K. Wen. "Method for random vibration of hysteretic systems". In: *Journal of the Engineering Mechanics Division* 102.2 (1976), pp. 249–263.

[110] J.M. Whittaker. *Interpolatory function theory*. Vol. 33. The University Press, 1935.

[111] Y. Zhang and A. Der Kiureghian. "Dynamic response sensitivity of inelastic structures." In: *Computer Methods in Applied Mechanics and Engineering* 108 (1993), pp. 23–36.

[112] Y. Zhang and A. Der Kiureghian. "Two improved algorithms for reliability analysis in reliability and optimization of structural systems." In: *Rackwitz R, Augusti G, Borri A, editors. Proceedings of the 6th IFIP WG 7.5 working conference on reliability and optimization of structural systems* (1994), pp. 297–304.

[113] W.Q. Zhu. "Recent developments and applications of the stochastic averaging method in random vibration". In: *Applied Mechanics Reviews* 49.10S (1996), S72–S80.

[114] W.Q. Zhu. "Stochastic averaging methods in random vibration". In: *Applied Mechanics Reviews* 41.5 (1988), pp. 189–199.

[115] O.C. Zienkiewicz and R. L. Taylor. *The finite element method: Solid mechanics*. Vol. 2. Butterworth-heinemann, 2000.

Index

Alibrandi, U., 112
Au, S.K., 4, 5, 78, 84, 109
Au-Beck algorithm, 78, 85, 87
Autocorrelation function
    Whittaker-Shannon expansion, 41

Band limit, 10
Basis function
    frequency domain, 14
    sinc interpolation, 38
    time domain, 10
Beck, J.L., 4, 5, 78, 84, 109
Bogolubov, N.N., 5
Bouc-Wen
    material model, 16, 88
Bracewell, R.N., 27

CDF
    Cumulative Distribution Function, 18
Constrained optimization problem, 12
Convergence
    Whittaker-Shannon expansion, 42
Crandall, S.H., 3

DDM
    Direct differentiation method, 54
Deodatis, G., 14, 37
Der Kiureghian, A., 3, 5, 7, 9, 37, 54, 106
Design point, 9
    augmented, 52
    high dimension, 110
Design point
    evolutionary, 84
Design-point excitation, 17
    bi-directional input, 62
Design-point response, 17

EFRF
    Evolutionary Frequency-Response Function, 80
ELM
    Equivalent Linearization Method, 5
EPSD
    Evolutionary Power Spectral Density, 78
    Kanai-Tajimi, 92
ETELM
    Evolutionary Tail Equivalent Linear Method, 84
ETELM-Au-Beck algorithm, 91
ETELS
    Evolutionary Tail-Equivalent Linear System, 78, 82
Evolutionary process, 79

First-passage probability, 22, 64
Fokker-Planck equation, 3
FORM
    First-Order Reliability Method, 3, 12
Fourier series
    expansion, 38
Fragility curve, 1, 23, 64
Franchin, P., 5
FRF
    Frequency-Response Function, 83
FRF, Frequency-Response Function, 14, 15
Fujimura, K., 3, 5, 7, 9, 106

Garrè, L., 6, 37, 106
Gaussian-noise, 38
Gradient vector, 12

augmented, 52
Grigoriu, M., 40

Hilbert space, 34
HLRF algorithm, 16, 54

Important hyper-ring, 109
Inner product space, 33
Integration step, 10
IRF
Impulse-Response Function, 10, 83
IS
Importance Sampling, 4

Koo, D.P., 5
Koo, H., 114
Krylov, N.M., 5

Li, C.C., 5
Limit-state surface, 11
concave, 112
convex, 112
saddle, 112

MCMC
Markov Chain Monte Carlo, 4
MCS, Monte Carlo Simulations, 4
Mean up-crossing, 64
Mean up-crossing rate, 21
Modulating function
frequency, 79
time, 79
Moment of closure, 3

Non-stationary process, 78
Nonparametric system, 13
Nyquist rate, 29

PBEE
Performance Based Earthquake Engineering, 1
PDF, Probability Density Function, 19
PEER
Pacific Earthquake Engineering Research Center , 1
Periodizing Shah distribution in the frequency domain, 28
Periodizing Shah distribution in the time domain, 28
Perturbation methods, 3
Priestley, M.B., 78
PSA
probabilistic structural analysis, 1
PSD
Kanai-Tajimi, 62

Rectangular wave process, 50
Reliability index, 12
evolutionary, 84
Rice, S.O., 14, 85
Roberts, J.B, 4

Sampling rate, 29
Sampling Shah distribution in the frequency domain , 28
Sampling Shah distribution in the time domain, 28
SDOF, Single-Degree-of-Freedom, 16
Sensitivity
input term, 56
restoring force, 56
Shah distribution, 27
Shinozuka, M., 14, 37
Spanos, P.D., 4
Spectral density, 10
Square-wave process, 10
Standard normal space, 39
augmented, 50
high dimension, 109
Stochastic averaging method, 4
Stratonovich, R.L., 4

Taylor series, 12
TELM
limitations and shortcomings, 109
Tail-Equivalent Linearization Method, 5, 9
TELS
Tail-Equivalent Linear System, 13

Uniformly modulated process, 79, 80

Vanmarcke, E.H., 85, 108

Volume error, 110

White-noise process, 10
    bi-component, 62
Whittaker-Shannon interpolation formula, 27,
        33, 38

Zhang, Y., 54
Zhu, W.Q., 4